

MADITRACE

A Review of Artificial Fingerprinting and 3D Printing for the Potential Tracking of Minerals in Complex Supply Chains

Deliverable D2.1

Version N°1.0

Authors: Laurance Donnelly (AHK), Quentin Dehaine (GTK), Shristi Ghosh (AHK), Ian Corfe (GTK), Robert Dunn (AHK), Dan Pop (AHK)



**Funded by
the European Union**

Funded by the European Union. Views and opinions expressed are however those of the author(s) only and do not necessarily reflect those of the European Union or HaDEA. Neither the European Union nor the granting authority can be held responsible for them.



Disclaimer

The content of this report reflects only the author's view. The European Commission is not responsible for any use that may be made of the information it contains.





Document Information

| | |
|--------------------------|--|
| Grant Agreement | 101091502 |
| Project Title | Material and digital traceability for the certification of critical raw materials |
| Project Acronym | MaDiTraCe |
| Project Coordinator | Daniel Monfort, BRGM |
| Project Duration | 1 January 2023 – 31 December 2025 (36 months) |
| Related Work Package | WP2 |
| Related Task(s) | T2.3 – Artificial Fingerprinting |
| Lead Organisation | Alfred H Knight (AHK) |
| Contributing Partner(s) | Geological Survey of Finland (GTK), Bureau de Recherche Géologique et Minière (BRGM) |
| Authors | Laurance Donnelly (AHK), Quentin Dehaine (GTK), Shristi Ghosh (AHK), Ian Corfe (GTK), Robert Dunn (AHK), Dan Pop (AHK) |
| Due Date | 30 September 2023 |
| Submission Date | 29 September 2023 |
| Revised Submission Date | 23 November 2023 |
| Revision Submission Date | 12 December 2023 |
| Dissemination level | Public (PU) |

History

| Date | Version | Submitted by | Reviewed by | Comments |
|------------|---------|-------------------|--|------------------|
| 29/09/2023 | 0.1 | Laurance Donnelly | Quentin Dehaine (GTK), Shristi Ghosh (AHK), Ian Corfe (GTK), Robert Dunn (AHK), Dan Pop (AHK), Harri Kaikkonen (GTK), Patrick Friedrichs (GTK), Daniel Monfort (BRGM) and Anne-Marie Desaulty (BRGM) | Draft for review |
| 01/12/2023 | 0.2 | Laurance Donnelly | Quentin Dehaine (GTK), Shristi Ghosh (AHK), Ian Corfe (GTK), Robert Dunn (AHK), Dan Pop (AHK), | Issued |





| | | | | |
|------------|---|-------------------|---|---------------|
| | | | Harri Kaikkonen (GTK), Patrick Friedrichs (GTK), Anne-Marie Desaulty (BRGM), Wolfram Kloppmann (BRGM) & Daniel Monfort (BRGM) | |
| 11/12/2023 | 1 | Laurance Donnelly | Mariana Terreros Lozano (LGI) | Quality Check |



Table of Contents

| | | |
|---------|--|----|
| 1 | Introduction..... | 21 |
| 1.1 | Global Context | 21 |
| 1.2 | Responsible Sourcing and Traceability | 21 |
| 1.3 | Illegal Mining, Illicit Minerals and Mining Crime | 22 |
| 1.3.1 | Provenance Determination | 22 |
| 1.3.2 | Traceability | 22 |
| 1.4 | Current Traceability Systems for CRMs | 23 |
| 1.5 | Report Objective | 24 |
| 2 | Overview of MaDiTraCe..... | 26 |
| 2.1 | Project Aim and Objectives | 26 |
| 2.2 | Artificial Fingerprinting | 27 |
| 3 | MaDiTraCe Commodities and Value Chains..... | 29 |
| 3.1 | Supply Chain Segments | 29 |
| 3.1.1 | LIB Supply Chains..... | 29 |
| 3.1.1.1 | Upstream graphite supply chains for anode production..... | 29 |
| 3.1.1.2 | Upstream lithium supply chains, cathode and electrolyte..... | 32 |
| 3.1.1.3 | Upstream cobalt supply chains for cathode production..... | 32 |
| 3.1.1.4 | Midstream LIB supply chains and recycling | 33 |
| 3.1.2 | REE Supply Chains for NdFeB Magnets | 33 |
| 3.1.3 | Geographical Distribution of the Li, Co, Graphite and REEs Supply Chains.. | 34 |
| 3.1.3.1 | Raw and processed materials..... | 34 |
| 3.1.3.2 | Battery component, battery cell and EV manufacturing | 35 |
| 3.1.3.3 | NdFeB magnets and wind turbine manufacturing | 37 |
| 3.2 | Requirements of Miners, Traders and Refiners | 37 |
| 3.2.1 | The MaDiTraCe Questionnaire, mapping of permitted taggant materials in metal industry..... | 37 |
| 3.2.1.1 | Element penalty (impurity) limits in the mining and metals industry..... | 37 |
| 3.2.2 | Managing Perception and the Potential for Blight..... | 39 |
| 4 | Artificial Fingerprinting and Tracing | 40 |
| 4.1 | Historical Development..... | 40 |
| 4.2 | Artificial Taggant Types, Properties and Uses | 41 |
| 4.2.1 | Artificial Taggant Restrictions | 42 |
| 4.2.2 | Forensic Taggants | 45 |
| 4.2.2.1 | Physical..... | 45 |
| 4.2.2.2 | Spectroscopic..... | 45 |



| | | |
|---------|---|-----|
| 4.2.2.3 | Chemical | 46 |
| 4.2.2.4 | DNA | 46 |
| 4.2.3 | Existing Taggants | 47 |
| 4.2.3.1 | Barcodes and barcode particles | 47 |
| 4.2.3.2 | Photonic nanocrystals, QD, fluorophores, lanthanides, nanophosphors | 49 |
| 4.2.3.3 | Physical unclonable functions | 55 |
| 4.2.3.4 | Plasmonic structures | 58 |
| 4.2.4 | Other Techniques | 59 |
| 4.2.4.1 | Raman spectroscopy | 59 |
| 4.2.4.2 | Synthetic polypeptide sequences | 60 |
| 4.2.4.3 | Aerospace materials | 60 |
| 4.2.4.4 | Non-optical detection | 60 |
| 4.2.4.5 | Tailorlux fibres | 61 |
| 4.3 | Existing Taggants and MaDiTraCe | 61 |
| 4.3.1 | AHK Preliminary Investigations | 64 |
| 5 | 3D Printing | 66 |
| 5.1 | Overview | 66 |
| 5.2 | Advantages of 3D Printing | 67 |
| 5.3 | Methods of 3D Printing | 67 |
| 5.3.1 | Range of Materials | 68 |
| 5.3.2 | Size Range | 70 |
| 5.3.3 | Prior Examples of Tracing and 3D Printing | 72 |
| 6 | Conclusions | 79 |
| 7 | Bibliography | 81 |
| 8 | Appendices | 97 |
| 8.1 | Appendix I: MaDiTraCe Questionnaire | 97 |
| 8.2 | Appendix II: Photolithography or Photochemical Machining | 101 |
| 8.3 | Appendix III: Stokes shift and Anti-Stokes shift | 102 |
| 8.4 | Appendix IV: Photoluminescence | 103 |



List of Figures

| | |
|--|----|
| Figure 1: The MaDiTraCe consortium (source: MaDiTraCe, 2023)..... | 26 |
| Figure 2: Simplified representation of the different stages of the REE-magnet and battery supply chains. | 30 |
| Figure 3: Supply chain stages for lithium, cobalt and graphite batteries and REE-magnets used in electric vehicles and wind turbines. Abbreviations are given in the text. | 31 |
| Figure 4: Geographical distribution of the global MaDiTraCe technology materials (Li, Co, Graphite, REEs) supply chains (source: GTK). | 36 |
| Figure 5: Identification taggants history timeline in the US (source: Seman <i>et al.</i> , 2019). .. | 40 |
| Figure 6: Example of anticounterfeiting taggants on currency notes (source: Arppe & Sørensen, 2017). | 43 |
| Figure 7: Uniquely encoded Microtrace taggants (source: Microtrace Solutions, 2023). ... | 45 |
| Figure 8: DNA based taggant products (source: Selectamark Security System, 2023). | 47 |
| Figure 9: (a) preparation of QD coated pollens using layer by layer (LbL) deposition process. (b) Probe binding, target-probe interaction, fluorescently labelled detection (source: Wang <i>et al.</i> , 2020). | 48 |
| Figure 10: Emission wavelength range of commercially used materials (source: Q. Grim <i>et al.</i> , 2015). | 49 |
| Figure 11: Illustration of CdS spheres printed on paper using inkjet printers (source: S. Wu <i>et al.</i> , 2017). | 50 |
| Figure 12: Invisible QR codes obtained using CdS spheres (source: S. Wu <i>et al.</i> , 2017). ... | 51 |
| Figure 13: (a) Photonic crystals alter motion of photons due to its periodic dielectric structure; (b) metallic NPs are selective with their absorption and scattering wavelength; (c) semiconducting NPs exhibit Stokes shift and Anti-Stokes shift (source: Ren <i>et al.</i> , 2020). . | 52 |
| Figure 14: UCNF controlled synthesis (source: Xu <i>et al.</i> , 2017). | 55 |
| Figure 15: Multiple layered particles with different physical characteristics in each layer (source: Gooch, Daniel, <i>et al.</i> , 2016). | 56 |
| Figure 16: Synthesis of a PUF key (source: Arppe & Sørensen, 2017). | 57 |
| Figure 17: (a) Self-assemble of CNTs in HfO ₂ trenches in a monolayer. Self-assembly is realised through ion exchange, (b) Randomly connected 2D CNT array (source: Q. Li <i>et al.</i> , 2021). | 58 |
| Figure 18: (a-c) SEM, dark field microscopy and AFM image of metal electrode. (d-f) SEM, dark field microscopy and AFM image of annealed electrode. (g) Close up SEM and chemical composition of hemispherical core-shell NPs (source: Q. Li <i>et al.</i> , 2021). | 59 |
| Figure 19: Peptide based taggant and its analysis (source: Gooch, Daniel, <i>et al.</i> , 2016). .. | 60 |
| Figure 20: 100/200 mesh MIP (courtesy of Microtrace), showing layers and colour sequence without UV(left and middle) and under UV(right) (source: Alfred H Knight International).. | 64 |
| Figure 21: MIP bonded into coated layer of the crystal-clear lacquer (source: Alfred H Knight International). | 64 |
| Figure 22: Differences between a) traditional subtractive manufacturing and b) additive manufacturing (source: Chen <i>et al.</i> , 2020). | 66 |
| Figure 23: Complex near-net shape metal 3D printed heat exchangers with internal structures unachievable via traditional manufacturing methods. Since the surface area to volume ratio and position of that surface area relative to air flow are critical in heat exchanger efficiency, 3D printing allows step change increases in performance over traditional heat exchangers (source: https://all3dp.com/1/better-heat-exchangers-with-additive-manufacturing/). | 67 |



| | |
|--|----|
| Figure 24: The seven principal methods of 3D printing, as defined in the ISO/ASTM 52900:2021 document on additive manufacturing terminology (source: ISO, 2021; de Pastre <i>et al.</i> , 2022). | 69 |
| Figure 25: Size of the 3D printing materials market by revenue in 2022 (source: Dadhania, 2023). | 70 |
| Figure 26: Size range of 3D printed objects. a) One of the largest 3D printed buildings, printed using concrete material extrusion with local materials as aggregate. b) 3D printed boat, printed using polymer material extrusion. c) 3D printed wind turbine blade mould, printed using polymer material extrusion. d) One of the largest 3D printed pressure chambers, approximately 1.5m tall, printed using metal WAAM. e) 3D printed 'benchy' boat benchmark print, printed using two photon polymerization, total length approximately 50 micrometres (source: Doherty <i>et al.</i> , 2020). | 72 |
| Figure 27: Two-photon lithography/two-photon polymerisation printing of sub-surface photoluminescent nitrogen-doped carbon quantum dots (source: Jaiswal <i>et al.</i> , 2021). | 74 |
| Figure 28: (a-i) Photos, UV luminescence images, and SEM images of aerosol jet 3D printed nanospheres, with g-i deposited at higher temperatures than a-f and producing predominantly spherical and highly luminescent nanosphere structures (source: Lin <i>et al.</i> , 2023). (j-n): Photoluminescent and mechanoluminescent ZnS/CaZnOS-based 3D printed ceramic spheres; j - photo, k - 290nm photoluminescence, l - 339nm photoluminescence, m - photo of spheres in plastic ball, n - mechanoluminescence of spheres agitated inside plastic ball in dark (source: Wang <i>et al.</i> , 2023). | 75 |
| Figure 29: Multi-material powder bed fusion 3D printing of internal QR codes. (a-c): schematic of three levels of concealment (none, partial, full). (d-g): optical and X-ray images of none-concealed and fully concealed samples (source: Wei <i>et al.</i> 2018). | 76 |
| Figure 30: Magnetic permeability differences in directed energy deposition multi-material steel 3D printing revealed by eddy current reading. Grid can be used for comparison and individual coding (source: Eisenbarth <i>et al.</i> 2020). | 77 |
| Figure 31: Ferromagnetic multi-material steel directed energy deposition 3D printing of internally coded information. a) Schematic for MBC's - magnetic band composites of non-magnetic 316L and magnetic 430 steel. b) Schematic for MPC's - magnetic pattern composites. c-e) magnetic flux (upper) and iron filing (lower) patterns for MPC's on c) surface, d) 1mm embedded below surface, and e) 1.5mm embedded below surface (source: Salas <i>et al.</i> , 2022). | 78 |
| Figure 32: Single material powder bed fusion fully dense 3D printed 316 L stainless steel QR and bar codes via crystallographic texture. (a) optical scanned QR code, (b) directed reflectance microscopy QR code, (c) optical scanned barcode, (d) directed reflectance microscopy barcode, (e) electron backscatter diffraction patterning of data blocks/bits within QR code showing varying crystal grain textures and orientations (source: Sofinowski <i>et al.</i> 2023). | 78 |

List of Tables

| | |
|--|----|
| Table 1: Maximum impurity levels and approximate penalties for copper and nickel concentrates (source: Salomon-de-Friedberg & Robinson, 2015). | 37 |
| Table 2: Anonymised preliminary response to the MaDiTraCe questionnaire, received from a mining company, indicating the elemental limits for potential artificial taggant particles. | 38 |



| | |
|--|----|
| Table 3: Anonymised preliminary response to the MaDiTraCe questionnaire, received from a precious metals refining company, indicating the elemental limits for potential artificial taggant particles..... | 38 |
| Table 4: Classification of anti-counterfeiting taggants based on characteristics and function (source: Arppe & Sørensen, 2017)..... | 44 |
| Table 5: Advantages and disadvantages of commercially available forensic taggants (source: Gooch, Daniel, et al., 2016)..... | 47 |
| Table 6: Different optical NPs with potential usage in anticounterfeiting (source: Ren et al., 2020)..... | 54 |
| Table 7: Summary of new materials and technologies..... | 62 |





Summary

Global commodity flows and regulatory framework relating to critical raw materials (CRMs), and battery raw materials in particular, are high on the European economic and political agenda. Companies are also facing increased pressure to responsibly extract, process and source geological raw materials. This is driven in part by, for example, the European Union Battery Regulation and European Union Directive on Corporate Sustainability Due Diligence. As a consequence, certification schemes, transparent and secure traceability, and decentralised confidential data handling will become imperative. In this context, the MaDiTraCe (Material and Digital Traceability for the Certification of Critical Raw Materials, CRM) project has been commissioned by the European Union.

MaDiTraCe, formally launched in Paris in January 2023, is a 36-month European Union project funded through the Horizon Europe Programme. The project aim is to reinforce the transparency, traceability, and sustainability of complex supply chains of CRMs including cobalt, lithium, natural graphite and rare earth elements. Notably, these supply chains are associated with batteries for electric vehicles and permanent magnets for wind turbines. There are 14 partners, from 7 countries, involved in the project. MaDiTraCe has a principal focus on the development of integrated technological solutions for the traceability and certification of CRMs into a digital passport. It is anticipated these solutions may prove the provenance and traceability of CRMs to comply with existing regulations and future European Union policies.

The tracking of minerals and commodities using artificial fingerprinting techniques and the potential use of 3D printed tracer particles technology, forms part of the MaDiTraCe Work Package 2. This report provides a review of existing artificial fingerprinting and 3D printing technology, and the potential for the development of an artificial taggant particle (ATP).

ATPs (also referred to in this report as 'artificial taggants' or simply 'taggants') were originally developed in the 1970s as an additive in explosives for the purposes of tracking. Since then, the technology has advanced significantly. A range of different ATPs are now commercially available for tracking items of value, anti-counterfeiting and monitoring. Typically, these are applied to currency, clothing, pharmaceuticals, chemicals, drugs, explosives, vehicles and watches.

To-date, ATPs have not been reported to be widely used for the tracking of minerals and metals commodities. Taggant technology is variable and complex, based largely on spectroscopic or electrical characteristics. These include: inks and dyes, micron-sized SU8 (epoxy-based negative photoresist) barcodes, cadmium selenide (CdSe), quantum dots (QDs) deposited onto sunflower pollen grains, silicon-based photonic crystal, inks with dispersed CdSe spheres, gold nanoparticles (AuNPs), silver nanoparticles (AgNPs), oxidised indole derivative on silicon nanoparticles (SiNPs), lanthanum-doped up-conversion nanoparticles (UCNP), physical unclonable functions (PUF) keys, carbon nanotubes (CNTs) and deoxyribonucleic acid (DNA). Further experimental work is also recommended on existing artificial taggant particles, including for example, Microtaggant Identification Particles (MIP®) produced by Microtrace Solutions, USA and artificial taggant particles produced by Tailorlux GmbH, Germany.

Unfortunately, during this review, there were no existing artificial taggants that were found to be directly applicable to MaDiTraCe materials. This was principally due to the inclusion



of components that may not be acceptable to the minerals and metals industries, insufficient data or complex and impracticable detection procedures. Potentially, silicon from gramineae plants and PUF keys warrant further experimental research investigations.

Essentially, the development of a new and innovative ATP is therefore required. This new taggant should be inert, free from penalty metals and components that are forbidden or restricted in the minerals and metals industries, possess a high encoding capacity, non-toxic, non-radioactive and, easily and cost-effectively detectable. As part of this review stage, a questionnaire was developed and will be provided to players within the mining, minerals and metals industry to help guide the properties and acceptable components of ATPs.

A moderate amount of research has been carried out into the use of 3D printing both for producing objects for tracing, and for tracing 3D printed objects themselves. Some of these incorporate existing artificial taggant particles (e.g., quantum dots and various nanoparticles), while others rely on the properties of either the printing process or the materials being printed with. A wide range of materials or composites is possible, and many of the 3D printing methods allow considerable freedom of design with regards to both internal and external shape. In the context of MaDiTraCe, incorporating existing taggant technologies into 3D printed particles would allow control over particle shape. It would also allow partial control over the materials used, in accordance with the requirements outlined above. This would in turn enable experiments on particle dispersion to move beyond existing taggant particle shapes, which were not designed for the purposes of artificial fingerprinting of lithium-ion batteries and rare-earth magnet supply chains.

Keywords

Artificial Fingerprinting, Artificial Taggant Particles, Critical Raw Materials, Li-ion Battery REE-magnet Traceability, Tracking, Tracers, 3D Printing.

Abbreviations and Acronyms

| Acronym | Description |
|---------|----------------------------------|
| 3TG | Tin, tantalum, tungsten and gold |
| ABS | Acrylonitrile butadiene styrene |
| AFM | Atomic force microscope |
| AgNP | Silver nanoparticle |
| AHF | Anhydrous hydrogen fluoride |
| ASA | Acrylonitrile styrene acrylate |
| ASM | Artisanal and small-scale mining |
| ASO | Antisense oligonucleotide |
| ATP | Artificial taggant particle |
| AuNP | Gold nanoparticle |
| CAM | Cathode active material |



| | |
|---------------------------------|--|
| CdS | Cadmium sulphide |
| CdSe | Cadmium selenide |
| CdTe | Cadmium telluride |
| CoC | Chain of custody |
| CNT | Carbon nanotube |
| CP | Conjugated polymer |
| CRM | Critical Raw Material |
| CViT | Cash and Valuables in Transit |
| DNA | Deoxyribonucleic acid |
| DPP | Digital product passport |
| DRC | Democratic Republic of the Congo |
| DSC | Differential scanning calorimetry |
| EHDP | Aerosol jet printing and electrohydrodynamic printing |
| EoL | End of Life |
| EPOX | 3,4 epoxycyclohexane methyl or 3,4 epoxycyclohexylcarboxylate |
| ESI-MS | Electrospray ionisation mass spectrometry |
| EV | Electric Vehicle |
| FTIR | Fourier transform infrared |
| GIGO | Garbage in, garbage out |
| HOMO | Highest occupied molecular orbital |
| HREE | Heavy rare earth element |
| IGF | Inter-Governmental Forum on Mining, Minerals, Metals and Sustainable Development |
| INTERPOL | International Criminal Police Organization |
| IR | Infrared radiation |
| ISC | Intersystem crossing |
| ISO | International Organization for Standardization |
| IUGS-IFG | International Union of Geological Sciences, Initiative on Forensic Geology |
| LA-ICP-MS | Laser ablation coupled with plasma mass spectrometry |
| LbL | Layer by layer deposition process |
| LIB | Lithium-ion battery |
| Li ₂ CO ₃ | Lithium carbonate |
| LiF | Lithium fluoride |
| LiOH | Lithium hydroxide |
| LiPF ₆ | Lithium hexafluorophosphate |



| | |
|-------------|--|
| LREE | Light rare earth element |
| LSM | Large-scale mining |
| LSPR | Localised surface plasmon resonance |
| LUMO | Lowest occupied molecular orbital |
| MFP | Material fingerprinting |
| MIP | Microtaggant® Identification Particle |
| MSP | Mixed nickel-cobalt sulphide product |
| NC | Nanocrystal |
| NIR-VIS | Near infrared and visible |
| NdFeB | Neodymium-iron-boron |
| NP | Nanoparticle |
| NPL | Nanoplatelet |
| NR | Nanorod |
| OECD | Organisation for Economic Co-operation and Development |
| OEM | Original equipment manufacturer |
| PA | Nylon (also known as polyamide) |
| PC / PC-ABS | Polycarbonate / Polycarbonate ABS alloy |
| PDA | Polydiacetylene |
| Pdots | Polymer dots |
| PE | Polyelectrolyte |
| PEEK | Polyether ether ketone |
| PET (PETG) | Polyethylene terephthalate |
| PETMP | Pentaerythritol tetra (3-mercaptopropionate) |
| PLA | Polylactic acid |
| PLQE | Photoluminescence quantum efficiency |
| PMMA | Polymethyl methacrylate |
| PP | Polypropylene |
| PUF | Physical unclonable function |
| PVP | Polyvinylpyrrolidone |
| QD | Quantum Dot |
| QR | Quick response |
| REE | Rare earth element |
| RET | Resonance energy transfer |
| RFID | Radio-frequency identification (also known as RFIT) |



| | |
|-------|---|
| RFIT | Radio frequency identification tag (also known as RDID) |
| RI | Refractive Index |
| RNA | Ribonucleic acid |
| RNAi | RNA interference |
| SAPC | Self-assembled photonic crystal |
| SEM | Scanning electron microscopy |
| SERS | Surface Enhanced Raman Scattering |
| SiNP | Silicon nanoparticle |
| SNR | Signal to noise ratio |
| SPR | Surface Plasmon Resonance |
| TCSPC | Time correlated single photon counting |
| TMPMP | Thiol monomers such as trimethylolpropane tris (3-mercaptopropionate) |
| TPE | Thermoplastic elastomers |
| TPP | Two-photon polymerization |
| TRL | Technology readiness level |
| UC | Upconversion |
| UCNP | Upconversion nanoparticle |
| UDMA | Urethane dimethacrylate |
| UNODC | United Nations Office on Drugs and Crime |
| WAAM | Wire arc additive manufacturing |
| X-CT | X ray computed tomography |

Symbols

| Symbol | Description |
|--------|-----------------------------------|
| 3D | Three-dimensional |
| ppm | Parts per million |
| μm | Micrometre (also known as micron) |
| wt% | Weight percent |
| ~ | Approximately |
| ® | Registered trademark |

Definitions

Adulteration



Also known as 'salting', adulteration is the wilful and premeditated tampering of all, or an amount of a material or product, by adding material of a higher or lower standard, quality, or value, without the other party's knowledge or consent.

Anti-stokes

Anti-Stokes lines correspond to photons with higher energy compared to the incident photon.

Artificial taggant particles

Small, usually micron-size artificially developed physical taggants or particles.

Autofluorescence

Autofluorescence (primary fluorescence) is the fluorescence of naturally occurring substances, such as chlorophyll, collagen and fluorite. Most plant and animal tissues show some autofluorescence when excited with ultraviolet light (e.g., light of wavelength around 365 nm).

Background autofluorescence

The natural emission of light by molecules that increase during enhanced cellular metabolism.

Base metals

Naturally occurring metals such as copper, zinc, lead and nickel that are more readily available and less expensive than precious metals, such as gold. Base metals tarnish, oxidise or corrode relatively quickly when exposed to air or moisture.

Blockchain

Digital technology that allows for data to be validated and subsequently stored as an immutable 'block' on a collectively owned and decentralised database, every block being validated based on previous blocks, making it very difficult to alter. Blocks are validated either by an algorithm or a third party in the field.

Cationic exchange

Cation exchange is where one cation is substituted for one or more other cations.

Chain of custody

The custodial sequence that occurs as ownership or control (physical or administrative) of the material supply is transferred from one custodian to another in the supply chain.

Critical Raw Materials

Critical Raw Materials (CRMs) are raw materials that are considered essential in the modern-day economy, and often clean technologies, with however a relatively high supply risk.

Fluorescence

Materials emitting optical radiation for the duration of light energy incident on it.



Fluorometry

The measurement of emitted fluorescent light.

Functional materials

Materials with discrete characteristics and functions.

Gramineae

A large and nearly ubiquitous family of monocotyledonous flowering plants commonly known as grasses. It includes the cereal grasses, bamboos and the grasses of natural grassland and species cultivated in lawns and pasture.

Heterostructures

Semiconductor structure in which the chemical composition changes with position. The simplest heterostructure consists of a single heterojunction, which is an interface within a semiconductor crystal across which the chemical composition changes.

Illegal Mining

Illegal mining is mining activity that is undertaken without state permission, in particular in absence of land rights, mining licenses, and exploration or mineral transportation permits.

Illicit Minerals

Illicit minerals are forbidden by laws, rules and customs, but may not necessarily be illegal.

Indole

An aromatic, heterocyclic, organic compound (C_8H_7N) with a bicyclic structure, consisting of a six-membered benzene ring fused to a five-membered pyrrole ring. Indole is widely distributed in nature and can be produced by a variety of bacteria.

Integrity

The quality of a sample or seal being whole and complete.

Lanthanide doped nano-particles

Exhibit unique luminescent properties, including tunable luminescence emission, narrow emission width, excellent optical stability, and long lifetimes from micro- to milli-seconds.

Ligand

A ligand is an ion or molecule which donates a pair of electrons to the central metal atom or ion to form a coordination complex. The word ligand is from Latin, which means "tie or bind". Ligands can be anions, cations, and neutral molecules.

Ligand field

In ligand field theory, the various d orbitals are affected differently when surrounded by a field of neighbouring ligands and are raised or lowered in energy based on the strength of their interaction with the ligands.



Magnesiothermic reduction

This reduction entails the reaction of magnesium with silica resulting in an interwoven composite product of magnesia (MgO) and silicon.

Metallic nanoparticles

Submicron scale artefacts made of pure metals (gold, silver, titanium, zinc, platinum, cerium, iron, thallium) or their compounds (oxides, hydroxides, sulphides, phosphates, etc).

Microdots

Small polymer discs 2-1000 μm in size.

Micronizing

To pulverize extremely fine.

Nano-photonics (Nano-optics)

The study of the behaviour of light on the nanometre scale, and the interaction of nanometre-scale objects with light.

Oligonucleotide

Short, single or double-stranded DNA or RNA molecules, and include antisense oligonucleotides (ASO), RNA interference (RNAi), and aptamer RNAs. ASO and RNAi oligonucleotides are intended mainly for modulating gene and protein expression.

Optoelectronic

The study and application of light-emitting or light-detecting devices, a sub-discipline of photonics. Photonics refers to the study and application of the physical science of light.

Outer ligand field

One of several theories that describe the electronic structure of coordination or complex compounds, notably transition metal complexes, which consist of a central metal atom surrounded by a group of electron-rich atoms or molecules called ligands.

Particle

A small, localized grain or fragment, which can be ascribed several physical or chemical properties, such as volume, density, or mass.

Penalty Elements

Penalty elements may change the physical properties of material and impede the proper operation of the smelting facility.

Phononic energy

Quantum of vibrational mechanical energy.

Photoacoustic effect

When a material generates sound waves on interaction with light waves.

Photobleaching



Photochemical alteration of chemical compounds to change their ability to fluoresce.

Photochromism

Defined as a reversible transformation of a chemical species between two isomers upon photoirradiation.

Photolithography

Manipulating light to etch desired features onto a surface by transferring the pattern onto a mask on the surface, then etching away the areas of the surface unprotected by the mask.

Photonic nanocrystals

Artificial structures with periodically modified refractive index, where the optical modulation of light propagation is realized by diffraction and refractive index contrast in one, two, or three spatial dimensions respectively

Photoluminescence quantum efficiency

The number of photons emitted per absorbed photons of the excitation source.

Photonics

Science of light waves.

Photostability

Testing of exposure to solar light/UV/visible light in solid, liquid and semisolid state to observe any physical/chemical changes.

Photothermal

Of or concerned with light and heat, especially the production of heat by light.

Piezoelectricity

Refers to the accumulation of electric charge in some solids (such as crystals and ceramics).

Polymer dots

Semiconducting polymer dots (Pdots) are a type of conjugated polymer (CP) nanoparticle with highly advantageous fluorescence properties and a growing breadth of applications in bioanalysis and imaging. Exceptional brightness is an advantage of Pdots.

Quantum Dots

Also called semiconductor nanocrystals, are semiconductor particles a few nanometres in size, having optical and electronic properties that differ from those of larger particles as a result of quantum mechanics.

Quantum heterostructures

Heterostructure in a substrate, where size restricts the movements of charge carriers forcing them into a quantum confinement. This leads to formation of a set of discrete energy levels at which the carriers can exist.



Quantum yield

Ratio of number of photons emitted to absorbed photons.

Pollen

A powdery substance produced by flowers of seed plants. It consists of pollen grains (highly reduced microgametophytes), which produce male gametes.

Radiative rate

Rate of light emission per unit carrier concentration, or radiative rate. A fundamental semiconductor parameter that determines the photoconversion efficiency of solar cells.

Rare Earth Elements

Group of elements including lanthanide elements (atomic numbers from 57 to 71), scandium, and yttrium. They are divided into two groups based on their atomic weights: Light REEs (LREEs) include cerium (Ce), lanthanum (La), praseodymium (Pr), neodymium (Nd), and samarium (Sm) while Heavy REEs (HREEs) include europium (Eu), gadolinium (Gd), terbium (Tb), dysprosium (Dy), holmium (Ho), erbium (Er), thulium (Tm), ytterbium (Yb), and lutetium (Lt).

Raman scattering

On interaction between light and air molecules, it is possible for incident photons to lose or gain energy such that the scattered photons have changed frequency. This inelastic scattering is referred to as Raman scattering.

Spiropyrans

Spiropyrans are photoswitches that can undergo reversible structural transformations through isomerization between ring-opened merocyanine and ring-closed spiropyran forms under the influence of stimuli such as stress, light, pH, and thermal effect.

Stochastic

Having a random probability distribution or pattern that may be analysed statistically but may not be predicted precisely.

Stokes

Stokes lines correspond to photons with lower energy compared to the incident photon.

SU-8

SU-8 is a high contrast, epoxy-based photoresist designed for micromachining and other microelectronic applications where a thick chemically and thermally stable image is desired. The exposed and subsequently cross-linked portions of the film are rendered insoluble to liquid developers.

Substitution

Substitution is the wilful and premeditated switching of all, or an amount of ore, mineral concentrate, refinery or smelter products, for material of a lower standard or quality, without the other party's knowledge or consent. It could also include the use of fake or counterfeit materials or products. This is illegal and considered a fraudulent practice.





Surface plasmon resonance

Collective oscillation of conduction band electrons that are in resonance with the oscillating electric field of incident light.

Taggant

Any chemical or physical marker added to materials to allow various forms of tracking, tracing and testing.

Thermochromic inks

Temperature dependent inks or dyes prone to temporary changes in colour on exposure to changing temperature.

Traceability

The ability to verify the history, location or application of a material or product at different stages of the value chain from the source to the market and up to the end-of-life, by documented recorded identification or other means.

Traceability systems

Systems (digital or paper-based) that records and follows the trail as products and materials come from suppliers and are processed and ultimately distributed as end products.

Upconversion fluorescence

A cross-correlation between the fluorescence and the probe laser pulse.

3D Printing

3D printing (also known as additive manufacturing) is the construction of a three-dimensional object from a CAD model or a digital 3D model. It can be done in a variety of processes in which material is deposited, joined or solidified under computer control, with the material being added together, typically layer by layer.

4f orbitals

The seventh f orbitals of the 4th electron shell (energy level).



1 Introduction

1.1 Global Context

The energy transition towards renewable and fossil-free energy and the electrification of transportation systems will require a substantial amount of geological resources (minerals), technology, metals and materials. These are likely to include cobalt (Co), lithium (Li) and graphite for rechargeable batteries used in electronic devices and electric vehicles (EVs). Additionally, Rare Earth Elements* (REEs), neodymium (Nd) in particular, for permanent magnets are used, notably in wind turbines (Pell *et al.*, 2021) and electric vehicle motors. However, the supply chains that deliver these engineered materials, from mining to manufacturing and end use, are complex, involving several countries and actors (e.g., exploration, resource and mining companies, traders, refiners and smelters), alongside social, environmental and economic impacts on both a local and global scale (Kaikkonen *et al.*, 2022; Pell *et al.*, 2021).

Consumers and downstream manufacturing companies, like original equipment manufacturers (OEMs), electronics and automotive companies, are becoming increasingly interested in the sustainability and responsibility of the upstream raw materials value chain of their end-products (RCS Global, 2017). New regulations are also encouraging greater transparency in raw materials supply chains, notably for battery metals (European Commission, 2020), and this will likely dictate global developments regarding raw materials sourcing. The buyers of minerals and metals are under pressure to be able to prove the geographical provenance of their raw materials (e.g., from which mines/miners or countries are they extracted), their production methods (e.g., which technologies are used and are they sustainable) and traceability* (e.g., 'who' handled the materials during transit, 'when', 'where' and for 'how long'?). This trend is even more important for technology materials as any sustainability or responsibility issues in their supply chain would be in contradiction with the environmental objectives they are expected to adhere to.

1.2 Responsible Sourcing and Traceability

Concerns about responsible sourcing cover mainly three aspects: (i) human rights abuses, (ii) environmental degradation and (iii) issues related to criminal activities and corruption. In many countries where minerals and metals are mined, especially those where artisanal and small-scale mining (ASM) occur, there are reports of human rights abuses including forced labour, child labour, and unsafe working conditions (Mancini *et al.*, 2020). For example, cobalt produced by ASM in the Democratic Republic of the Congo (DRC) reportedly includes undignified working conditions, violence against women and child labour (Amnesty International, 2016).

Environmental degradation refers to the environmental impacts induced by mining activities such as deforestation, soil erosion, water pollution and loss of biodiversity. Lithium extraction from brines in the South American 'lithium triangle' (Chile, Bolivia and Argentina) uses large quantities of water, with consequences for local wildlife and human populations. Furthermore, lithium extraction from spodumene, which is extracted from hard-rock deposits (*i.e.*, pegmatites) in places such as Australia, utilises high-temperature (> 1000°C) energy-intensive processes (Pell *et al.*, 2021; Sanderson, 2021). Finally, the illegal trafficking, theft and trade in minerals and metals is a major global problem, especially for the so-called conflict minerals: namely tin, tantalum, tungsten, and some types of gold (3TG), to fund





armed conflict in the Great Lakes region in Africa. This activity does not only involve conflict minerals, but also precious minerals and metals (gold), platinum group minerals (PGMs) and base metals* (e.g., copper) (INTERPOL, 2021).

To mitigate the risks associated with the environmental impacts of illegal mining* it is necessary to ensure socially and environmentally responsible sourcing of technology raw materials, which could be assisted via improved traceability schemes along the supply chains. Traceability refers to the ability to track a material or product at different stages of the value chain from the source (mine) to the refiner, the market and up to the end-of-life (EoL), therefore allowing the origin of the source material to be proved at any of these stages. Traceability solutions rely on a *Chain of Custody** (CoC), which means the documentation of all organisations taking physical and/or administrative ownership or control of a product during production, processing, shipping, and retail (ISEAL, 2016).

It should be noted that, 'traceability' (who handled it, when and where) refers to the physical tracing and tracking as they move through the supply chain from the mine to the load port and disport ('cradle to grave'). Whereas provenance determination (also called 'predictive geolocation') is to determine the geographical location from where a mineral or metal sample* was derived or refined, to verify whether or not it originated from a conflict source or from a mine or processing plant aligned with criminal activities.

1.3 Illegal Mining, Illicit Minerals and Mining Crime

The illegal trafficking, theft and trade in minerals and metals is a major global problem. Illicit minerals* and metals may become 'legitimised' via money laundering schemes and enter the supply chain after they have been refined, usually at a different geographical location to their origin (Donnelly and Ruffell 2021, IUGS-IFG 2023). The beneficiaries are often well-organised syndicates, criminal gangs, cartels or terrorist organisation. This activity involves precious minerals and metals, platinum group minerals and conflict minerals (tin, tungsten, tantalum, and gold). Minerals and metals have inherent variability in terms of their physical, chemical (e.g. isotope ratios), morphological, textural, structural and mineralogical characteristics. This variability can be attributed to a number of factors including for example their geological origin, post mining mineral processing, beneficiation or the blending of different streams. It is these inherent properties that potentially enable minerals to become analysed to determine their provenance and traceability. It is anticipated the use of artificial taggant particles (ATP) could become incorporated into a high assurance strategy to determine mineral provenance and traceability. Publications and general guidance on illegal mining can be found in Zabyelina and van Uhm (2020); INTERPOL; UNODC; THEMIS; IGF; OECD; IUGS-IFG.

1.3.1 Provenance Determination

An objective of provenance determination (predictive geolocation) is to determine the geographical location from where a mineral or metal sample was derived or refined, to verify whether or not it originated from a conflict source or from a mine or processing plant aligned with criminal activities.

1.3.2 Traceability

Traceability refers to the physical tracing and tracking of precious minerals and metals as they move through the supply chain from the mine to the refiner and market. Traceability includes chain of custody, sample security, bagging, tagging and certificate of origin, due



diligence audits, registry of minerals producers and traders, the use of artificial taggant particles (ATPs), a geoforensic passport, elemental profiling and mineralogical profiling.

1.4 Current Traceability Systems for CRMs

The traditional traceability systems* in the mining industry and for CRMs supply chains are essentially paper-based or document-based following the usual, 'bag, seal and tag' methodology to trace the origin of a truckload, shipment or cargo. These documents can be falsified or faked, therefore making these traceability systems highly susceptible to fraud and adulteration*.

Solutions to bring traceability to the CRMs supply chains are currently being developed in several companies and research projects. These solutions essentially rely on digitalisation, big data and cloud technologies and are connected to the overall digital development in different industrial sectors and transportation.

Most of these digital traceability solutions are based on blockchain* to provide immutable records for traceability through decentralized databases. This is for instance the traceability solution adopted for cobalt artisanal mining in the DRC for the so-called 'model mines' and, 'hybrid artisanal-industrial mines'. These are developed upon the premise of digitally monitoring material flows and compliance with rigorous traceability mechanisms, envisioning future possible integration in blockchain-designed solutions (Calvão & Archer, 2021). Examples include the Mutushi project in Kolwezi launched in 2017 through a partnership between Trafigura and Chemaif (up to 5000 artisanal miners) or the project by Zhejiang-based Huayou Cobalt (through its local subsidiary Congo Dongfang Mining), also developed in 2017, in the Kasulo and Kamilombe mining concessions (up to 14,000 miners), (Calvão & Archer, 2021). The 'Better Cobalt Sourcing Program', and more recently renamed 'Better Mining', is operated by RCS Global Group and currently implemented in the DRC cobalt mines. It audits, verifies data, monitors mining sites and offers digital traceability services. More recently, RCS has led the creation of the 'Responsible Sourcing Blockchain Network' (RSBN), a membership-based collaborative endeavour involving organisations that includes IBM, Ford and Glencore. It seems however, that the latter does not exist anymore and has been replaced by commercial traceability services (Vine and Claritas). Despite the implementation of digital and blockchain-based solutions, there are a number of limitations to this approach when confronted with the practicalities of cobalt mining in the DRC (Calvão & Archer, 2021). Apart from technical constraints, blockchains share the same 'garbage in, garbage out' (GIGO) limitation as other extensive data systems. While the data stored in a blockchain is immutable, its usage does not guarantee its accuracy from the outset (Kaikkonen *et al.*, 2022; RCS Global, 2017). In jurisdictions where criminal activity and corruption are commonplace, blockchain solutions would not solve the problem of upstream traceability since the input information may not be reliable (Calvão & Archer, 2021). Similarly, the risk of adulteration (whereby material from different sources is added and mixed together with the certified material) challenges the feasibility of digital solutions for 'model mines'. Additionally, COVID-19 and a fluctuating cobalt price led Huayou, to suspend buying from artisanal sources (Calvão & Archer, 2021).

Consequently, there exist commercial prospects for technological solutions that can complement existing traceability systems by verifying the data within the system. Such complementary technology could be physical traceability systems, which rely on the materials properties and characteristics. These can be natural fingerprints, which are intrinsic properties (e.g., mineral, physical or geochemical properties) or artificial





fingerprints, whereby the material is voluntarily artificially altered (e.g., by the addition of particles or taggants with unique properties and/or laser inscription) to certify its origin and ensure traceability (Kaikkonen *et al.*, 2022). The former technology has already been developed for various minerals and materials, such as the marking of gemstones (Dalpé *et al.*, 2010; Pornwilard *et al.*, 2011), gold (Augé *et al.*, 2015; Pochon *et al.*, 2021), uranium/yellow cake (Keegan *et al.*, 2008, 2012; Wotherspoon *et al.*, 2014), coltan (H.-E. Gäbler *et al.*, 2011; Melcher *et al.*, 2008), base metals (H. E. Gäbler *et al.*, 2020; Martyna *et al.*, 2018; Melcher *et al.*, 2021) and other minerals (Kaikkonen *et al.*, 2022; Melcher *et al.*, 2021). These are mostly developed at the regional scale and focus on the upstream of the value chains (ores and concentrates). This approach is known as, 'analytical fingerprinting' (Schütte *et al.*, 2018), the 'analytical proof of origin' (Melcher *et al.*, 2021), 'geo-based traceability' (Dehaine *et al.*, 2020), a 'geoforensic passport' (Metalor, 2021) and microtaggant[®] identification particles (MIP) or 'microtaggants' (Microtrace Solutions, 2023). However, in essence the principle is always the same, *i.e.*, to confirm or determine the origin of a given material (ore, concentrate, or smelter/refinery material or product) by analysing its properties linked to the geological environment of the mine from where the material originated and to subsequent treatment and transformation. However, minerals and metals have inherent variability in terms of their physical, chemical (e.g., isotope ratios), morphological, textural and mineralogical characteristics (Dehaine *et al.*, 2020; Desautly *et al.*, 2022; Kaikkonen *et al.*, 2022; Pochon *et al.*, 2021). This variability can be attributed to a number of factors including for example, their geological origin, post mining mineral processing, beneficiation or the blending of different streams.

In some cases, these natural or intrinsic fingerprints may not suffice to detect any anomalies and certify the material origin and the use of artificial fingerprints may be required. Artificial fingerprinting, whereby the material is artificially altered (e.g., by addition of particles or tracers with unique properties to the material itself or its container, laser inscription and marking), has already been implemented in many industries including: fuels, chemicals, pharmaceutical, explosives, cotton, gems and diamonds.

The success of any new traceability solution, in terms of commercial applications, are dependent on the existing range of available solutions and future markets within the CRMs supply chain. Over time, the growing consumer focus on sustainability and the regulatory demand for sustainable and ethical business practices, like those seen from the EU, will fuel the requirement for traceability solutions (Kaikkonen *et al.*, 2022).

1.5 Report Objective

This report focuses on artificial fingerprinting technologies for tracking raw materials in complex supply chains. The objectives and principal research questions addressed in this report are as follows:

1. Where in the CRMs supply chains is artificial fingerprinting the most needed?
2. What are the specific needs of the industry and requirement for the potential artificial fingerprinting technologies?
3. What are the existing artificial fingerprinting technologies and are there any potentially applicable to CRMs supply chains traceability?
4. Is there a potential for 3D printing technology to be used to produced tailored artificial taggant particles* (ATPs) for CRMs supply chains?



D2.1 A Review of Artificial Fingerprinting and 3D Printing for the Potential Tracking of Minerals in Complex Supply Chains

Following an introduction to the MaDiTraCe project, a brief overview of the MaDiTraCe commodities value chain is presented followed by an analysis of the current industry needs in terms of raw material traceability with a special focus on artificial fingerprinting technologies. Additionally, a review of existing artificial fingerprinting technologies and their industrial application is presented. Finally, the potential for using 3D printing technologies to produce artificial tracers is discussed.





2 Overview of MaDiTraCe

MaDiTraCe (Material and digital traceability for the certification of critical raw materials*) is a 36-month European Union project funded through the Horizon Europe Programme (contract number 101091502, <https://cordis.europa.eu/project/id/101091502/fr>) coordinated by BRGM (French geological survey). This project was launched in January 2023 and aims to reinforce the transparency, traceability and sustainability of complex supply chains of critical raw materials (CRMs) including cobalt, lithium, natural graphite and rare earth elements. Bringing together 14 partners from 7 countries (Figure 1), the project will develop and integrate technological solutions for traceability and certification of critical raw materials, their processed forms and the derived end-products into a digital product passport. In parallel to the digital traceability, the use of intrinsic information, contained in the material itself will be developed providing information notably on the provenance of the raw material in derived substances and end products. Notably, the geochemical and mineralogical fingerprints of the investigated ores of critical raw materials, alongside artificial tracking. These solutions could enable key industry players to prove the reliability of their sustainability claims, comply with current regulation and anticipate future policies.

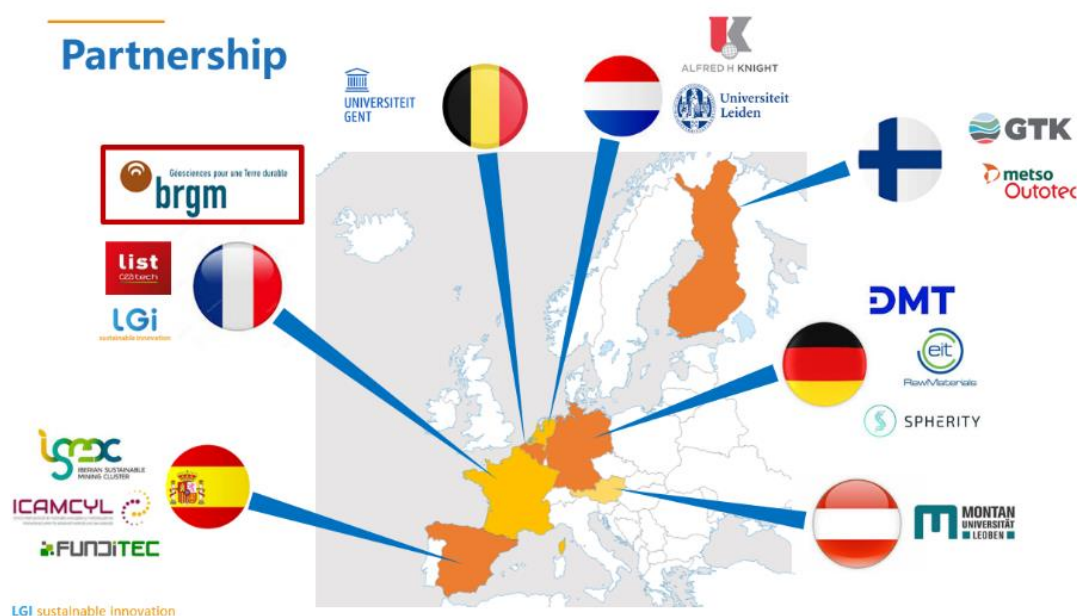


Figure 1: The MaDiTraCe consortium (source: MaDiTraCe, 2023).

2.1 Project Aim and Objectives

MaDiTraCe aims to enlarge and integrate the portfolio of technological solutions for traceability and certification of responsible and sustainable CRMs supply chains into a Digital Product Passport (DPP), compatible with the EU battery passport, through CRMs tracking and supply chains transparency for four key commodities (lithium, cobalt, graphite, REEs/Nd) that are relevant to different supply chains, primarily EV batteries and permanent magnets.

In the future, independent digital and analytical methods for tracing CRMs will be developed and integrated into a generic certification scheme, covering responsible and sustainable CRMs across the mineral supply chains from mining to manufacturing and



recycling. The project seeks to address the complexities of mineral supply chains, including points of aggregation, transformation and circular economy aspects, through coherent DPPs. This will be defined by identifying and solving current gaps in due diligence and assessing industry needs to comply with sustainability standards and regulations.

MaDiTraCe will provide a methodological digital framework and components to facilitate the integration of existing identification, assessment and tracing methods into a trusted blockchain-based platform. Such decentralised methodology addresses barriers of the current system, notably confidentiality, transparency, risk of fraud, costs and lack of standardisation. The information flow in the digital trail will be formalised in a way to be compatible with and support the implementation of DPPs as compliance and audit tool.

MaDiTraCe also aims to develop material fingerprinting (MFP) based on material geochemical properties, characteristics and artificial fingerprinting approaches, as an independent tool to support traceability and certification schemes. This intrinsic information constitutes a non-counterfeitable fingerprint and an independent traceability support from the information provided by the producers to the digital trail.

MaDiTraCe will look into integrating the certification according to sustainable standards for mineral resources in DPP. MaDiTraCe will support the harmonisation of sustainability reporting standards by building on the CERA 4in1 (www.cera4in1.org) certification system through the addition of DPP technology.

This methodology will enable downstream industrials to prove the reliability of their sustainability claims, complying with regulation in force notably, the EU Battery Regulation, EU Directive on Corporate Sustainability Due Diligence and German Supply Chain Act. MaDiTraCe's has a strong stakeholder process (WP1) with upstream and downstream partners from academics to industry, including mining to manufacturing, and large networks involved via the consortia (EIT-RM) and clusters (ISMC) participating in the project. Continuous interaction with this industrial and policy-oriented stakeholder community on the traceability technology (WP2 and WP3) and the certification schemes (WP4) developed in the project will ensure it stays in line with industrial needs and expectations with respect to regulatory compliance. It will also facilitate implementation and exploitation (WP5) of the project outcomes. The high-level objectives are (www.maditrace.eu):

1. Improve supply chain data transparency and traceability.
2. Set up technological solutions for tracking raw material flows (material passports).
3. Identify and address gaps in due diligence.
4. Develop comparable criteria, reporting and audit approaches.
5. Contribute to sustainable sourcing of raw materials.

2.2 Artificial Fingerprinting

Artificial fingerprinting forms part of MaDiTraCe's Work Package 2, which is dedicated to technological solutions for raw materials traceability. Task 2.3 on 'Artificial Fingerprinting' seeks to, 'develop a new artificial fingerprinting technology using 3D printed tracer particles (TPs) in selected supply chains, with specific focus on mineral concentrates'. Task 2.3 comprises the following stages:

1. A review of existing methods for potential use of 3D printed tracer particles technologies. Analysis (with MaDiTraCe industrial partner input) of mining, minerals



- and metals industry requirements to ensure solutions are fit-for-purpose and commercially relevant,
2. Design and manufacture of 3D printed tracer particles using appropriate materials (e.g., minerals, metals, bioplastic mineral/metal composites) based on specifications from the review,
 3. Test and validation of 3D printed tracer particles in a selected supply chain (assess impacts of transshipment, storage times and environmental conditions, financial evaluation, etc.) for artificial fingerprinting of raw materials in the selected supply chains, with a specific focus on mineral concentrates, using 3D printing notably.

This report is the first deliverable of Task 2.3, and will help evaluate existing artificial fingerprinting technologies and the potential for the use of artificial taggant particles (ATP) and 3D printing technologies.

As part of the research, an analysis of the requirements for the mining, minerals and metals industry will be undertaken to ensure any solutions provided are fit-for-purposes and commercially relevant with support from MaDiTraCe industrial partners.





3 MaDiTraCe Commodities and Value Chains

3.1 Supply Chain Segments

The supply chains of batteries for EVs and REE-magnets for wind turbines are complex and consist of multiple stages involving a range of commodities, including lithium, cobalt, natural graphite and REEs, which are the focus of the MaDiTraCe. In particular, the project focuses on the NiCo-based Li-ion battery value chain and sintered neodymium-iron-boron (NdFeB) magnets.

Globally these supply chains comprise the stages as illustrated in Figure 2. Mining extracts these metals from primary sources (ores), mineral processing produces mineral concentrates, metallurgy (hydrometallurgy or pyrometallurgy) produces intermediate products and refining forms sufficient purity chemicals. These chemicals are then used for advanced materials synthesis to form battery materials and components such as cathode, anode and electrolyte (for lithium, cobalt and graphite) or REE-magnets. The latter are then used to manufacture synchronous motor (for wind turbines) or tractions motors (for EVs) while battery components are used to manufacture cells which are then housed in modules within a battery pack and then integrated into the EV, stationary energy storage unit or consumer electronics.

Once used, a portion of the metals end-up in scrap from end-of-life products such as batteries, scrap metal and permanent magnets. This scrap, along with residues and side streams from other stages of the value chain (such as swarf for REEs, a residue from cutting magnets during magnet manufacturing), represent secondary resources that can be recycled and therefore re-enter the value chain at various stages depending on their nature.

To improve the traceability of RE magnets and lithium-ion battery raw material, it is critical to understand all the stages in these complex supply chains. An overview of these supply chains focusing on lithium, cobalt, graphite and REEs is shown in Figure 3.

3.1.1 LIB Supply Chains

3.1.1.1 Upstream graphite supply chains for anode production

Graphite, a naturally occurring allotrope of carbon, stands out as the sole non-metallic element that exhibits remarkable electrical and heat conductivity. In lithium-ion batteries (LIB), graphite is commonly utilized as the material for the negative electrode, while intercalated lithium compounds serve as the positive electrode's material. Battery-grade graphite can be produced from two primary sources; natural graphite or synthetic graphite. Among natural graphite, only flake graphite finds application in battery production. It is found in high-grade metamorphic rocks such as marbles, schists, and gneisses, where it forms through either fluid deposition or graphitization (Mitchell & Deady, 2021; Pell *et al.*, 2021). Besides flake graphite, other forms of natural graphite include amorphous (microcrystalline) graphite and vein (lump) graphite. On the other hand, synthetic graphite is produced through a complex manufacturing process, using petroleum coke or other carbon-rich materials. Graphite processing consist mainly of mechanical processes (sorting and sizing) as well as froth flotation to obtain concentrates with the desired particle size distribution and remove impurities. This is followed by purification and refining to meet the stringent quality requirements for lithium-ion battery applications.



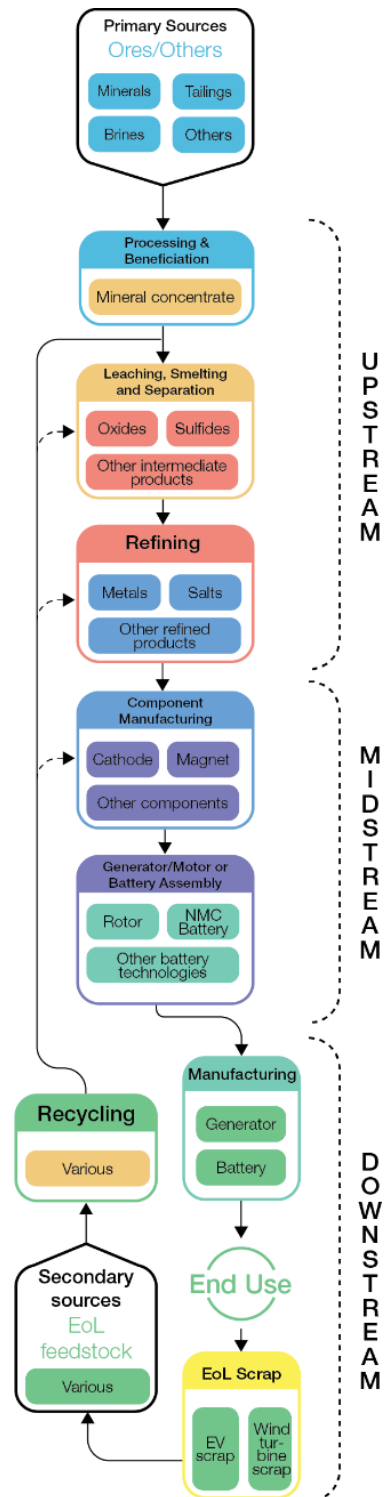


Figure 2: Simplified representation of the different stages of the REE-magnet and battery supply chains.

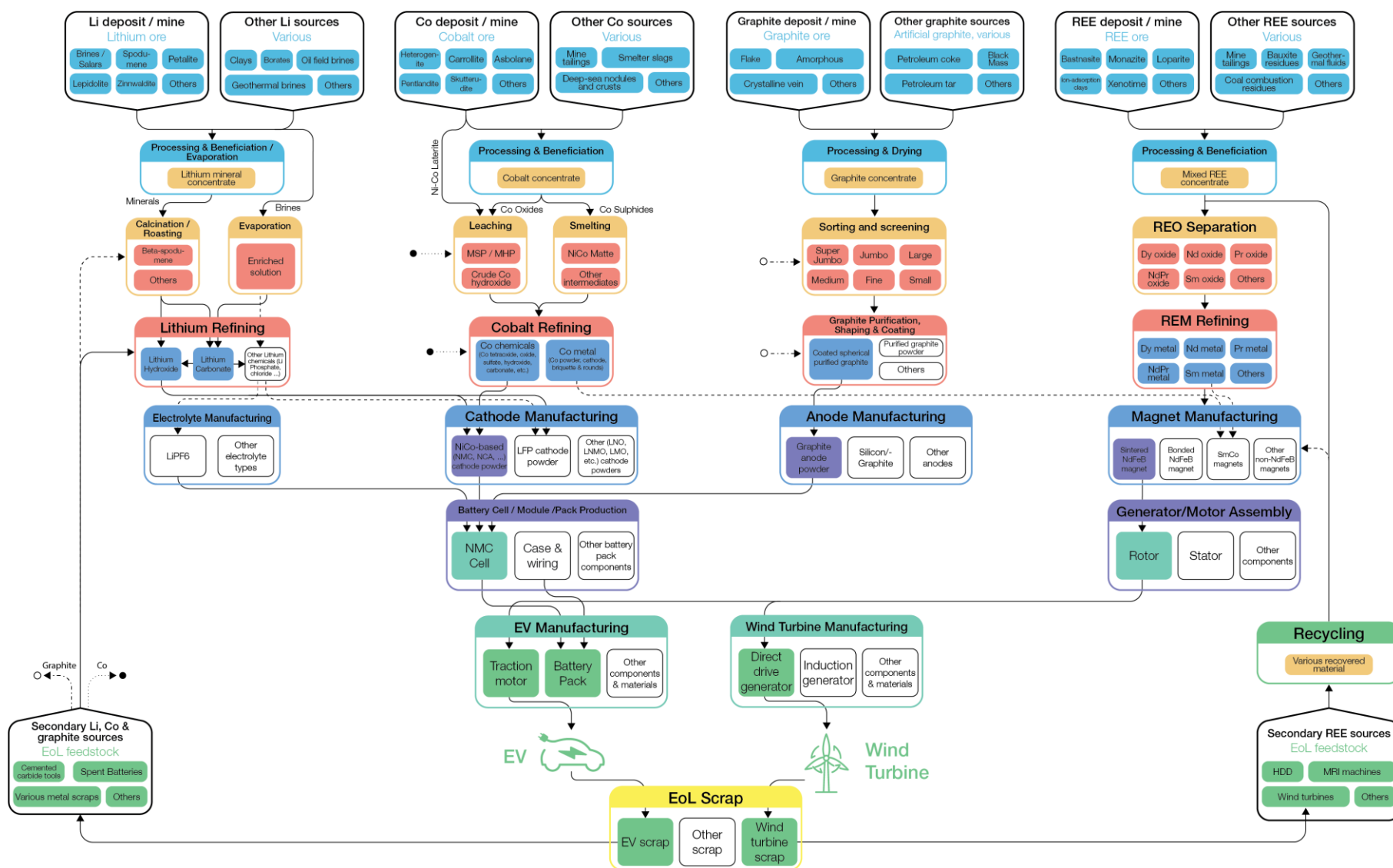


Figure 3: Supply chain stages for lithium, cobalt and graphite batteries and REE-magnets used in electric vehicles and wind turbines. Abbreviations are given in the text.



To be deemed suitable for battery applications, graphite must possess high purity levels, with carbon content exceeding 99.95 wt%. Additionally, graphite needs to have spheroidal particles ranging in size from 10 to 25 μm to ensure efficient operation. Spherical graphite is produced by micronizing*, shaping, and rounding flake graphite (Jara *et al.*, 2019). This transformation increases the surface area and allows for better contact with lithium ions during battery charging and discharging cycles.

3.1.1.2 Upstream lithium supply chains, cathode and electrolyte

Lithium is primarily obtained from two main sources. Hard-rock deposits hosting lithium-bearing minerals and lithium-rich brines. Lithium-rich brines are solutions of salts of lithium, sodium, potassium and other salts, with most economic brine resources found in salars within high- elevation basins but also geothermal and oil field brines. Hard-rock lithium deposits consist mainly of lithium pegmatite and to a lesser extent rare-metal granites or sedimentary deposits, clays or borates (Pell *et al.*, 2021). Brines are pumped to the surface and concentrated through solar evaporation to obtain an enriched solution. On the other hand, lithium-bearing minerals, such as spodumene and lepidolite, are mined from hard-rock deposits and concentrated through crushing, grinding and froth flotation with some processes involving sorting, magnetic separation, and gravity concentration (Meng *et al.*, 2021). The mineral concentrates undergo a thermal treatment through calcination or roasting before leaching to extract lithium into solution. Once lithium is in solution, the refining stage consists of the purification of the solution mainly via precipitation to remove major impurities such as calcium, magnesium, aluminum, and iron, followed by lithium concentration using ion exchange or evaporation. Crystallization, carbonation, or electrodialysis is finally conducted to produce lithium compounds, mainly lithium carbonate (Li_2CO_3) and lithium hydroxide (LiOH), of chemical or battery grade, or lithium chloride which are further refined to lithium metal from these precursors or related compounds (lithium fluoride, LiF) used in the electrolyte solutions (Tran & Luong, 2015).

3.1.1.3 Upstream cobalt supply chains for cathode production

Cobalt production mainly occurs as a by-product of copper from sediment-hosted copper deposits or nickel from magmatic nickel sulphide or nickel laterite deposits (Dehaine, Tijsseling, *et al.*, 2021). The processing route and intermediate cobalt products vary greatly depending on the deposit type and ore type (oxide or sulphide), ore mineralogy and the presence of other by-products (copper, zinc and PGMs). Sediment-hosted copper-cobalt deposits comprise a weathered (oxide) ore blanket overlying a primary sulphide ore at depth through a transition zone. Oxide ores are leached, most of the time without preconcentration, whereas sulfidic ore is concentrated through froth flotation, after which the concentrate is roasted before leaching. Mixed ores are more problematic and often require pre-concentration through froth flotation before leaching (Dehaine, Filippov, *et al.*, 2021; Tijsseling *et al.*, 2019). Cobalt is then often precipitated as a cobalt hydroxide intermediate product after having gone through several purification process steps. Cobalt from magmatic nickel sulphide deposits is recovered along with nickel through froth flotation as both metals are mostly hosted by the same mineral (pentlandite). The concentrate is then commonly smelted to produce a nickel-cobalt matte, which is then refined through hydrometallurgical processes to produce cobalt powder or cobalt metal. For nickel laterites, cobalt is produced through hydrometallurgical processes, mostly high-pressure acid leaching of limonite ore to produce a mixed nickel-cobalt sulphide product (MSP) or hydroxide product. Depending on the specific process design, intermediate or





final cobalt products are cobalt sulfide, cobalt hydroxide, cobalt carbonate cobalt powder or cobalt metal (Dehaine, Tijsseling, *et al.*, 2021).

3.1.1.4 Midstream LIB supply chains and recycling

Lithium salts along with cobalt and other metal (nickel, manganese) salts or metal oxides are then mixed to make precursor for the cathode active materials (CAM). Layered oxides with mixed transition metal composition are typically prepared over a co-precipitation route. After filtering and washing to remove impurities, the material is dried and sieved before it is mixed with a stoichiometric amount of a lithium salt. The as-prepared cathode powder is then deagglomerated and may optionally be surface treated to stabilize the electrode/electrolyte interface and performance (Schmuck *et al.*, 2018).

Anodes are produced by combining spherical graphite with a binder and conductive additives. These components are then coated onto a current collector and assembled with the cathode, separator, and electrolyte to form a complete Li-ion battery cell.

Current electrolytes are almost exclusively based on lithium hexafluorophosphate (LiPF_6) as conducting salt that is dissolved in organic carbonate solvents. LiPF_6 is produced by reacting lithium fluoride with phosphorous pentachloride in anhydrous hydrogen fluoride (AHF). It is then further purified with additional AHF to reach various purity classes from 99.00% for industrial grade to 99.99% for EV plus grade (Schmuck *et al.*, 2018).

Finally, the cathodes and anodes, as well as other components like electrolytes, copper foil and separators, are moulded to form individual cells. These cells are then packed into modules to build a lithium-ion battery.

The recycling of graphite from end-of-life batteries is complex and not currently well developed. The recycling process typically involves several stages, including dismantling and disassembling the end-of-life products, followed by mechanical or thermo-mechanical processes to produce a fine powder known as black mass (Donnelly 2022, Donnelly *et al.*, 2021a, b, c; 2022, 2023; Vanderbruggen *et al.*, 2021; Dade *et al.*, 2022, Schwich *et al.*, 2021). The latter can be fed to pyrometallurgical or hydrometallurgical processes (or a combination of both). The reclaimed metals and graphite can then be reintroduced into the manufacturing cycle to produce new battery products or serve as a valuable source for various industrial applications.

3.1.2 REE Supply Chains for NdFeB Magnets

Most REE are currently produced from the mining of primary ores as co-products since they are always found in the same deposits with some deposits containing primarily LREEs and others containing more HREEs (mainly dysprosium). The most important deposit type for LREEs and neodymium are carbonatite-related in which REE are hosted in bastnäsite and monazite, xenotime as well as iron oxide minerals (Chen, 2011; Pell *et al.*, 2021). The separation processes for such ores employs various stages including magnetic and gravity concentration but rely primarily on flotation (Jordens *et al.*, 2013). Processed material production includes REE separation to separate individual rare earths from concentrates, generally in oxide form through a chemical intensive process involving solvent extraction to separate and purify the individual REEs to oxides and metal refining through electrowinning and sodium reduction to convert rare earth oxides to metals (Gupta & Krishnamurthy, 2004).

Magnets are produced from alloys or powders that combine rare earth metals such as neodymium and praseodymium with iron and boron. Sintered NdFeB magnets are



manufactured through a powder metallurgy route involving induction melting of the metals, strip casting sometimes followed by hydrogen decrepitation to reduce the grain size further. The powder is then aligned and pressed under a magnetic field and finally sintered at 1000-1100°C (Smith *et al.*, 2022). Once formed, the sintered magnets are machined to the desired shape and coated with a thin metal film of nickel (5-10 microns) as a protection against corrosion. Next, the magnet is magnetized in a high magnetic field to align the magnetization of the grains in the magnet (Smith *et al.*, 2022). Sintered NdFeB magnets have many uses across a broad spectrum of applications most notably for consumers electronics (e.g., hard disk drives, cell phones and loudspeakers), within the synchronous generator of wind turbines and the direct drive motors of EVs (Smith *et al.*, 2022).

Currently, most rare earth recycling is based on swarf, the leftover material generated when cutting magnets during their production. Although end-of-life magnet recycling to create new magnets or extract individual rare earth elements is limited in scale, there is hope for future expansion due to the development of various promising methods. In general, the recycling process for magnet-containing end-of-life (EoL) products occur in two loops; magnet recovery (short-loop) and REE recovery (long-loop) through various hydrometallurgical, pyrometallurgical or electrochemical routes (Smith *et al.*, 2022 and Mishra *et al.*, 2023).

3.1.3 Geographical Distribution of the Li, Co, Graphite and REEs Supply Chains

The different stages of the value chains for lithium, cobalt, graphite and REE are distributed around the world, however the balance between the production volumes of the different countries involved in these different stages from mining to technology production is increasingly leaning towards China which dominates the downstream value chains.

3.1.3.1 Raw and processed materials

The majority of global REE mine production, is coming from China (BayanObo mine, Inner Mongolia), and to a lesser extent the United States (Mountain Pass mine, California), Myanmar (illegal mining in Kachin state), and Australia (Mount Weld mine) (Smith *et al.*, 2022). The current identified reserves are in China, Vietnam, Brasil and Russia (USGS, 2023).

Graphite is mined predominantly in China (65% in 2022), but global production is becoming more diversified, with many greenfield graphite mining projects being developed including in Tanzania, Mozambique, Canada and Madagascar (IEA, 2022; USGS, 2023). But this dominance is even more pronounced for the refining stage with nearly all spherical graphite supply ensured by China in 2022 (Benchmark, 2022).

Most of the current cobalt mine production originates from the sediment-hosted copper-cobalt deposits in DRC (Dehaine, Tijsseling, *et al.*, 2021), which accounted for 76% of the global cobalt mine supply in 2022. However, a significant proportion of cobalt mines in DRC are operated or owned by Chinese companies or consortia (e.g., CMOC Group/Tenke-Fungurume, China Nonferrous Metal Mining/Deziwa) resulting in about 44% of the global mine supply in 2022 being Chinese owned or controlled (Darton Commodities, 2023). The Swiss-based company Glencore is the largest cobalt miner with its two large mines in DRC (Mutanda and Katanga), as well as its Canadian operations in Sudbury (Ontario) and Murrin-Murrin laterite mine in Australia. Indonesia became the second largest producer due to the development of various nickel laterite projects. China controls the cobalt refining with 91% of the world's cobalt chemical supplies refined in China in 2022 and 76% of global cobalt





refined production (chemicals and metal). Less than 7% of global cobalt mine supply is refined within the country of extraction (Darton Commodities, 2023). Around 20% of the global cobalt refined production is produced in Europe, mostly Finland.

Around 47% of the lithium produced in 2022 was extracted from hard-rock (spodumene pegmatite) deposits in Australia, such as the Greenbushes pegmatite (Western Australia), while the rest of the production was dominated by salars/brines from South America (Argentina, Chile) with Chile being the largest producer accounting for about 30% of the 2022 lithium production (USGS, 2023). Examples include Salar de Atacama (Chile), Salar del Hombre Muerto (Argentina) and Salar de Uyuni (Bolivia), which represent the vast majority of the currently identified lithium reserves (Munk *et al.*, 2016). Major lithium suppliers include a mixture of large chemical and mining companies including: Sociedad Química y Minera de Chile SA and Abermarle (Chile), Pilbara Minerals (Australia), Allkem (Australia), Livent Corporation (United States) and Ganfeng Lithium Co. (China), accounting for more than half the world lithium production (IEA, 2022). Often lithium is refined by the mining company together with the extraction except for Australian spodumene miners which mostly export concentrates to China, resulting in lithium refining being also highly concentrated in China (Benchmark, 2022). In Europe there are some lithium exploration projects such as Vulcan, Eramet and Lithium de France for geothermal brines in Germany and France and hard rock exploration in Spain, Portugal, England, France (Imerys) and Finland (Keliber).

3.1.3.2 Battery component, battery cell and EV manufacturing

Battery cell component production is also highly concentrated with two-thirds of global battery cell production, as well as around 80% of the production of cathode and over 90% of anode material, happening in China and controlled by a few companies (IEA, 2022, 2023):

- Seven companies are responsible for about 55% of global cathode material production capacity. Key players include: Sumitomo (Japan), Tianjin B&M Science and Technology (China), Shenzhen Dynanonic (China), and Ningbo Shanshan (China).
- Four companies are responsible for half of global production capacity of battery components including: Ningbo Shanshan (China), BTR New Energy Materials (China) and Shanghai Putailai New Energy Technology (China). The top-six companies are all Chinese and account for two-thirds of global production capacity.
- One company alone, Jiangxi Tinci Central Advanced Materials (China), produces 35% of global electrolyte salt. The top electrolyte producers include: Zhangjiagang Guotai-Huarong New Chemical Materials (China), Shenzhen Capchem Technology (China), and Ningbo Shanshan (China).

Battery cell production is also highly concentrated, with the top-three producers in 2021, CATL (China), LG Energy Solution (Korea), and Panasonic (Japan), accounting for 65% of global production (IEA, 2022).

China also accounts for about 54% of EV production capacity, followed by Europe, which is responsible for over one-quarter of global EV assembly, and the United States with around 10% of EV production capacity (IEA, 2023).



D2.1 Artificial fingerprinting for tracking raw material flows in complex supply chains

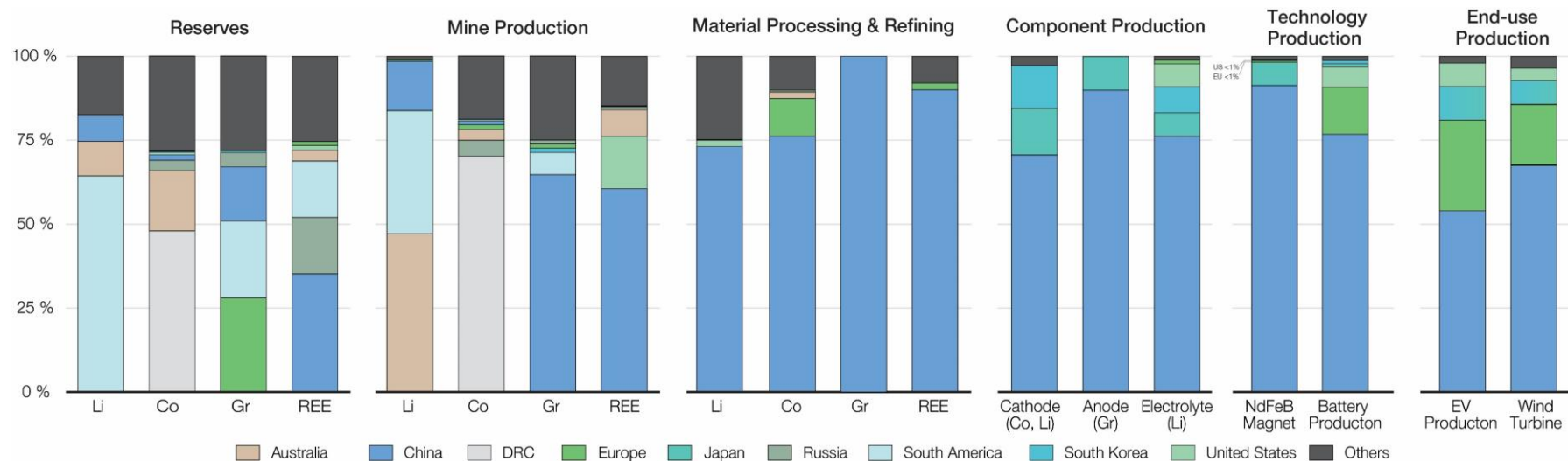


Figure 4: Geographical distribution of the global MaDiTraCe technology materials (Li, Co, Graphite, REEs) supply chains (source: GTK).

Reserves and mine production based on USGS (2023). Cobalt refining based on Darton Commodities (2023). Graphite refining based on spherical graphite supply (Benchmark, 2022). REE refining and NdFeB magnet alloy manufacturing are estimates based on current understanding of where concentrate from specific producers is separated and expert consultations, data from U.S. Department of Energy (Smith *et al.*, 2022). Cathode, anode and electrolyte production on 2022 capacity data (Bloomberg, 2022). Battery cell production is based on battery cell production capacity data (Elements, 2023, based on data from BNEF). End-use production based on 2021 capacity data, Wind turbine corresponds to the average of nacelle (Part which host the generator containing the NdFeB magnet) production capacity for on- and offshore (Elements, 2023b). Europe includes EU-member states plus Norway, Turkey, UK and Ukraine; South America includes Argentina, Bolivia, Brazil and Chile.





3.1.3.3 NdFeB magnets and wind turbine manufacturing

The major producers of NdFeB magnets, alloys, and powders are China (92%), Japan (7%), Vietnam (1%) and Germany (<1%), (Smith *et al.*, 2022). Manufacturing of wind turbines is also heavily concentrated geographically with Chinese companies accounting for more than 55% of the total capacity deployed in 2021, followed by European companies, with around 35%, and American ones, with less than 10% (IEA, 2023). The top 15 manufacturers accounted for almost 90% of the total capacity deployed in 2021.

3.2 Requirements of Miners, Traders and Refiners

Artificial taggant particles (ATP) could potentially comprise different material types, including for example: minerals, metals, bioplastic composites containing minerals and/or metals or organic component. It was considered necessary to engage with potential stakeholders to provide an appropriate specification of the types and chemistry of artificial taggant materials.

3.2.1 The MaDiTraCe Questionnaire, mapping of permitted taggant materials in metal industry

As part of this preliminary review a questionnaire was designed and it is recommended to be submitted to key stakeholders and industry participants throughout the duration of the MaDiTraCe project (Appendix I). The questionnaire aims to gather stakeholder input to guide the specifications of appropriate materials for the development of prototype artificial taggant particles and subsequent large-scale production of artificial taggant particles.

3.2.1.1 Element penalty (impurity) limits in the mining and metals industry

The ATP composition must meet the requirements of the miners, shippers, refiners and other receivers. These requirements can be owing to several factors such as health and safety regulations, dimensional tolerances, chemical reactivity, or quality and performance standards. For instance, Europe's largest copper producer, Aurubis, has produced a list of maximum impurity levels allowed for copper and nickel concentrates, as given in Table 1.

Table 1: Maximum impurity levels and approximate penalties for copper and nickel concentrates (source: Salomon-de-Friedberg & Robinson, 2015).

| Element | Penalty Limit (%) | Penalty, \$/t per extra 0.1 % |
|-------------------|-------------------|-------------------------------|
| Arsenic | 0.2 | 2 |
| Higher arsenic | >0.1 | >5 |
| Antimony | 0.05 | 15 |
| Bismuth | 0.02 | 25 |
| Cadmium | 0.03 | 30 |
| Fluorine | 0.03 | 15 |
| Lead | 1 | 0.3 |
| Mercury | 0.005 | 3000 |
| Nickel and cobalt | 0.5 | 1 |
| Selenium | 0.03 | 15 |
| Zinc | 3 | 0.3 |

Each smelter has differing limitations and this is reflected by the penalties imposed on incoming impurities. In some cases, such as arsenic, the penalty per incremental unit





escalates with increasing concentration. Certain smelters may even reject potential feeds outright because of a particular element existing in higher concentration. It is to be understood that, if an impurity is penalised, any corresponding metal value is not paid for presenting a 'double' opportunity to the concentrate provider. For example, the penalty for excessive nickel may not appear to be high, but the lost nickel value itself can be appreciable. If the metal is lost to the smelter's final discard slag, this also represents a waste of the original resource.

Similarly, the ATP material specification must adhere to such standards. Therefore, this questionnaire is aiming at receiving at least the boundary conditions for material selection from several mineral and metal industries (Table 2).

The ATP could be added to the concentrate blends at the producing mine or concentrator. In addition to the elemental composition limitations it must be:

- Non-magnetic.
- Nonradioactive.
- Non-visible with the naked eyes.
- Cause no colour change.
- Sizes must be preferable comparable to the sizing of the product shipped.
- Align with health and safety regulations.
- Minimal and insignificant quantity.
- Some industries specifically require the taggant to evaporate via melting processes.

Table 2: Anonymised preliminary response to the MaDiTraCe questionnaire, received from a mining company, indicating the elemental limits for potential artificial taggant particles.

| Not permitted | Permitted within limits | No restrictions |
|--------------------|-------------------------|--|
| Bismuth | Antimony (<300 ppm) | Iron |
| Cadmium | Arsenic (<500 ppm) | Nickel |
| Chlorine | Lead (<500 ppm) | Phosphorus |
| Carbon | Mercury (<50 ppm) | Silicon |
| Oil-based plastics | Tellurium | Selenium |
| - | - | Sulphur |
| - | - | Tin |
| - | - | REE (Ce, Dy, Er, Eu, Gd, Ho, La, Lu, Nd, Pr, Pm, Sm, Sc, Tb, Tm, Yb and Y) |
| - | - | Non-oil-based plastics |
| - | - | Biomaterials |
| - | - | Ceramics |

Table 3: Anonymised preliminary response to the MaDiTraCe questionnaire, received from a precious metals refining company, indicating the elemental limits for potential artificial taggant particles.

| Not permitted | Permitted within limits | No restrictions |
|---------------|-------------------------|-----------------|
| Arsenic | Antimony | - |
| Cadmium | Bismuth (0.1%) | - |
| Chlorine | Iron | - |
| Mercury | Lead | - |





| | | |
|---|--------------------|---|
| - | Nickel | - |
| - | Selenium (0.5%) | - |
| - | Sulphur (2% on Ag) | - |
| - | Tellurium (0.5%) | - |
| - | Tin (0.5%) | - |

3.2.2 Managing Perception and the Potential for Blight

The use of ATPs must not compromise the integrity* or reputation of a product, a producer, or give any reason to cause blight. The additional tracer material added must be as low in quantity as possible. For instance, concentrates with high levels of impurities being sold to smelters leads to the miner facing penalties that marginally reduces their revenues and choice of smelters. Furthermore, since the ATP is a secondary material, addition of high volume will inhibit movement and transaction of the original amount of material, thereby leading to increased cost for lower volume.

The sizing of taggants must be such that comminution procedures do not render their physical or chemical properties purposeless.

Managing the perception of the ATP and reducing the potential for blight is therefore fundamentally important. However, this could be complex to achieve, especially if ATPs are used covertly to track commodities, but discovered by a receiver.

ATP perception is likely to depend on the industry insight, which can be gained through effective communications, transparency and standards detailing permitted and restricted elements.

The global supply chain often recalls products whose authenticity is called into question because consumer problems are seen or perceived. The additional cost of ATP inclusion must be associated with a benefit of the products/materials being genuine. As such, managing the perception of ATPs and mitigating the risks for blight should become an important aspect of the MaDiTraCe research phase as new ATPs are developed.



4 Artificial Fingerprinting and Tracing

Artificial taggants are chemical or physical markers used to demarcate objects for the purpose of identification. Taggants may be applied or affixed to an object overtly to deter, or covertly to detect for example, adulteration or substitution*. Taggants can also be 'encoded' and their presence, or absence, can be used for the purpose of authentication. They have been used for authenticating products from counterfeits in the pharmaceutical, currency, clothing, and electrical industries, but have rarely been used in the mining, minerals and metals industries.

4.1 Historical Development

In 1970, the need for explosives regulations outside of a declared state of war was realised under the Organised Crime Control Act - 1970 (Figure 5). This was act of congress aimed at, *'facilitating the eradication of organised crime in the USA, by strengthening the evidence-gathering process, by adopting new penal prohibitions, and by creating increased sanctions and numerous remedies to deal with unlawful activities'* (USA Government, 1970). It became a requirement for explosives to be marked with manufacturer name, explosive type and a date or batch code (Seman *et al.*, 2019). These markings were to be in the immediate wrapping around the explosive to serve as an identification taggant to track and identify the sale of undetonated explosives. However, the identification of explosives post-detonation posed a particular challenge, which required a forensic recovery of the residues.

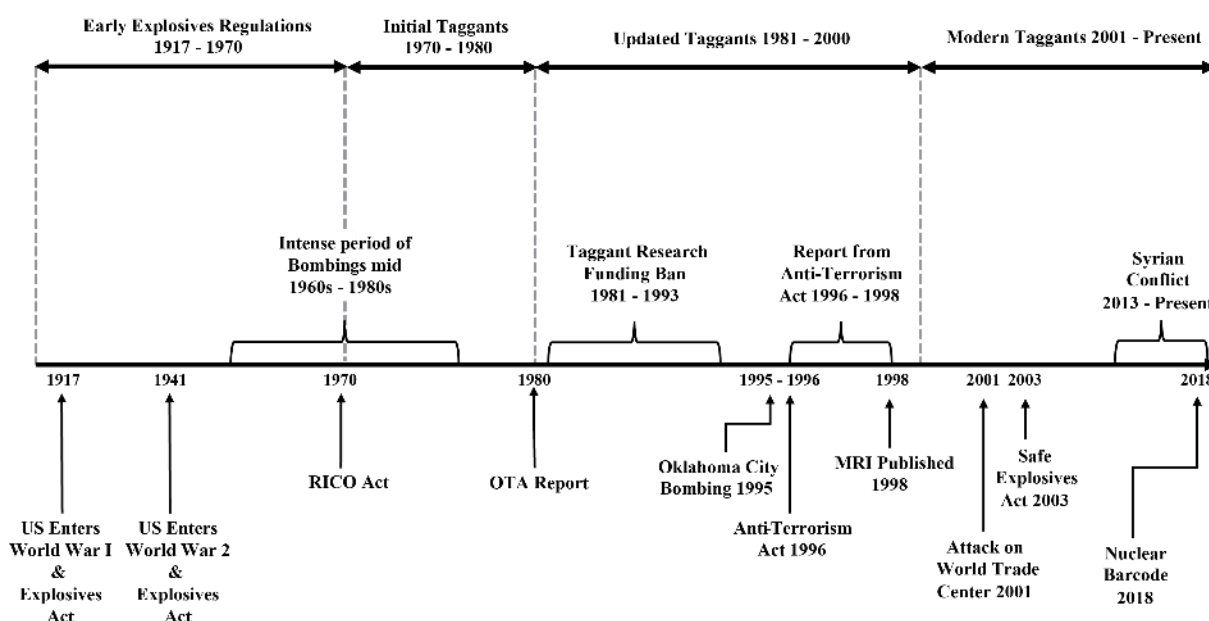


Figure 5: Identification taggants history timeline in the US (source: Seman *et al.*, 2019).

Five significant factors were considered as particularly relevant, as follows:

1. The taggants could be recovered as residue in post-blast debris.
2. The survivability of taggants could ensure information encoding after the explosion.
3. The amount of information stored within the taggant was relevant.
4. Taggant-explosive compatibility (e.g., chemical reactivity).
5. Cost.



D2.1. Artificial fingerprinting for tracking raw material flows in complex supply chains.

The first taggants developed were radiological. Active isotopes were added to explosives and these allowed rapid recovery. However, the potential health hazard in exposing people to radiation brought about additional regulations (Seman *et al.*, 2019). As a result, research subsequently focused on chemical taggants, including the use of different ethanol concentrations of rare earth salts and physical taggants.

In the 1980s a physical taggant was eventually developed by the 3M Corporation, which comprised layers of coloured plastics stacked together, and considered as a viable candidate. The technology was subsequently acquired by Microtrace Solutions LLC, and taggants were used for brand protection and anti-counterfeiting purposes. The term 'taggant' was subsequently developed from the trademarked name 'Microtaggant® Identification Particles' (MIP) for a variety of applications (Microtrace Solutions 2023).

Generally, there are now two main types of taggants included in explosives. Firstly, to help detect the potential presence of a bomb, bullets or construction explosive used for example during the screening of luggage at an airport. Secondly, to assist law enforcement investigate the detonation of a bomb.

4.2 Artificial Taggant Types, Properties and Uses

The main characteristics and properties of artificial taggants are as follows:

- Contain unique encoded chemical and/or materials or chemistries.
- Distinct physical and chemical properties to meet its specific requirements.
- Behave as virtual fingerprints.
- Used covertly, for example by law enforcement to track commodities.
- Used overtly, to deter potential theft, adulteration or substitution.
- Detected with basic, low-cost or low complex equipment, which facilitates the real-time, in-situ verification of a taggant's presence or absence.
- The taggants should be complex and difficult to replicate or duplicate.
- Taggants act as permanent markers. Although, in the mining, minerals and metals industry they might be destroyed during mineral processing, refining and smelting.
- Negligible or low manufacturing costs.
- High encoding capacity.
- Non-destructive modes of detection.
- Chemically inert (unreactive)
- Non-toxic.
- Non-radioactive.

Artificial taggants are now commonly used for a variety of purposes, which include the following (





Table 4):

- The tracking of a variety of commodities, including technology items (e.g., phones and laptop computers) and consumer products (e.g., food).
- Permanent markers used in staining currency for tracking theft during Cash and valuables in transit (CViT).
- Firearm and cartridge casing coatings to establish their handling.
- Custom holograms in medical and currency industries.
- Thermochromic* inks in consumer packaging, product labels and safety warnings.
- Tamper evident construction labels and tapes.
- Invisible barcodes.
- Watermarks for digital assets.
- Laser marking for information writing directly onto internal layer of seals or labels.
- Electronic tracking using frequency identification (RIF).
- Money and banknote authentication.
- Tax stamp authentication.
- Banknote authentication.
- Anticounterfeiting (e.g., alcohol, cigarettes, and pharmaceuticals).
- Construction, engineering and building materials.

4.2.1 Artificial Taggant Restrictions

Manufacturers of taggants might consider their products to be versatile and adoptable for various applications. However, their commercial usage is generally restricted to the following (Gooch, Daniel, *et al.*, 2016):

- **Property marking:** Taggants specific to valuable items such as vehicles and electronics. The functional materials* involved are usually invisible without optical devices. Selectamark® has been extensively working in this sector by incorporating chemical etching and Deoxyribonucleic acid (DNA) taggant solution.
- **Anti-counterfeiting:** Predominantly used in industries such as pharmaceutical, currency and clothing and conventionally using barcodes and hologram technology.
- **Tracking:** This requirement is of prominence within the hazardous chemicals, illegal drugs and explosives industry.
- **Monitoring:** These taggants are applied onto exterior surfaces of private or commercial commodities, or items of value (e.g., watches and vehicles). Easily transferrable inks or dyes onto the surface of items can be used to provide evidence of possession in the event of a crime such as theft.



D2.1. Artificial fingerprinting for tracking raw material flows in complex supply chains.

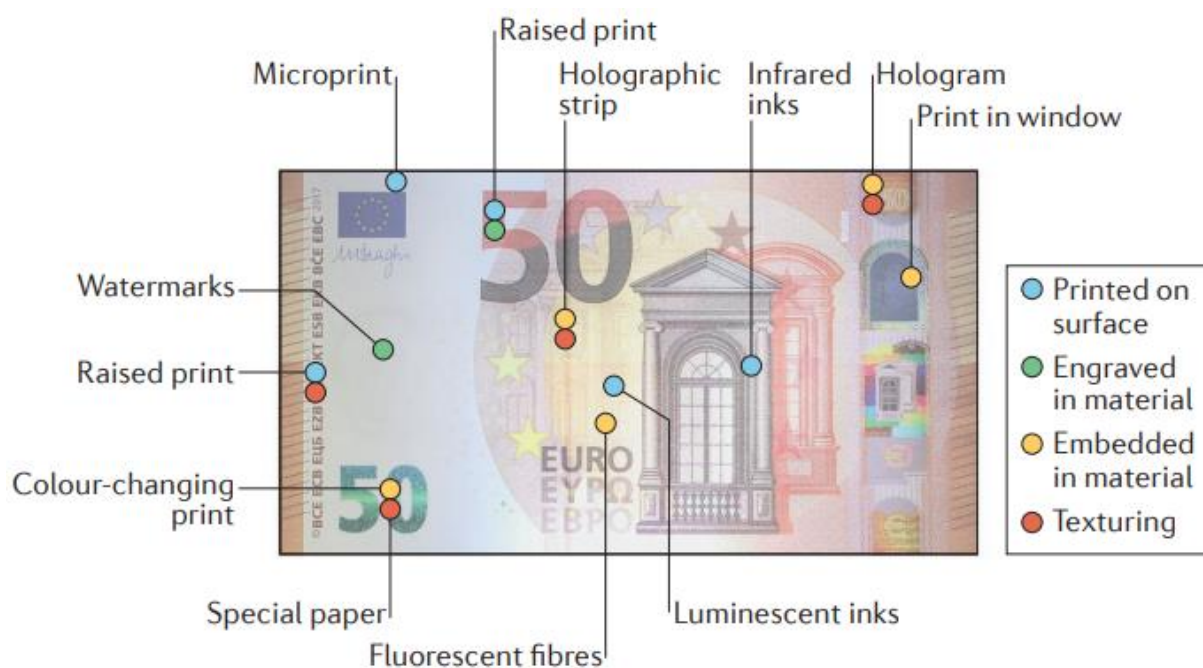


Figure 6: Example of anticounterfeiting taggants on currency notes (source: Arppe & Sørensen, 2017).



Table 4: Classification of anti-counterfeiting taggants based on characteristics and function (source: Arppe & Sørensen, 2017).

| Approach | Taggant | Detection | Method of encryption |
|--|--|---|---|
| Substrate structures (cloneable) | | | |
| Hologram (in material) | Hologram | Visual | Restricted access to printing technology |
| Watermark (in material) | Watermark | Visual | Materials, high precision and complexity of printing technology |
| Graphic tag: engraved (in material) | Microdot with text or coloured stripes | Visual or low-magnification tags | Microscopic, physical characteristics and availability |
| | Fluorophore-dyed particles or fibres with photobleached QR- or barcode | Fluorescence* imaging and confocal microscopy | Microscopic, physical characteristics and composition |
| | Laser written, photoactive tags | | |
| Graphical tag: microfabricated (in a material) | Striped nano or microwires by alternating materials | Imaging and fluorescence imaging | Microscopic, physical characteristics and composition |
| | Photonic crystals | Visual | Colour, responsive to magnetic field |
| Surface tags (cloneable) | | | |
| Printed tags: (on surface) | Colorimetric inks | Visual | Colour, thermal change |
| | Fluorescent inks | Fluorescence imaging and mass spectrometry | Colour, composition, excitation wavelength and ink availability |
| | Lanthanide inks | | |
| | Upconverting nanophosphor inks | | |
| | Qdots or Cdote inks | | |
| Structured surface (on surface) | Plasmonic surface or Raman probe | Raman imaging | Composition and graphical |
| Embedded tags (cloneable) | | | |
| Molecular tags (in material or on surface) | Nucleic acid tag | Sequencing and fluorescence imaging | Sequence, colour and length |
| | Peptide tag | Mass spectrometry | Sequence and length |
| | Polymer tag | Mass spectrometry | Sequence and length |
| | Lanthanide tag | Elemental analysis | Composition |
| | Thermal tag and phase change nanoparticles | Calorimetry | Composition |
| Random patterns (physical unclonable functions) | | | |
| Random 2D pattern (in material or on surface) | Intrinsic surface topology of the product | Surface Scattering | Random surface topology |
| | Spherical cholesteric liquid crystals | Reflection | Random optical pattern |
| | Randomly distributed nanostructures | Fluorescence imaging, Raman imaging and current | Random pattern, area, number of pixels and position |
| Random 3D pattern (in material or on surface) | Scattering speckle token | Scattering | Random pattern, laser wavelength, and angle and relative position |
| | Fingerprint textures | Imaging, Raman scattering* and fingerprint minutiae | Random pattern, position, type and direction |



4.2.2 Forensic Taggants

Forensic taggant technologies are used to prevent criminal offences by associating a commodity with a unique piece of information. Nanotechnology has greatly helped in forensic investigations in the fields of toxicology biology, questioned documents and fingerprint detection. However, one challenge with nanomaterials is achieving a consistent production with the desired surface characteristics on a large scale. Most of the existing nanomaterials either encrypt information or use naturally occurring randomness.

4.2.2.1 Physical

Physical taggants comprise materials with different properties such as solid particle size, appearance and structure (Gooch, Daniel, *et al.*, 2016). A larger and optimised surface is necessary since encoding capacity is greatly dependent on it. The built-in codes need to be analysed using visual methods such as low-power microscopy. However, owing to their relatively larger particle sizes, they cannot be used for covert operations. Examples include 'Microdots*', which contain micro-sized photographic information that can be revealed through optical magnification. Datadot® and Microtrace® (Figure 7) use microdot technology by incorporating different inks or varnishes (Microtrace Solutions, 2023). Some taggants consist of small plastic particles each made from materials of different colour. They are attached in differing sequential layers to produce specific designs (3M Security Solutions, 2023).



Figure 7: Uniquely encoded Microtrace taggants (source: Microtrace Solutions, 2023).

4.2.2.2 Spectroscopic

Spectroscopic taggants involve a combination of materials with varying optical properties. These are combined to produce a unique sequence of intensities and emission wavelengths (Gooch, Daniel, *et al.*, 2016). Non-toxic organic dyes with fluorescence properties in different regions of the visible spectrum are substantially used. Companies such as Luminex® are at the forefront of such taggant materials and they use a combination of cyanine, phthalocyanine and squaraine-based fluorophores.

Inexpensive and widely available materials lead to a higher chance of illegal manufacturing of the taggants. Organic dyes also exhibit broad spectral emission overlap, short



fluorescence times and sensitivity to photobleaching*. This leads to increased manufacturing requirements, insufficient detection time and unsustainable material utilisation. Research is concentrating mainly on overcoming these disadvantages and preparing more sophisticated optical materials with elements such as rare earths, as their optical properties are extremely difficult to duplicate (Gooch, Daniel, *et al.*, 2016).

Colorimetric and fluorometric methods have been widely used for currency anticounterfeiting. A group of conjugated polymers known as polydiacetylenes (PDA), with their alternating 'ene'-'yne' structures, provide novel structural and optical properties.

4.2.2.3 Chemical

Chemical taggants are similar to spectroscopic taggants. However, these tend to be encoded with a unique sequence using a set of tracers, which may either be present or absent from the mixture as a means of encoding. Examples include the UK's largest manufacturer of forensic marker technology, SmartWater® and SmartSpray®, utilises rare-earth elements, which are identified by their concentration through laser ablation coupled with plasma mass spectrometry (LA-ICP-MS). Authentix® uses isotopic components as chemical markers for authentications of fuels, consumer products and agrochemicals (Authentix, 2023).

4.2.2.4 DNA

DNA taggants use the coding ability of deoxyribonucleic acid (DNA). A range of methods have been developed for the storage of non-genetic data within DNA molecules. Manufacturers such as Selectamark Security Systems® (Figure 8) (Selectamark Security Systems, 2023), TraceTag® (TraceTag International, 2023), Haelixa (Haelixa, 2023) and Applied DNA Sciences® (Applied DNS Science, 2023) produce forensic marking agents that can infer identity via the use of unique oligonucleotide* sequences. DNA Gensee has been working on a metabarcoding technology which constitutes of DNA extraction, polymerase chain reaction amplification and sequencing using patented molecular tools. It allows them to search for the tiniest traces of DNA at the heart of a product. The technology can hold relevance in this project however, the scope is outside our area of expertise.

A significant portion of the current taggant research is aimed at developing chemical anti-counterfeiting taggants, their optical readout methods and the implementation of these taggants in the respective supply chains. The advantages and disadvantages of forensic taggants are summarised on Table 5.



Figure 8: DNA based taggant products (source: Selectamark Security System, 2023).

Table 5: Advantages and disadvantages of commercially available forensic taggants (source: Gooch, Daniel, *et al.*, 2016).

| Coding Type | Advantages | Disadvantages |
|---------------|--------------------------------------|--|
| Physical | Simplistic analysis Inexpensive | Limited coding capacity Less covert |
| Spectroscopic | Simplistic analysis Inexpensive | Subject to counterfeiting Limited coding capacity |
| Chemical | Analysis sensitivity More covert | Prone to misidentification Incomplete recovery |
| DNA | High coding capacity Low toxicity | Expensive analysis Possible degradation |

4.2.3 Existing Taggants

4.2.3.1 Barcodes and barcode particles

The commonly used fabrication techniques for barcode particles include photolithography*, chemical synthesis, moulding and microfluidics (Appendix II). Barcodes use specific chemical, physical, optical and morphological properties. However, the morphology has so far been limited to spherical shapes and smooth surfaces. Most manufacturing techniques are expensive, time-consuming and labour intensive. As a result of this, the use and scale-up of barcodes have been limited (Rao *et al.*, 2004).

Nano-photonics

Nano-photonics* are being extensively used for the microfabrication of barcodes. This technology has found application in combinatorial chemistry where several chemical reactions take place on micron-sized structures. A research group at the University of Southampton (Banu *et al.*, 2005) has been successful in manufacturing micron-sized SU8 (epoxy based negative photoresist) barcodes encoded with diffraction gratings. They can be detected by illuminating them with laser in a microfluidic channel. Several million distinct barcodes are possible with this technology.



The fabrication procedure used is called 'photolithography' or 'photochemical machining' (Appendix II). The end products were designed to carry a periodic pattern capable of detection via observation of field diffraction pattern. The factors which determine the encoding capacity are bar lengths and laser wavelength capacity. However, one limitation of this technique is the resolution that can be achieved by photolithography.

Pollen

The flowers of seed plants produce a powdery substance called pollen*, which comprises genetic information needed to fertilise a plant. Most pollen grains range from 10 to 70 μm in diameter. They have been used as intrinsic marker systems for geolocation and provenance determination.

A high demand for barcoding particles has been observed in the biomedical industry (Wang *et al.*, 2020). Researchers from Fudan University and Southeast University, China, integrated quantum dots (QDs) into natural biomass sunflower pollens using a layer-by-layer (LbL) deposition process (Wang *et al.*, 2020) (Figure 9).

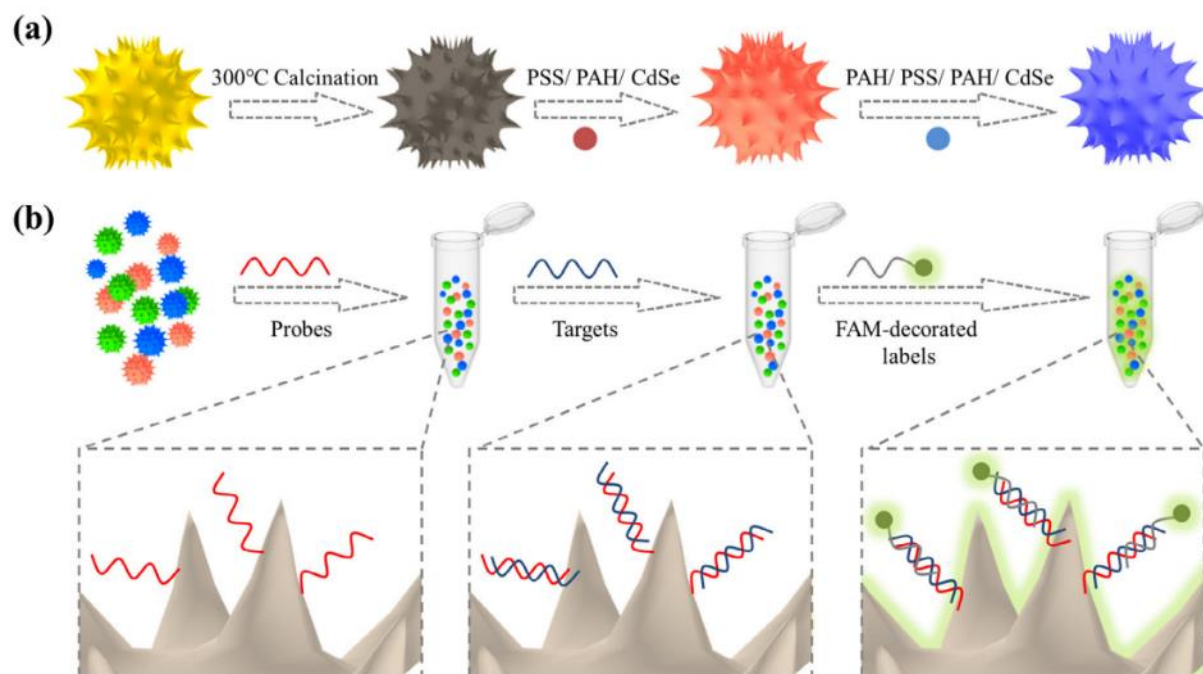


Figure 9: (a) preparation of QD coated pollens using layer by layer (LbL) deposition process. (b) Probe binding, target-probe interaction, fluorescently labelled detection (source: Wang *et al.*, 2020).

This demonstrated a novel approach, which made use of the prickly surface morphology of the pollen. Pollen grains are micron-sized, robust in maximal conditions and abundant. The prevalent optical method requires employment of fluorescent dyes. Conventional organic or inorganic dyes are prone to photobleaching, require multi-photon lights, and experience property alteration due to fabrication related quenching. QDs are well known for overcoming all these intrinsic issues and also allow a broad absorption spectrum, high quantum yield*, and narrow emission spectra.

The pollens underwent calcination treatment* for background autofluorescence* removal. Furthermore, they were layered with polyelectrolyte (PE) film layers and cadmium selenide



(CdSe). QDs were introduced into this film through a layer by layer (LbL) deposition process. Multi-coloured barcodes can be generated by depositing varied shapes and sizes of QDs.

4.2.3.2 Photonic nanocrystals, QD, fluorophores, lanthanides, nanophosphors

With the steady rise in counterfeits, a broad range of nanoparticles (NPs) such as metallic NPs, organic dyes, QDs, lanthanide-doped NPs have been widely investigated for anticounterfeiting. Amongst them, lanthanide doped up-conversion NPs (UCNPs) have been found to be one of the most efficient for the ease of tunability of optical properties. Some of the characteristics to be considered when selecting optical materials for anticounterfeiting are as follows:

- Easy control of abundant optical states to carry authentic information.
- Optical characteristics such as absorption, reflection, fluorescence and scattering.
- High photoluminescence* quantum efficiency (PLQE).
- Exhibit covert-overt transformation on tuning photonic bandgaps.

A range of the NP geometries include QDs, nanorods (NRs), nanoplatelets (NPLs) and other heterostructures* (e.g., dots-in-dots, dots-in-rods, dots-in-plates) (Hines & Guyot-Sionnest, 1996). This class of material is diverse due to its multi-faceted fabrication steps and includes organics, aqueous media, cation exchange reactions and polymer-assisted synthesis. They have proved to be successful but are limited by their use of rare-earth elements and toxic elements such as cadmium, mercury and lead. Visible, infrared (IR) range of spectral radiations can also be obtained using heavy-metal-free materials (Figure 10). The questionnaire responses (chapter 3.2.1) corroborate the toxic elements in Figure 10 (e.g., Cd toxicity).

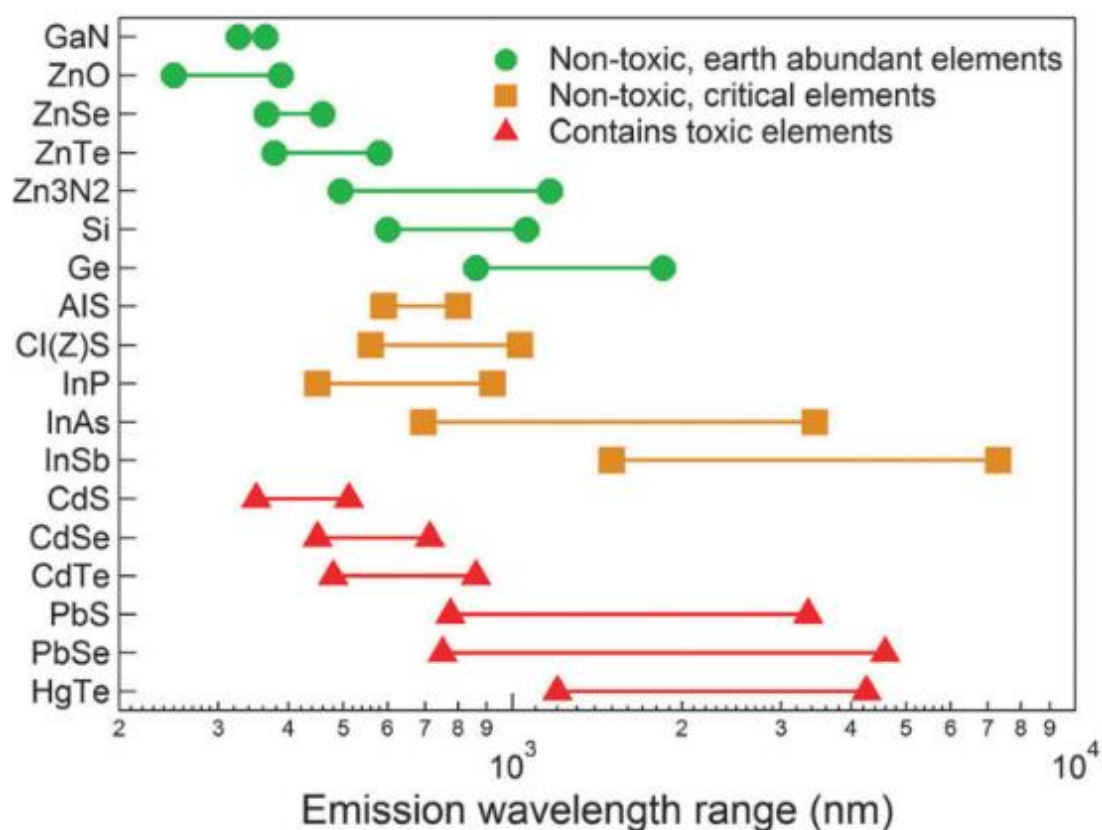


Figure 10: Emission wavelength range of commercially used materials (source: Q. Grim *et al.*, 2015).

Photonic nanocrystals

Photonic nanocrystals (NCs) have an internal periodic dielectric structure. Due to the repetitive variation in refractive index (RI), it allows or prohibits the propagation of certain electromagnetic waves. For instance, researchers from the Ulsan National Institute of Science and Technology, Korea (Nam *et al.*, 2016) effectively proposed a novel and cost-effective fabrication (using ink-jet printing) technique for silica-based (500nm diameter) mono-layered, self-assembled photonic crystal (SAPC). With this procedure, they were able to overcome the cost/time-ineffectiveness of top-down manufacturing techniques like photolithography, two photon patterning and direct-writing assembly. The NPs exhibited structural colouration by controlling the light illumination and the background. There are significant research and investigations on inkjet printers for structural colour patterns (Singh *et al.*, 2010; Yakovlev *et al.*, 2016; Park & Moon, 2006). Inks containing monodisperse CdS spheres were printed on paper and exhibited different colouration depending upon viewing angle (Figure 11) (S. Wu *et al.*, 2017).

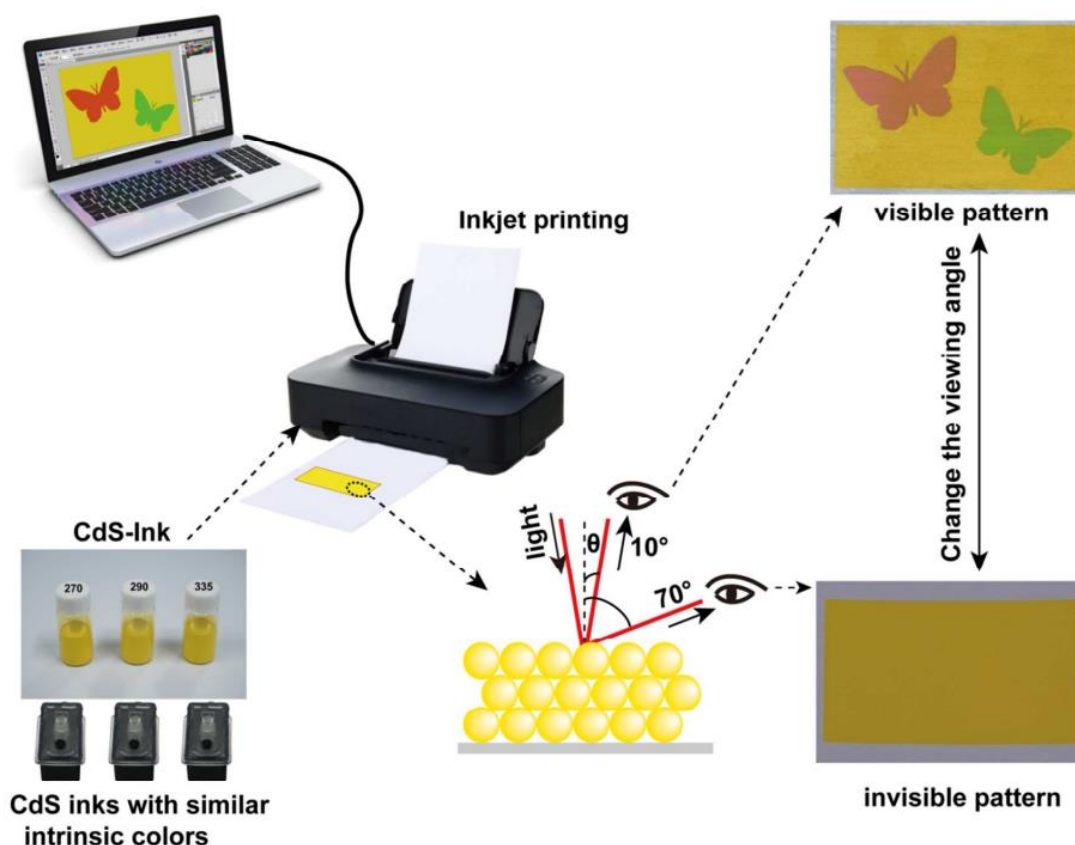


Figure 11: Illustration of CdS spheres printed on paper using inkjet printers (source: S. Wu *et al.*, 2017).

With this technology, no external stimuli (such as, light, temperature, electricity or magnetic field) are required for proving authenticity and the print remains in its original form. The durability tests, spanning six months, also generated promising results with reflectivity remaining absolutely unchanged. Mesoporous silica nanoparticles (Bai *et al.*, 2014) and polymer nanoparticles (P-X Wang *et al.*, 2016) exhibit similar characteristics depending on vapour absorption, which alters its refractive index. Not only does this method allow ease of detection with the naked eye (by viewing at different angles), non-compulsory external stimuli but, the ability to observe moisture ingress as well (Figure 12).



D2.1. Artificial fingerprinting for tracking raw material flows in complex supply chains.

Both CdS and CdSe release toxicity into the soil owing to the poisonous Cd. Therefore, several industries do not permit their processing (as observed in 3.2.1.1). Quantum dots made of CdSe are valuable in photonics, serving as single-photon sources, dopants for fibre sensors, sensitizers for photovoltaic cells, and luminescent markers for biomedical research (with the quantum dots sometimes fabricated with a shell of zinc sulphide to reduce toxicity). Many of these uses require only small quantities of the quantum dots. These materials hold a lot of potential and therefore their usage requires more proactive research in to whether they will be a problem when they enter the environment.

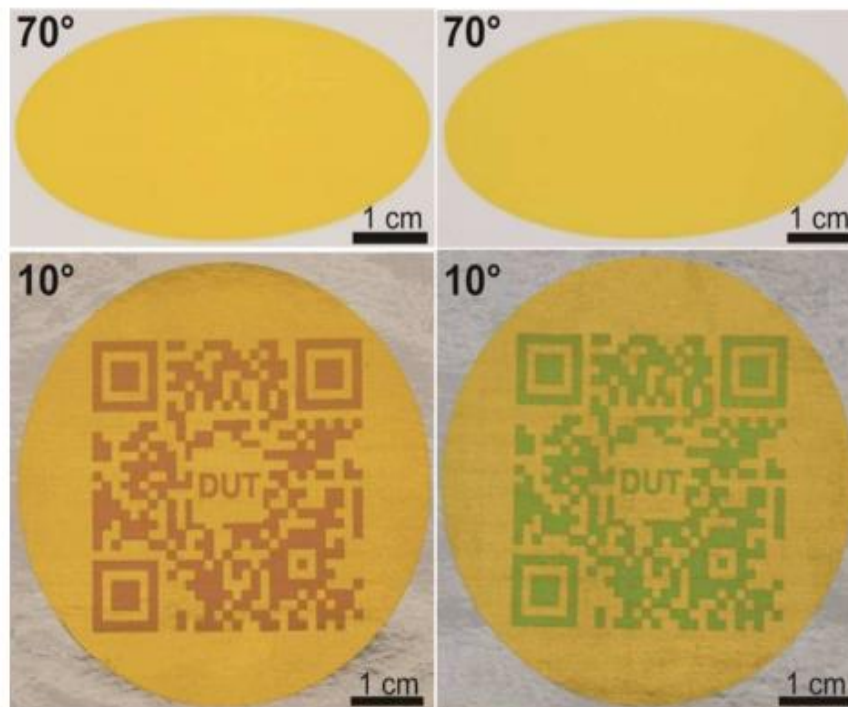


Figure 12: Invisible QR codes obtained using CdS spheres (source: S. Wu *et al.*, 2017)

Metallic nanoparticles

Metallic NPs* exhibit an absorption spectrum depending on their surface structure and surface plasmon resonance* (SPR). On excitation, electrons jump from their valence band to a higher energy orbital called the conduction band. The collective oscillation of all the conduction electrons in resonance with the electric field produced by polarised, incident light is referred to as the SPR. For example, gold NPs and silver NPs respond to specific wavelengths depending on their morphology (Lin *et al.*, 2018). Moreover, these gold nanorods and nanospheres also exhibit a photothermal* effect depending on their shape and size. Due to excitation of electrons by incident light, some materials generate thermal energy and these specific heat signatures can be detected and imaged by an infrared camera (Kang *et al.*, 2018).

Semiconducting nano particles

Semiconducting nanoparticles (Figure 13) exhibit the highest range of nanomaterials to select from as they include all the III-V and II-VI combination of elements from the periodic



table (Xu *et al.*, 2017; Jiang *et al.*, 2016). They have multiple energy labels at conduction and valence bands and exhibit both Stokes* and Anti-Stokes* shift (Appendix III).

Silicon nanotechnology has opened up opportunities in the fields of biology, electronics and energy in the form of silicon NPs (SiNPs), silicon nanowires and nanoribbons. Investigation using zero dimensional fluorescent SiNPs has yielded interesting results. Silicon is the second most abundant element on Earth and is known for negligible toxicity however, expensive and/or toxic silicon precursors are generally needed (Y. Wu *et al.*, 2016; Q. Li *et al.*, 2013). Since illegal extraction of SiO₂ is widespread and is damaging to the environment, it could be beneficial to consider biological precursors. Research has revealed that surface ligands* (e.g., N-H groups, diphenylamine, cyanine dye series and carbazole) on SiNPs produce a large impact on its fluorescent properties. Nonetheless, it is quite difficult to control its emission spectrum. Through experiments, distinct excitation wavelength dependent photoluminescence (Appendix IV) has been successfully obtained by introducing oxidised indole* derivatives on SiNPs (Q. Li *et al.*, 2013). This was realised through photoluminescent energy measurement and time correlated single photon counting (TCSPC). Indole usage is advantageous since its optoelectronic module application proves its biocompatibility and high photoelectric activity (Hines & Guyot-Sionnest, 1996). Research into thermal decomposition and magnesiothermic* reduction has been utilised to manufacture SiNPs (10-40 nm) from rice husk (Liu *et al.*, 2013). Silicon from Gramineae* plants (e.g., rice husks, sugarcane bagasse and wheat straws) can be altered into SiNPs (4 nm) with a high quantum yield of 15%, exhibiting strong fluorescence under microwave radiations.

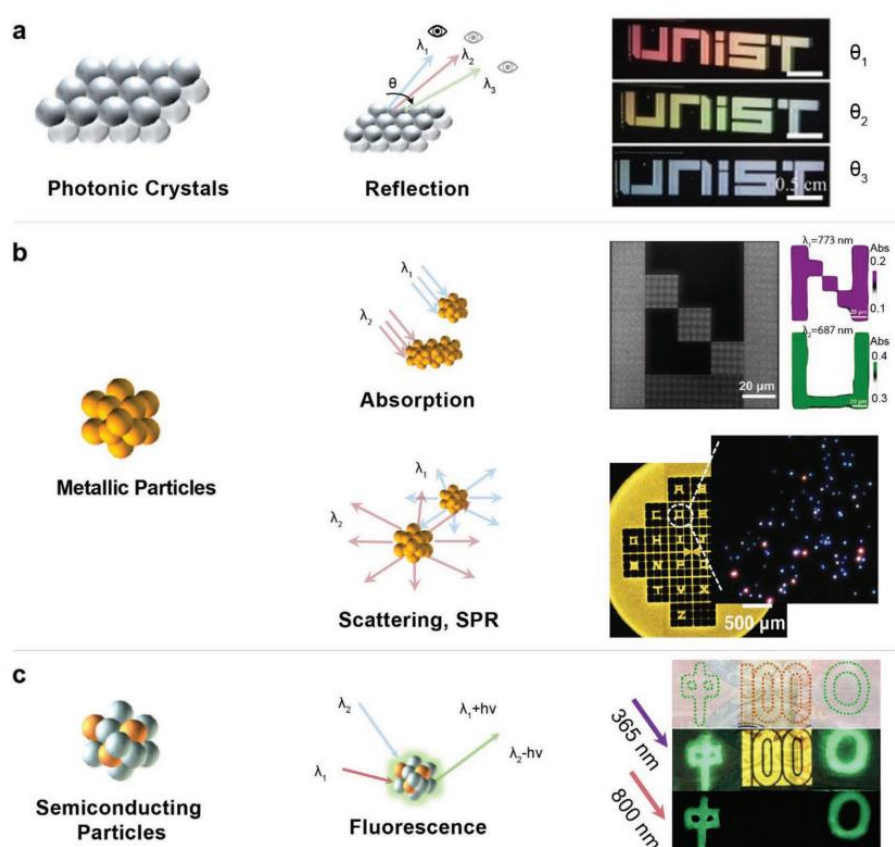


Figure 13: (a) Photonic crystals alter motion of photons due to its periodic dielectric structure; (b) metallic NPs are selective with their absorption and scattering wavelength; (c) semiconducting NPs exhibit Stokes shift and Anti-Stokes shift (source: Ren *et al.*, 2020).



Polymer hosts doped with semiconductor NPs bring together the processing characteristics of polymers and fluorescence properties of semiconductors (Table 6) (Rajeshwar *et al.*, 2001). There exists a comprehensive batch of such materials (in the form of inks) that can be patterned using inkjet printing. However, in-situ fabrication of QD NCs is still a challenge. Semiconducting QDs exhibit excellent optoelectronic properties owing to; size-dependent quantum confinement effect and Stokes shift as a consequence of overlap between emission and absorption spectra (Yan *et al.*, 2022). Therefore, detection strategies can often yield incorrect output as resonance energy transfer (RET) causes reabsorption. Nevertheless, doping can enhance their inherent properties. However, it comes at the price of rare-earth ions or other metals being used as optical activators. For example, Mn^{2+} doped QDs display emissions within the orange spectral window and a large Stokes shift (F. Li *et al.*, 2017). Therefore, QDs can potentially have application in anticounterfeiting labels.

Polymer dots* have received attention recently as a result of their remarkable brightness, great photostability, fast radiative rate*, and excellent biocompatibility, albeit their anticounterfeiting applications are under researched and untested. To date, their research has commercially extended to photothermal neuron activation and photoacoustic* imaging (Lyu *et al.*, 2017; Lyu *et al.*, 2016). Weik-Kai Tsai and co-workers (Tsai *et al.*, 2017) developed a novel strategy for fabrication of a light-responsive fluorescent nanomaterial with photochromic spiropyran molecules integrated in semiconducting polymer dots. Spiropyran* derivatives were incorporated into polymer matrices and photo-switching efficiencies checked before application in anticounterfeiting (Tsai *et al.*, 2017). However, polymer dot NPs have been specifically used for patterning onto flexible photonic and optoelectronic devices, barcodes and other consumer products such as pens and bicycles. Their potential applications in anticounterfeiting within the mineral supply chain requires further research.

Upconversion nanoparticles

Rare-earth NPs exhibit upconversion (UC) luminescence* due to the ease of 4f orbital transitions thereby minimizing outer ligand field effect* (Bünzli, 2010; Auzel, 2004; Rathaiiah *et al.*, 2015). 4f shells in the atomic structure of elements do not feel the influence of the nucleus due to shielding caused by inner electrons. This results in easy movement of electrons leading to radiation exchange (sometimes in the form of fluorescence). Rare earth matrices generate UC luminescence in the violet to near-infrared region under constant wave excitation at 980 nm.

For bio-imaging, fluorescent probes play an important role in labelling molecules of interest and fluorescence amplification. Most probes to date have involved QDs, fluorescent proteins, organic dyes and metal complexes. However, these materials use one-photon excitation which have a few limitations, which includes (a) DNA damage, (b) low signal-to-noise (SNR) ratio due to background autofluorescence, and (c) low penetration depth. Rare-earth upconversion nanophosphors have proved to be useful in bio-imaging for their large penetration depth and absence of background fluorescence (L.-Q. Xiong *et al.*, 2009; L. Xiong *et al.*, 2009). Particularly, lanthanum-doped, upconversion nanoparticles (UCNP) have a longer life, sharp emission lines, large anti-Stokes shift, non-blinking and higher photostability. These materials include an inorganic host, sensitizer and activator. The host matrices are usually oxides, halides (fluorides, chlorides, bromides and iodides), oxysulfides, vanadates and phosphates.




Table 6: Different optical NPs with potential usage in anticounterfeiting (source: Ren *et al.*, 2020).

| Nanomaterials | Advantages | Disadvantages | Optical Encoders |
|--|---|--|--|
| Photonic Nanocrystals | | | |
| SiO ₂ NPs, CdS NPs, polymer NPs, metal oxide NPs | Unique colours, unlimited codes | A complex fabrication process for each code | Structural colour based on viewing angle Solvent vapor/swelling responsive colour Viewing angle dependent fluorescence enhancement |
| Metallic Nanoparticles | | | |
| Au NPs, Ag NPs | High stability, easy synthesis | No visible optical features to the naked eye as anticounterfeiting marks | Absorption spectrum Photothermal effect Scattering light |
| Semiconducting Nanoparticles | | | |
| Silicon NPs | Biocompatibility, high stability, can be obtained from biomass | Harsh conditions, specific equipment required to obtain nanocrystalline crystals | Stokes emission |
| Quantum dots (CdS, CdTe, CdS/ZnS/ZnS:Mn ²⁺ /ZnS) | Photostable, tuneable, excitation and emission spectra, the narrow emission band | Photo-blinking, cytotoxicity | Stokes emission |
| Carbon/graphene dots | High quantum yield, low toxicity, low cost, enables multimode emission, long lifetime value, can be obtained from biomass | Fluorescence mechanism is not clearly understood, the long-lived phosphorescence depends on special substrates | Stokes emission Anti-stokes emission Long persistence phosphorescence |
| Perovskite (APbX ₃ and its hetero-structure, A = Sc or CH ₃ NH ₃ , X = Cl, Br, I) | Tuneable emission wavelength, narrow emission peak, temperature-responsive, enables multimode emission | Poor stability in the humid environment usually contains hazardous ions (e.g., Pb) | Stokes emission Anti-stokes emission |
| Polymer dots | Photostability, structural stability, eco-friendly | Relatively broad emission peak, poor in morphology control | Stokes emission |
| Upconversion Nanoparticles | | | |
| REE NPs | Photo stability, high penetration depth, longer life, absence of background fluorescence, sharp emission lines | Complex process, costs not know and real-time in-situ applications may be limited. | Anti-stokes emission |



The typical host fluoride crystal structures are NaYF_4 and CaF_2 (Chen *et al.*, 2012). Their dominant characteristics include good chemical stability, low phonon energy, and their ability to be doped with lanthanide through cationic exchange*. Synthesis processes such as thermal co-decomposition method, high temperature co-precipitation method, have matured and allow size and morphology control. With alteration between a combination of lanthanide ions as sensitizers and activators with their abundant energy levels, the optical diverseness is enormous. As a result, their application in anticounterfeiting measures offers new possibilities (Han *et al.*, 2016). The complication arises due to need for drastic synthesis scale-up. Currently the aforementioned techniques yield less than 100 mg of the final product for every batch. This enhances the drawback with reproducibility of UCNP production (Figure 14).

Recently, there has been substantial development of large-scale synthesis processes such as a facile hydrothermal method and solid-liquid thermal decomposition. However, the main issue is of scarce starter materials and their high prices (Yao *et al.*, 2016).

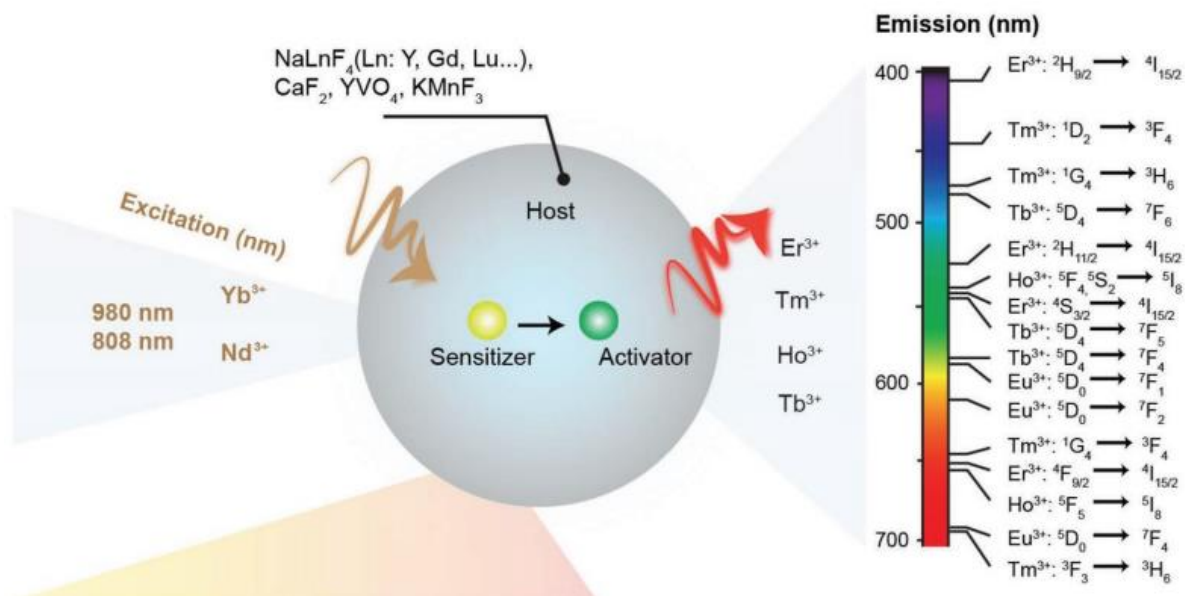


Figure 14: UCNP controlled synthesis (source: Xu *et al.*, 2017).

4.2.3.3 Physical unclonable functions

For the protection of consumer products, radio frequency identification tags (RFITs), holograms and chemical tagging have been significantly used in livestock, equipment and asset tracking. However, due to the cloneable attribute of the existing technology, research has concentrated on combining optical readout, pattern recognition, encrypting data and storing information. This has led to development of anticounterfeiting taggants called physical unclonable functions (PUFs) (Arppe & Sørensen, 2017). PUFs combine layers of distinct materials with specific characteristics. Each layer is to contain unique information in the form of random codes obtained through a digital process (Figure 15).



Figure 15: Multiple layered particles with different physical characteristics in each layer (source: Gooch, Daniel, *et al.*, 2016).

A high encoding capacity can be achieved by having a greater encoding area. Instead of imprinting unique information, if present technology permits, different materials can be randomly deposited onto a specific layer following a stochastic* process.

Figure 16 describes the production process of a PUF key. Researchers have successfully synthesized six taggants each with a distinct optical response and embedded all of them into the same tag (Arppe & Sørensen, 2017). The tag comprised of substrate, a taggant layer and a top coating. The sequence followed for allocation of these six taggants within the tag is a result of a stochastic process and the encoded information can be decrypted in 1D or 2D. Decoding produces results regarding either the presence or absence of taggants as a result of their chemical response to external stimuli. The PUF key is fully functional once the optical readout has been well-established. Of the other PUF keys reported in literature, a stochastic sequence of luminescent inks or dyes (or, barcodes) seem convincing. The stability of both the PUF key and the readout, alongside multiple colours to yield multiple responses are deterministic factors.

A weak PUF was realised by producing a multilayered plasmonic tag on a standard microscope glass slide (Yao *et al.*, 2016). On deposition of zinc oxide, silver and polyvinylpyrrolidone (PVP), the silver layer exhibits low adhesion and zinc oxide deposition degradation take place conjointly. The label can be authenticated by comparing images taken by smartphones with recognition software. The low cost tagging mechanism lacks the higher authenticity control achieved by spectroscopic taggants.

Also, refining of oxide-based minerals requires them to undergo reduction through elevated temperature reactions. Along with reduction of the mineral, zinc oxide in the taggant will reduce to zinc and allow its ingress into the mineral or the minerals ingress into the PUF lattice. Not only does this constitute a loss of chemical and physical properties of the added marker, but it could contaminate the mineral.



D2.1. Artificial fingerprinting for tracking raw material flows in complex supply chains.

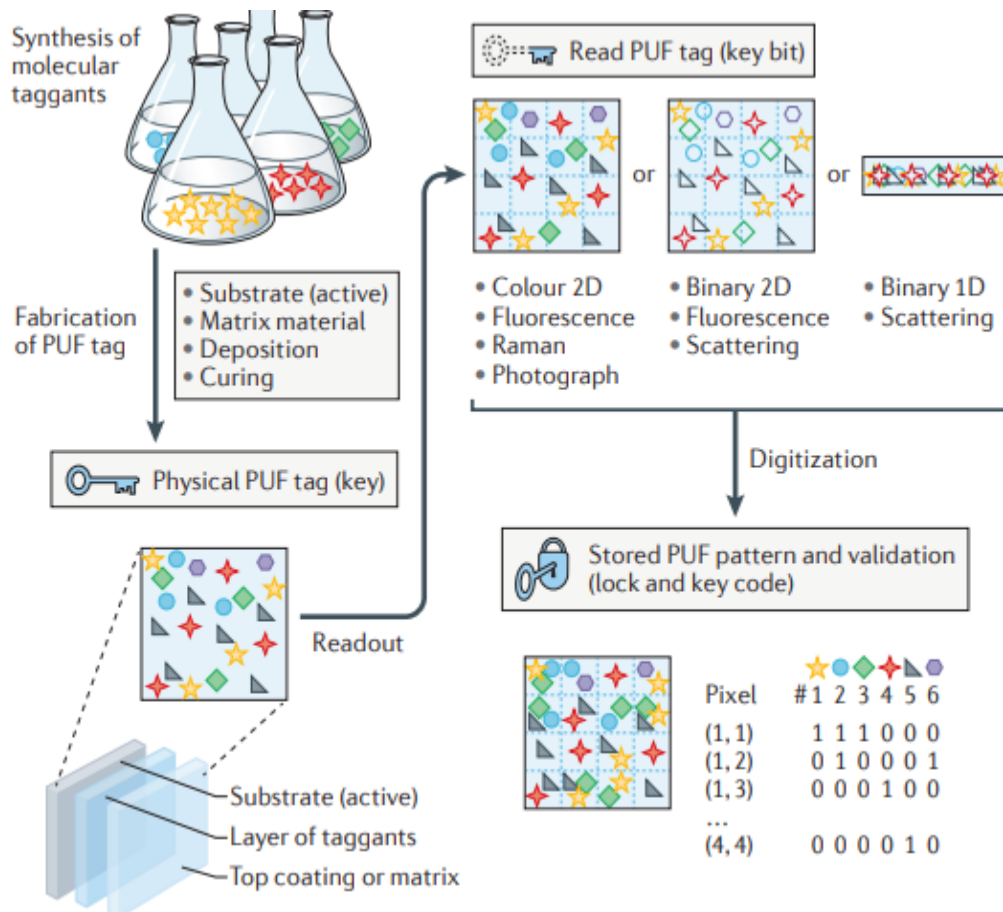


Figure 16: Synthesis of a PUF key (source: Arppe & Sørensen, 2017).

Silicon chips in transistors are prone to counterfeiting, tampering and information leakage through side channel attacks (such as, by measuring power consumption, electromagnetic radiation and timing). Silicon PUFs make use of process-variation induced mismatches. Therefore, they are vulnerable to environmental factors and noise. Self-assembled carbon nanotubes (CNTs) deposited onto HfO_2 has found application as the channel material of transistors (Figure 17). The alternative is hard-to-forge and low-cost. However, limited semiconducting purity and non-ideal assembly inhibits its ready usage in the field. This technology enables a new operating principle for hardware security beyond conventional PUFs.

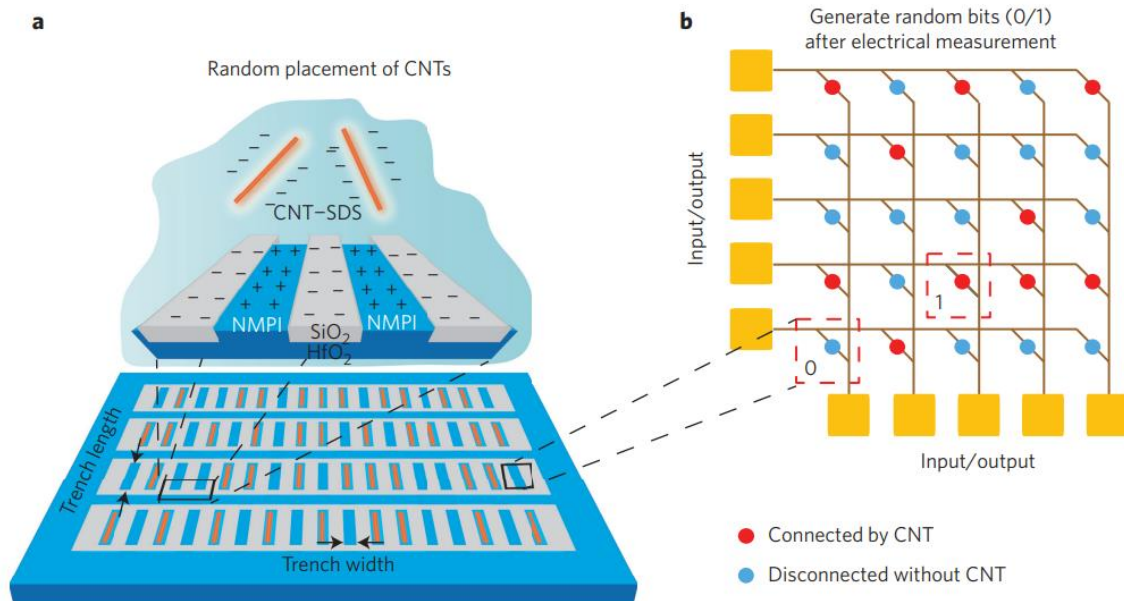


Figure 17: (a) Self-assembly of CNTs in HfO_2 trenches in a monolayer. Self-assembly is realised through ion exchange, (b) Randomly connected 2D CNT array (source: Q. Li et al., 2021).

4.2.3.4 Plasmonic structures

Localised surface plasmon resonance (SPR) is characteristic of constituting materials and surrounding conditions. Gold NPs have been observed to self-assemble due to LSPR and have shown great potential in photoelectronic devices, flexible electronics, and others. Core-shell NPs were proposed as electrodes for anticounterfeiting in the electronics industry. Core-shell NPs were introduced intentionally and unintentionally into microelectronics (specifically electrodes of different semiconductors such as GaAs, GaN). Figure 18 exhibits detection of these NPs using scanning electron microscopy (SEM), atomic force microscope (AFM) and dark-field microscopy image of an electrode. Some commonly used electrodes exhibiting good plasmonic properties include gold, copper and aluminium owing to their high conductivity (Q. Li et al., 2021).

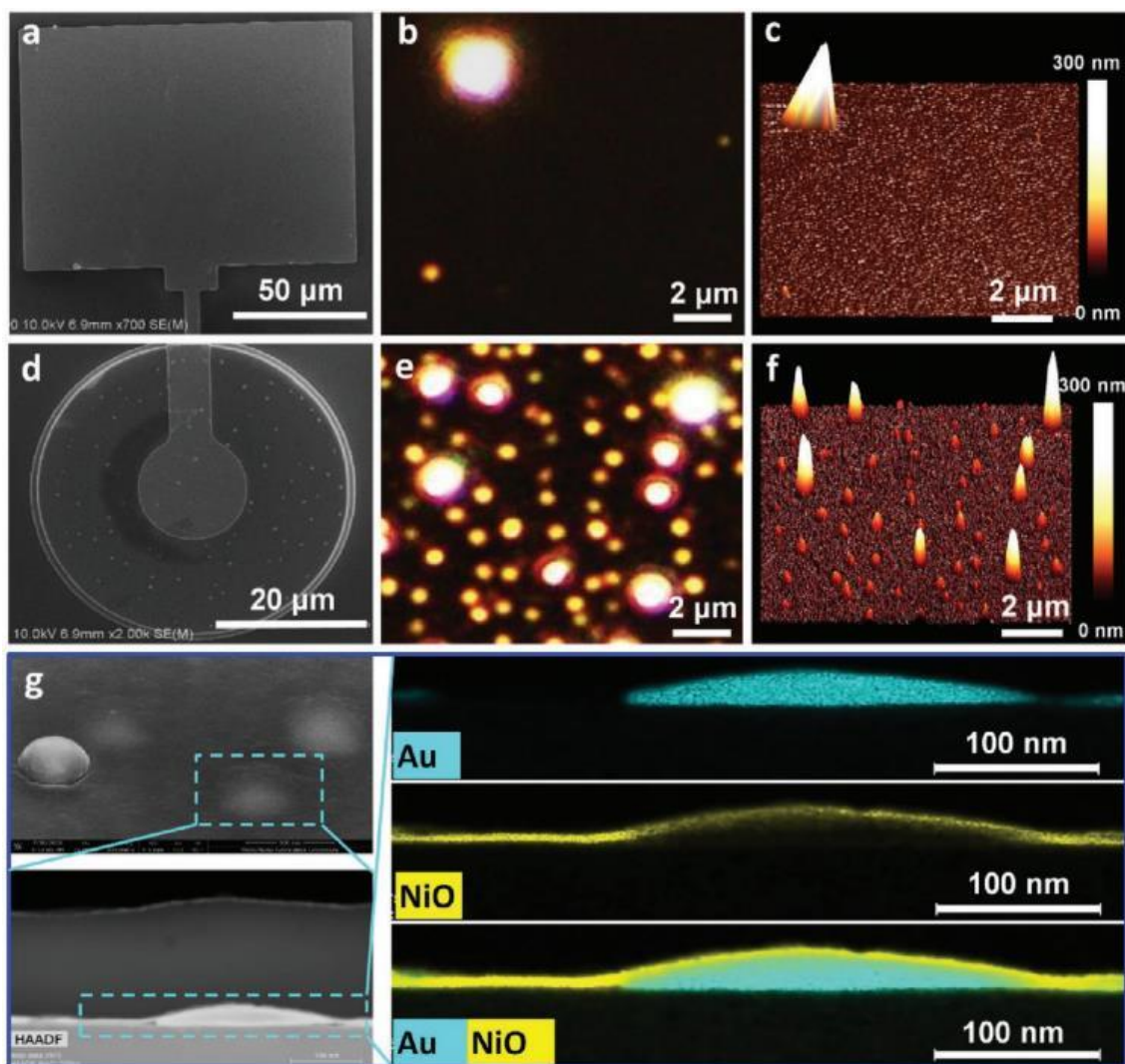


Figure 18: (a-c) SEM, dark field microscopy and AFM image of metal electrode. (d-f) SEM, dark field microscopy and AFM image of annealed electrode. (g) Close up SEM and chemical composition of hemispherical core-shell NPs (source: Q. Li et al., 2021).

4.2.4 Other Techniques

4.2.4.1 Raman spectroscopy

To reduce the production and circulation of counterfeits, some of the present taggant technologies are being examined using Raman spectroscopy (R. Li et al., 2016; Zhou et al., 2014). As with the spectroscopic methods, the compounds are prepared to have a distinct spectral fingerprint. The shift takes place from absorption of light energy to analysis of spectral radiation owing to inelastic scattering of monochromatic laser light.

The sensitivity of detection of tracer components can be further increased through Surface Enhanced Raman Scattering (SERS) by directly conjugating Raman-active compounds to a number of metallic NPs. Researchers have designed a coding technique to use the NP characteristics beyond fluorescence by extracting the discrete melting temperatures of a solid particles panel within a taggant mixture to produce a unique thermal barcode (Natan et al., 2007). Differential scanning calorimetry (DSC) can be used to detect the presence or absence of these 'phase-change' NPs in a linear thermal scan, which generates a melting point peak for each component (Duong et al., 2014). Nonetheless, only a very small portion of NPs have been developed for this purpose (Hyun et al., 2014).



4.2.4.2 Synthetic polypeptide sequences

Developments with synthetic polypeptide sequences have been successful (Gooch *et al.*, 2015). Since the 1980's, the usage of uniquely ordered amino acids has been considered to be a plausible solution to inferring identity (Kydd, 1982). An oil-based medium constituted of hydrophilic peptide molecules is applied onto the surface of an object. As a result of illegal handling, the reagent is transferred onto the offender. Detection is carried out by fluorescence tracers. These hydrophilic peptides are then isolated from the medium using liquid-liquid extraction, which allows their mass and sequence to be determined by electrospray ionisation mass spectrometry (ESI-MS) (Figure 19).

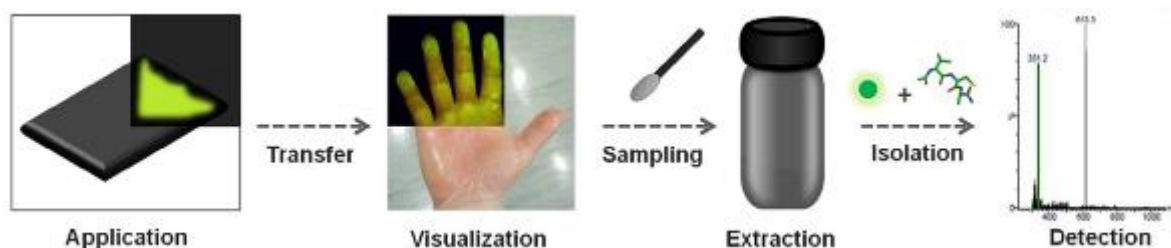


Figure 19: Peptide based taggant and its analysis (source: Gooch, Daniel, *et al.*, 2016).

Peptide taggants have proved to be advantageous as a substitute for single-component biomolecular coding over DNA based marking systems. Polypeptide chains have a significantly greater statistical coding capacity, due to the 22 different natural amino acids that may be used as individual sequence units (DNA only has four). Some researchers have specified that 10 amino acids can code up to 4×10^{13} distinct sequences (Hyun *et al.*, 2014). ESI-MS techniques are also quicker and are becoming exceedingly portable. In terms of cost, polypeptides can be synthesised at low cost, are environmentally friendly and comparatively inert. Chemical modification can bring about even higher stability (Nam *et al.*, 2016).

4.2.4.3 Aerospace materials

Aerospace grade materials exhibit high performance characteristics, such as high strength to weight ratio, durability, and ductility. For instance, titanium alloys display promising characteristics and their 3D printing, albeit costly, is a widely accepted manufacturing process. Its properties of very high strength, corrosion resistance, high melting point and low thermal expansion may be relevant to the production of a taggant. However, there is no evidence of titanium taggants being researched or possessing spectroscopic properties (e.g., fluorescence) (personal communications, Dr Rong Lan, Coventry University, UK).

4.2.4.4 Non-optical detection

In addition to spectroscopic characteristics, other properties that could be used for detection are as follows:

- Electricity, piezoelectricity* (whereby mechanically stressed materials produce electricity).
- Magnetism.
- Sound-light interaction with matter.



4.2.4.5 Tailorlux fibres

Tailorlux GmbH, located in Münster, Germany, helps companies ensure transparency in supply chains, circularity, and product protection. Their method uses scalable near infra-red and visible (NIR/VIS) spectroscopy to detect the chemical fingerprint of materials or create unique signatures with individual markers. These markers can be integrated into raw materials or products and read reliably with handheld sensors in the field.

The markers are available as dispersions, masterbatches, or individual fibres for easy industrial integration. Alternatively, their application uses intelligent dispensing systems, generating initial data for digital twins. These markers are invisible to the human eye and do not affect the marked material. They are resistant to high temperatures, pressure, mechanical impact, and harsh chemicals, remaining readable even if the product degrades or burns. These markers can also serve as forensic evidence in destructive analysis methods. Since the marking is flexible it can be integrated into many products, for example; automotive, PCBs and electronics, leather, security prints, fibres and filaments, glue, glass, foams.

4.3 Existing Taggants and MaDiTraCe

A summary of available taggants is provided in Table 7, giving the advantages and disadvantages and potential applications for MaDiTraCe. Unfortunately, none of the existing taggants seem to be directly and readily transferable to track minerals and metal commodities. This is primarily since they already contain components such as particular metals, minerals, rare earth elements etc., which could compromise the integrity or perception of the materials being tracked, or, they are not cost-effective or require sophisticated or complex detection techniques. However, the following warrant further research:

- **Silicon NPs:** Silicon NPs obtained from biomaterials could be relevant for MaDiTraCe, but require spectroscopic characteristics. Moreover, Silicon based slags are used as part of smelting processes to remove impurities (e.g., gangue minerals). Therefore, the usage of silicon NPs as a taggant could potentially impart the additional benefit of easy removal during melting. However, the extraction of silicon from bio-resources to produce NPs could be a complex, costly and time-consuming process.
- **Carbon nanotubes (CNTs) and carbon nanowires:** The applicability of CNTs and carbon nanowires in the minerals and metals sector requires further research and is limited by the present technology readiness level (TRL). Current production methods of graphene are very expensive, energy and resource intensive and the production rate is low. Moreover, mining of natural graphite is limited by the dust emissions, water and soil contamination due to run-off and contamination of storage facilities it causes. However, the amounts needed for tracking are far smaller than batteries, and the amount being mined is rapidly increasing because of increasing battery requirements
- **PUF keys:** The technology outlined by PUF keys are potentially promising for MaDiTraCe. Nonetheless, advanced synthesis procedures require more investigation.
- **FTIR:** Experimenting with the FTIR emission spectrum and fluorescence spectroscopy of pollen grains, as artificial tracers, could yield prospective results. However, this is likely to require biological and palynological expertise.



Table 7: Summary of new materials and technologies.

| Taggant Types | Advantages | Disadvantages | Potential Application in MaDitraCe |
|--|--|---|---|
| SU8 Barcodes. | Theoretically millions of unique identifiable codes for particles as small as 50 microns in length are possible. | Photographic resolution restriction. Semi-transparent nature of SU8. Signal to noise ratio very low. | SU8 is expensive. However, nano-embossing technique can provide potential results. |
| QDs in sunflower pollens. | Prickly surface morphology of pollens. Pollens are robust in maximal conditions. Pollens are abundant. | Broad absorption spectrum. High quantum yield. Narrow emission spectra. | Mapping auto-background fluorescence of the pollen grains can provide promising results. |
| Organic dyes (such as, cyanine, fluorophores). | Organic dyes are non-toxic. Inexpensive. Widely available. | Prone to photobleaching. Require multi-photon lights. Quenching alters properties. Insufficient detection time. Low signal-to-noise ratio (background fluorescence). Prone to illegal manufacturing. | Application is currently limited by disadvantages. |
| Si-based photonic crystal. | Cost/time effective. Only requires light illumination & background control. | Requires external light source. | Insufficient data available. Requires experimentation. |
| CdS spheres. | Different colouration at different angles. No external stimuli needed. Reflectivity remains unchanged for long durations. Ease of detection. Invisible anticounterfeiting pattern. | Only applicable to labels. Toxicity of Cd | Understanding supply chain segments can help better understand the relevance of this technology in MaDiTraCe. |
| AuNPs, AgNPs. | Exhibit photothermal effect. Respond to specific wavelengths depending on morphology. | Absorption spectrum depends on surface structure SPR dependent . Highly sensitive to grinding condition. Affected by unwanted contamination. | Material is highly expensive. Material handling can cause issues such as AuNP absorption into human body and causing eye and skin irritation. |
| Oxidised indole derivative on SiNPs. | Si is the most abundant element on earth and indole is biocompatible. Si is relatively environment friendly (negligible environmental toxicity) Negligible human toxicity. | Difficult to control emission spectra. | Exhibit properties relevant to MaDiTraCe. Moreover, SiNPs can be derived from bio-resources such as rice husk. |





D2.1. Artificial fingerprinting for tracking raw material flows in complex supply chains.

| | | | |
|--|---|---|--|
| | High photoelectric activity. | | |
| QDs. | Exhibit optoelectronic effect due to quantum confinement effect. Doping enhances characteristics. | Small Stokes Shift. Often yields incorrect output. Needs REEs, which are expensive. | Contains expensive and toxic materials (such as Cd^{2+}). However, previous experimentation with doped CdS/ZnS QDs has displayed properties relevant to this project. |
| Lanthanum-doped UCNPs. | Longer life. Sharp emission lines. Large Anti-Stokes shift. High photostability. Large penetration depth. Absence of background fluorescence. | Expensive materials. Involves radiative loss during relaxation of excited electrons. | Technology maturity needed in terms of size and morphology control. Very optically diverse but, cost and availability pose a big challenge. Offers new possibilities however, manufacturing procedures require significant scale-up. |
| PUF key. | High encoding capacity. Stochastic sequence of luminescent inks or dyes. | Material dependent. Requires advanced synthesis processes. | New and diverse technology with potential for MaDiTraCe. |
| CNTs | Difficult to forge. Low cost. Not vulnerable to environmental factors. | Limited semiconducting purity. Non-ideal assembly. | New operating principle. Mainly relevant in hardware security. Insufficient data on relevance to MaDiTraCe. |
| Microtaggant® Identification Particles (MIP) | Established as tracers. Ease of detection with hand-held sensors and microscopy Invisible to the naked eye. Cost-effective. | Comprise metal elements. Particle shape and morphology may inhibit homogenous distribution and coverage. Limited research on applications for minerals and metals. Based outside the European Union. | Further experimental research is required, following on from the work conducted by AHK, GTK and Microtrace solutions. |
| Tailorlux GmbH | Established as tracers. Ease of detection with hand held sensors. Invisible to the naked eye. Track record of being used to provide forensic evidence. Based within the European Union. | Chemical composition to be determined and relevance for the tracking of minerals and metals. No previously used for minerals and metals. | Experimental research recommended with AHK, GTK and Tailorlux GmbH. |





4.3.1 AHK Preliminary Investigations

AHK Technical Department conducted preliminary experimental investigations using 'Microtaggant® Identification Particles (MIP)' or 'taggants' that were supplied by Microtrace LLC based in the USA (Microtrace, 2023). Their composition and structure have been specifically engineered to allow the MIP to efficiently fluoresce under the influence of a UV light and to allow for the creation of customer specific products. The objective was to test the MIPs to determine if they could be added to a base metal concentrate, in bulk or as a laboratory sample, to facilitate the tracking of the material in the global supply chain (Figures 20 and 21).

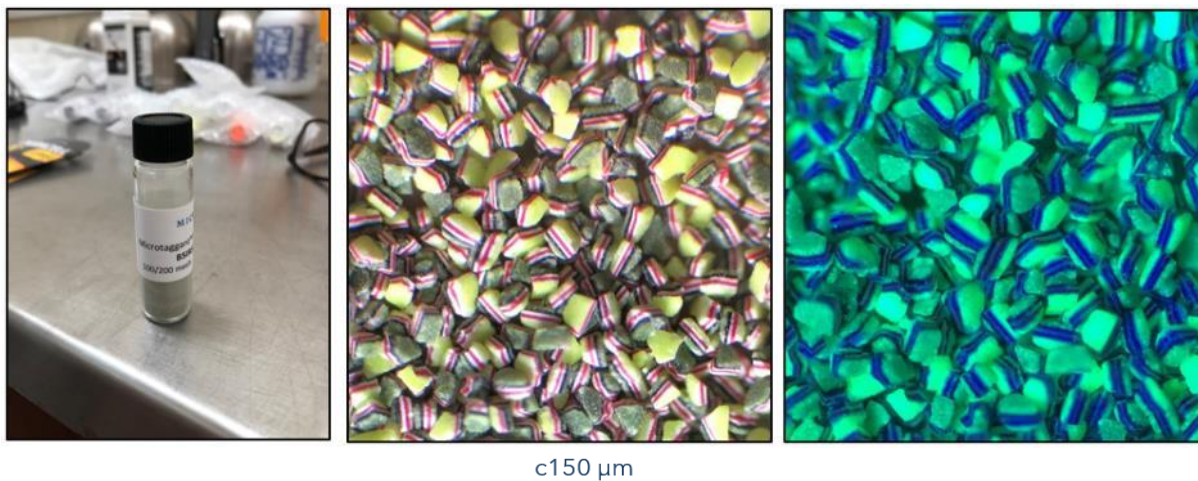


Figure 20: 100/200 mesh MIP (courtesy of Microtrace), showing layers and colour sequence without UV(left and middle) and under UV(right) (source: Alfred H Knight International).

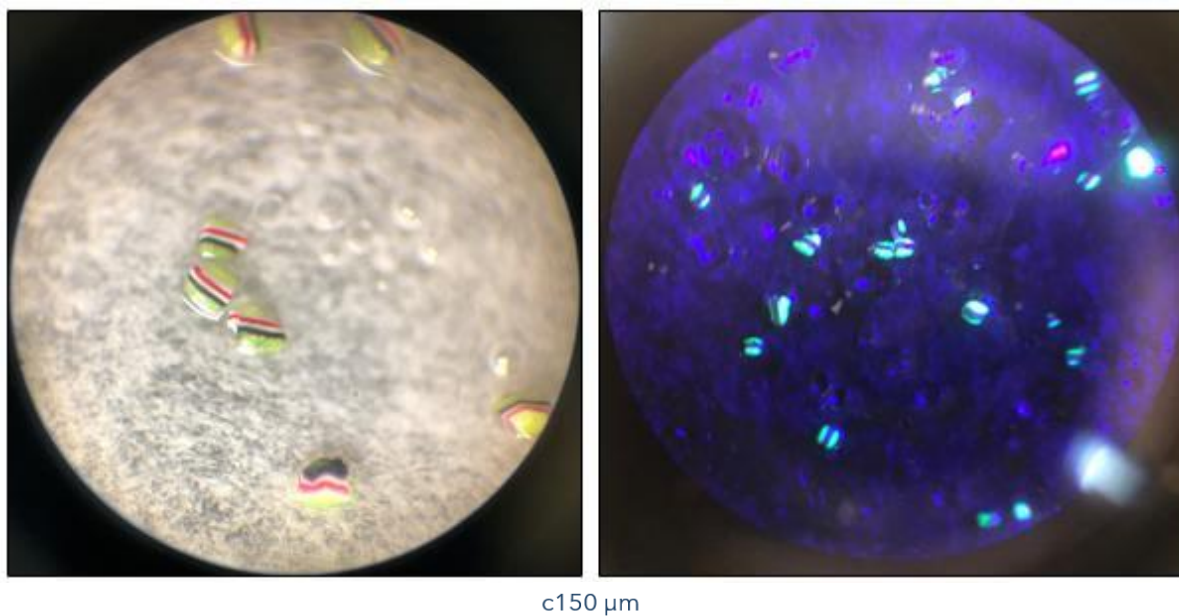


Figure 21: MIP bonded into coated layer of the crystal-clear lacquer (source: Alfred H Knight International).

The MIPs were applied to a copper concentrate sample by mixing one-gram of 100/200 mesh MIP sample with approximately 100 mL of Polyvine clear crystal lacquer and 50 mL of water. The mixture was applied using an atomising spray gun to ensure a homogenous



D2.1. Artificial fingerprinting for tracking raw material flows in complex supply chains.

coverage. There was complete coverage of the samples surface area and good distribution of the MIP's over the material. In addition, the application of the MIP's with lacquer/water, allowed the MIP's to bond with the material and remain on top of the exposed surface of the material contained in a hard lacquer coat. The MIPs, invisible to the naked eye, were detected using a 'uvBeast' UV torch light, which performed better than an infrared laser pen.

The MIPs were also analysed using Interactive SEM-EDS, LA-ICP-MS and X-CT tomography. The results showed a range of metals and minerals to be present, some of which may not be favourable for inclusion in metal concentrates, either due to stakeholder requirements, or perception of their inclusion.

It was concluded that further research is required to further characterise the MIPs. Their shape and composition are considered as potentially unsuitable for the application intended. However, these preliminary results and the experience gained, opens up the possibility of creating new MIPs that are better suited to the mining, minerals and metals industries applications, in terms of both material content and shape.





5 3D Printing

5.1 Overview

In this section we review the potential of 3D printing technologies for the manufacture of artificial tracking particles to be used for traceability, focusing on various stages in the value chains of lithium-ion rechargeable batteries and rare-earth magnets. 3D printing (also known as additive manufacturing) has been around in conceptual form for almost 50 years (Jones 1974) and in practical form for about 40 (Bagheri & Jin 2019). Jones (1974) described a method of 'joyful three-dimensional doodling'. It encompasses a wide range of methods and technologies. These are united by the principal of adding material to the object being formed rather than subtracting material from a larger initial piece of material, as in most traditional manufacturing methods (Figure 22). For a large part of its history as a method, 3D printing was considered most useful for either prototypes (hence rapid-prototyping as an additional alternative name) or high value, one-off or very low number customised objects in fields such as medical, aerospace, defence, oil and gas and motorsport etc. (Jordan 2019). However, recent developments and advances in machines, techniques, and software, have allowed it to move into the realm of 'mass-customisation' (Jordan 2019; Savolainen & Collan 2020). This was foreshadowed by Jones (1974) with his description of 'infinitely flexible mass production'.

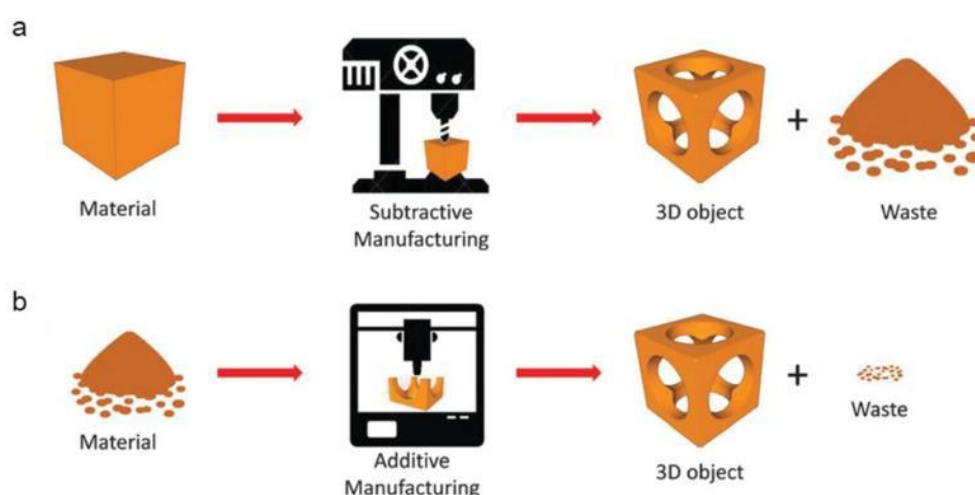


Figure 22: Differences between a) traditional subtractive manufacturing and b) additive manufacturing (source: Chen *et al.*, 2020).

'Mass-customisation' is where the numbers of items produced is less than full mass-production. However, because the use of digital design and 3D printing means items can be rapidly iterated, customised, and produced without lost lead-time and costs, they can be produced in hundreds to tens of thousands and so can no longer be considered as the realm purely of prototyping or one-off/limited run production builds. Fully individualised and customised products such as shoes, sportswear, sports equipment and sports safety equipment, where detailed personal measurements and per-customer customisation are used, are areas of rapid 3D printing growth (Beiderbeck *et al.*, 2020). This is also particularly the case for multiple small items, which with some 3D printing methods can be optimised for fitting the maximum number into the whole of the build volume, lowering per-part manufacture time and cost, yet can still be rapidly iterated, improved and customised (Garzaniti *et al.*, 2018).



5.2 Advantages of 3D Printing

In addition to the possibilities offered by full customisation of individual parts for prototyping, production, and mass customisation of production, as discussed above, there are a number of additional advantages that 3D printing has over traditional manufacturing methods (Ngo *et al.*, 2018). In addition to full customisability, tooling cost can be reduced over many manufacturing types, since each new shape in moulding and casting processes requires a new set of tooling, even for minor changes. Complex near net shape (*i.e.*, close to the desired final product) objects can be manufactured, which reduces the costs of finishing processes required. External and especially internal structures otherwise not possible with conventional manufacturing techniques can be achieved, allowing dramatic increases in efficiency and performance in some applications (Figure 23). In the case of tracking particles, this could include the ability to vary the external particle shape to allow experimentation to optimise the dispersion of tracking particles in various materials at different stages in the supply chains investigated in MaDiTraCe. Linked to this is the possibility of using digital 3D data from geological samples of minerals, ores in the supply chain to inspire the design of artificial tracking particles produced (the concept of geo-inspiration, Butcher & Corfe 2021). The ability to spatially vary the internal microstructure allows site-specific mechanical, thermal, chemical or magnetic properties (Sofinowski *et al.*, 2022). Light weighting is a particular advantage in the aerospace industry, allowed by generative digital design and complex internal and external structures (Martinez *et al.*, 2022). The additive nature, leading to a reduction in waste, provides both environmental and cost advantages (Griffiths *et al.*, 2016).



Figure 23: Complex near-net shape metal 3D printed heat exchangers with internal structures unachievable via traditional manufacturing methods. Since the surface area to volume ratio and position of that surface area relative to air flow are critical in heat exchanger efficiency, 3D printing allows step change increases in performance over traditional heat exchangers (source: <https://all3dp.com/1/better-heat-exchangers-with-additive-manufacturing/>).

5.3 Methods of 3D Printing

According to the ISO/ASTM 52900:2021 document on additive manufacturing terminology (International Organization for Standardization [ISO], 2021), seven different process categories or principal methods of 3D printing exist (Figure 24):



- Binder jetting, where a liquid binder is applied to a bed of dry powder particles: metals, polymers, sand, gypsum, concrete and ceramics etc. (Ziaee & Crane 2019).
- Directed energy deposition, where material (typically metals) is melted during deposition by laser/electron beam or plasma arc (Svetlizky *et al.*, 2021).
- Material extrusion, where polymer-based filaments or beads, or pastes of metals, ceramics, concretes, foodstuffs etc., are continuously extruded with or without being heated in or near the nozzle (Buswell *et al.*, 2018; Nachal *et al.*, 2019; Goh *et al.*, 2020; Ang *et al.*, 2023).
- Material jetting, where, similar to a 2D printer, material (resin, biological material) is sprayed as jets of tiny droplets from numerous nozzles and cured almost instantly with e.g., UV light (Gopinathan *et al.* 2018; Gulcan *et al.*, 2021).
- Powder bed fusion, where powder (principally polymers and metals, but also pharmaceuticals) is fused or sintered with energy from a laser or electron beam in layers, and new powder rolled over the top for the next layer (Bhavar *et al.*, 2017; Bain 2019; Sing & Yeong 2020; Awad *et al.*, 2021).
- Sheet lamination, where paper, polymer or metal sheets are cut with lasers or cutting tools, and layered and bonded with welding or adhesives (Gibson *et al.*, 2021).
- Vat photo-polymerisation, where liquid photocuring resins in a vat (which may also contain ceramics or biomaterials) are cured with, typically, UV light produced and projected via various means (Bagheri & Jin 2019; Li *et al.*, 2020; Oezkan *et al.*, 2021).

5.3.1 Range of Materials

Of these seven principal methods, powder bed fusion and vat photo-polymerisation are the most common in industry, and material extrusion in education and home/hobby settings. Metal powder, polymer filaments, photopolymer resins and polymer powders were in descending order the largest market sectors by revenue in 2022, with polymer powders expected to grow to second by 2033 (Figure 25). The production of correctly sized and shaped particles for powder bed fusion 3D printing, is itself an increasingly rapidly growing industry and research area (Vock *et al.* 2019). These particles are mostly metal alloys (commonly of titanium, stainless steel, aluminium, and also cobalt-chrome and copper) and polymers (commonly nylon, TPU [thermoplastic polyurethane], polypropylene). In vat photo-polymerisation, the polymers are typically urethane dimethacrylate (UDMA), thiol monomers such as trimethylolpropane tris(3-mercaptopropionate) (TMPMP) or pentaerythritol tetra(3-mercaptopropionate) (PETMP), 3,4 epoxycyclohexane methyl or 3,4 epoxycyclohexylcarboxylate (EPOX) (Bagheri & Jin 2019). For material extrusion, a wide range of polymers is commercially available, including polylactic acid (PLA), acrylonitrile butadiene styrene (ABS), polyethylene terephthalate (PET or PETG), thermoplastic elastomers (TPE) including thermoplastic polyurethane (TPU) and thermoplastic copolyester (TPC), nylon (also known as polyamide (PA)), polycarbonate (PC), acrylonitrile styrene acrylate (ASA), polypropylene (PP), polycarbonate ABS alloy (PC-ABS), polymethyl methacrylate (PMMA), polyether ether ketone (PEEK) etc. (Dey *et al.* 2021). However, each of these principal methods of 3D printing, and the other four less common methods, allow for a wide range of materials and composites of multiple materials. Many metals and metal alloys are printable from powdered material beyond the standard titanium, steel and aluminium (Vock *et al.*, 2019). Ceramics are perhaps the most common of these, with a wide range of decorative and technical ceramic materials printable via a number of different techniques (Chen *et al.*, 2019). Construction materials include concrete (Buswell *et al.* 2018) and concrete replacements such as alkali activated geopolymers (Panda *et al.*, 2017), and





D2.1. Artificial fingerprinting for tracking raw material flows in complex supply chains.

can include supplementary materials (Nodehi *et al.*, 2022). Polymer composites with reinforcement materials such as carbon or glass fibres to improve the material characteristics are also commonly used (Sanei & Popescu 2020; Monticeli *et al.*, 2021). Similarly, minerals can be incorporated into 3D printed composites or directly printed (Gao *et al.*, 2021; Raut *et al.*, 2021; Tumer & Erbil, 2021; Wen *et al.*, 2021; Zhao *et al.*, 2023).

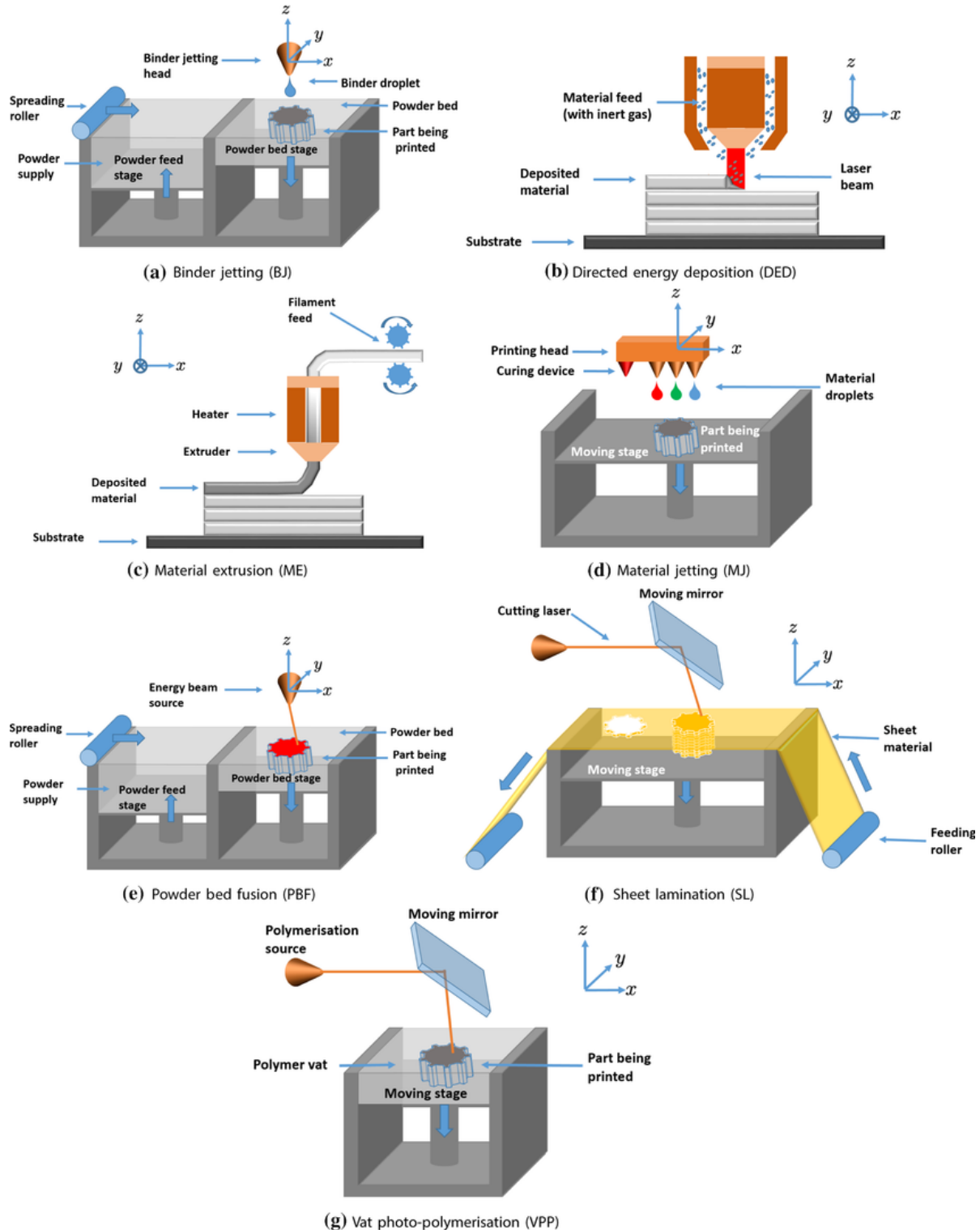


Figure 24: The seven principal methods of 3D printing, as defined in the ISO/ASTM 52900:2021 document on additive manufacturing terminology (source: ISO, 2021; de Pastre *et al.*, 2022).

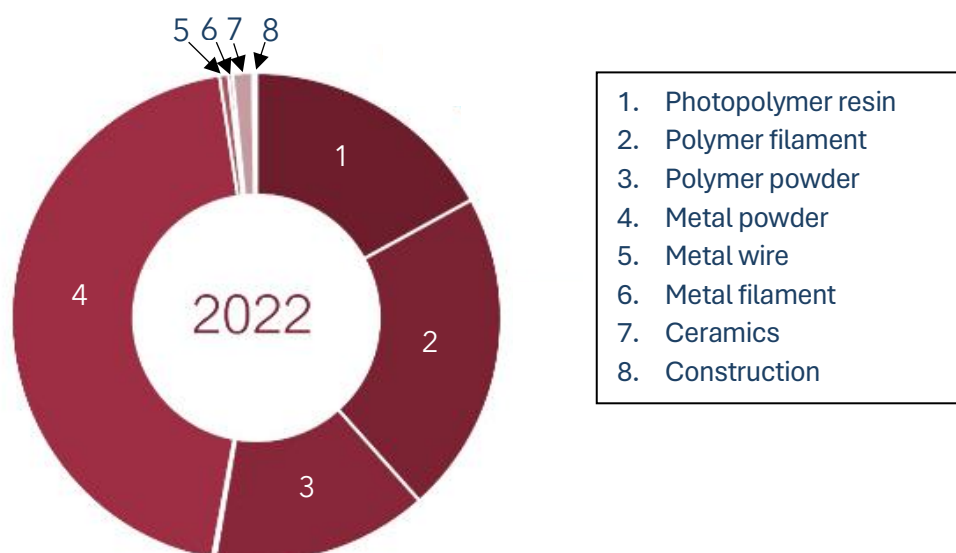


Figure 25: Size of the 3D printing materials market by revenue in 2022 (source: Dadhanian, 2023).

Complying with the requirements of the cobalt, lithium, graphite and rare earth element material value chains, and the stakeholders in the various steps of these value chains in the MaDiTraCe project, is potentially a difficult challenge. This is because of the problems with contamination due to the inclusion of materials in tracking particles (cf. subchapter 3.2), which may not be acceptable to the minerals and metals industries, either because of the materials involved or the perception of their inclusion. However, the wide range of materials available and previously 3D printed with should allow these issues to be overcome. Similarly, the ability to potentially 3D print with metals, minerals and composites with similar composition to the materials being traced, at some or all of the steps in their value chains, is a good reason to explore the use of this technology for material traceability in lithium-ion battery and rare earth element magnet production.

The durability requirements for producing tracking particles are somewhat uncertain, because it is currently unknown how early and how far along the value chain such particles will be needed. The results from isotopic fingerprint studies in other work packages within MaDiTraCe will help to clarify this, as will the questionnaire developed within this work package. Whether particle shape, the properties of additional included tracking materials, or both need to be retained, and for how many stages of the value chain, will also be investigated. The durability will be determined by the 3D printing materials and method used, the nature of any additional tracking materials added, and the processes the particles go through, some of which may involve high temperatures or strong chemical processing. Since the range of materials for 3D printing listed above ranges from basic polymers through technical polymers and metals to technical ceramics, it is likely that the base 3D printing material at least can be chosen to fulfil the durability requirements.

5.3.2 Size Range

3D printing can be used to make objects over a wide size-range, from cars, boats, and entire multi-story buildings down to the nano-scale (Figure 26). Different technologies and materials are suitable for the different scales. At the largest scale, meters, tens and hundreds of meters, 3D printed construction of buildings is accomplished using material extrusion from nozzles guided by either industrial-scale robotic arms or gantry installations, using



D2.1. Artificial fingerprinting for tracking raw material flows in complex supply chains.

concrete or concrete-like materials (Buswell *et al.*, 2018; Buswell *et al.*, 2022). Compared to other combinations of methods and materials, such 3D printing allows only a more limited range of 3D objects and geometries due to the material properties of the concrete or other cementitious materials, principally its setting time. Polymer printing has also been accomplished at large scale, using either the same industrial-scale robotic arms as used in concrete printing, oversized versions of existing polymer 3D printing machines, or gantry installations (Shah *et al.*, 2019; Pignatelli & Percoco 2022). Wire arc additive manufacturing (WAAM) allows medium-large scale metal 3D printing, but frequently requires additional machining and surface finishing due to the relatively large scale of the wires used (Rodrigues *et al.*, 2019). Sheet lamination can also be carried out at a medium-large scale (Gibson *et al.*, 2021). The other major 3D printing techniques are generally at small-medium scale, from the millimetres to tens of centimetres range for final objects and with resolutions of tens of microns to millimetres. While each of these has also been adapted for micro- and/or nano-scale 3D printing with resolutions in the single micrometre or tens to hundreds of nanometres range, additional methods such as two-photon polymerization (TPP), aerosol jet printing and electrohydrodynamic printing (EHDP) have particular benefits when printing at such small scale (Mao *et al.*, 2017; Lin *et al.*, 2023).

Similarly to the wide range of materials available for 3D printing with, the wide range of scales potentially allows for the tailoring of tracking materials produced by 3D printing for the MaDiTraCe project to the required scale, be it larger scale for single identification plates for materials in transit or storage, or the micro- or nano-scale for artificial taggant particles for in-material tracing and fraud protection.



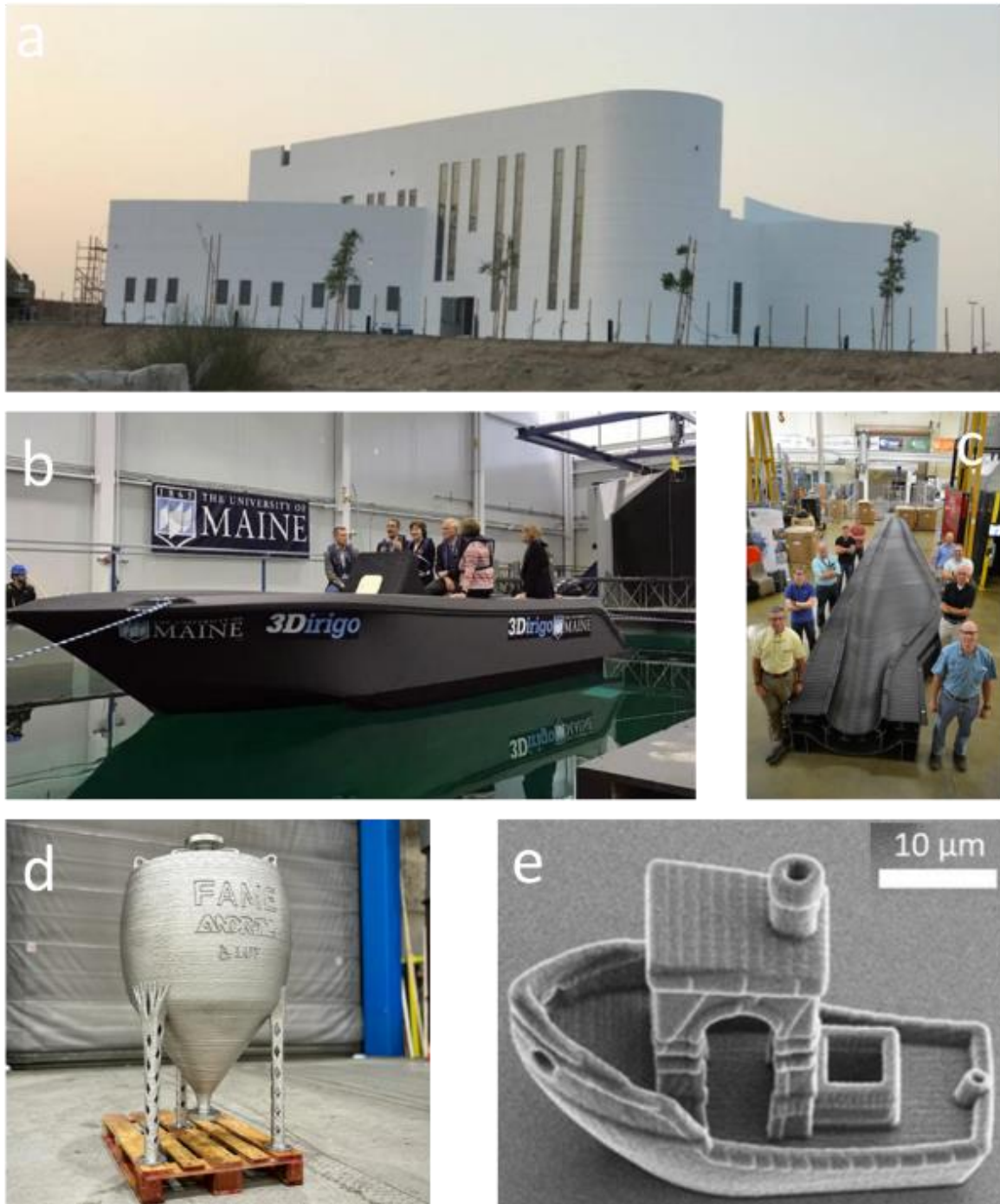


Figure 26: Size range of 3D printed objects. a) One of the largest 3D printed buildings, printed using concrete material extrusion with local materials as aggregate. b) 3D printed boat, printed using polymer material extrusion. c) 3D printed wind turbine blade mould, printed using polymer material extrusion. d) One of the largest 3D printed pressure chambers, approximately 1.5m tall, printed using metal WAAM. e) 3D printed 'benchy' boat benchmark print, printed using two photon polymerization, total length approximately 50 micrometres (source: Doherty *et al.*, 2020).

5.3.3 Prior Examples of Tracing and 3D Printing

There is literature already published that examines 3D printing in the context of traceability, though it is primarily focused on modifying 3D printed components to allow their tracing and as protection against counterfeiting (Chen, F. *et al.*, 2019; Sola *et al.*, 2021; Trinci and Sola 2023) rather than specifically manufacturing tracer objects via 3D printing. Concepts



D2.1. Artificial fingerprinting for tracking raw material flows in complex supply chains.

range from the relatively simple to the more complex. As above, most are designed around the requirement to be able to track and identify 3D printed parts themselves, though some of the techniques used could be adapted for tracking material flows in the battery and rare earth magnet supply chains in the MaDiTraCe project (Table 8).

Table 8: Summary of new 3D printable tracking technologies.

| 3D printing tracing method | Advantages | Disadvantages | Potential Application in MaDiTraCe |
|--|--|---|---|
| 2-photon polymerization with subsurface photoluminescent quantum dots | Sub-micron scale of encoded information | Polymer material may not be sufficiently durable | Encoding large information amounts into small particles subsurface |
| Aerosol jet 3D printing of microscale luminescent europium-doped yttrium oxide nanospheres | Easy surface encoding of large information amounts | Encoding on particle surface may not be durable, resolution may not be sufficiently small | Surface encoding of large particles/tracking tags for bulk bags etc |
| Photoluminescent and mechanoluminescent ZnS/CaZnOS-based ceramics | Durability of ceramic material, dual detection (photo- and mechano-luminescence) | Particle size currently too large | Tracing through processes requiring durability, inline particle detection during grinding |
| Material jetting nanoscale quantum dot random distribution | Low concentration fluorescence detection | Polymer material may not be sufficiently durable | Addition to more durable 3D printed particles |
| Multi-material metal magnetic encoding | Entirely internal information encoding | Magnetism may be undesirable for some value chains and processes | Metal printing of particles for durability and matching materials being traced |
| Rare earth element inclusion in multiple 3D printing methods | Easy detection at low ppm amounts | Rare earth elements may be undesirable for some value chains and processes | Addition to other 3D printed materials at low concentrations allows multiple 3D printing methods to be considered |
| Crystallographic texture control of metal and polymer 3D printed materials | Fully dense, internal, single material data encoding | More complicated detection methods required | Internal data encoding using relatively simpler 3D printing methods |



Radio-frequency identification (RFID) tags have been embedded into golf balls using 3D printing (Kantareddy *et al.*, 2017). In medicine, patient-specific targeted drug delivery was explored using 3D printed ‘intelligent implants’ combining local drug delivery devices with RFID technology. Passive RFID tags can be used to encode patient specific information that can be used to identify the presence of an implant and the details of the drug delivery it is facilitating. Four methods of 3D printing were studied, namely material extrusion, vat photo-polymerisation, binder jetting and powder bed fusion (Akmal *et al.*, 2018). In the food packaging industry, optical barcodes were transformed into RFID tags using 3D printing so that both techniques can be used in parallel (Catarinucci *et al.* 2020). In the pharmaceuticals industry, traceability was investigated using 2D inkjet printing to print QR codes onto 3D printed drug loaded tablets (Trenfield *et al.*, 2019). 3D printed chipless RFID tags were produced using polymer material extrusion, relying on information encoded in inner voids of the tag that is retrieved via a plane wave interrogation system that provides energy that is scattered back to the reading system (Terranova *et al.*, 2020). Two-photon polymerization 3D printing incorporating photoluminescent nitrogen-doped carbon quantum dots below the surface of a tag enabled sub-micron scale patterned fluorescent information encoding, visible under UV illumination (Jaiswal *et al.*, 2021), see Figure 27. Binary digits were encoded on the surface of 3D printed drug tablets manufactured via material extrusion (by varying the layer thickness of internal layers of the print) and detected using a flatbed scanner (Windolf *et al.*, 2022).

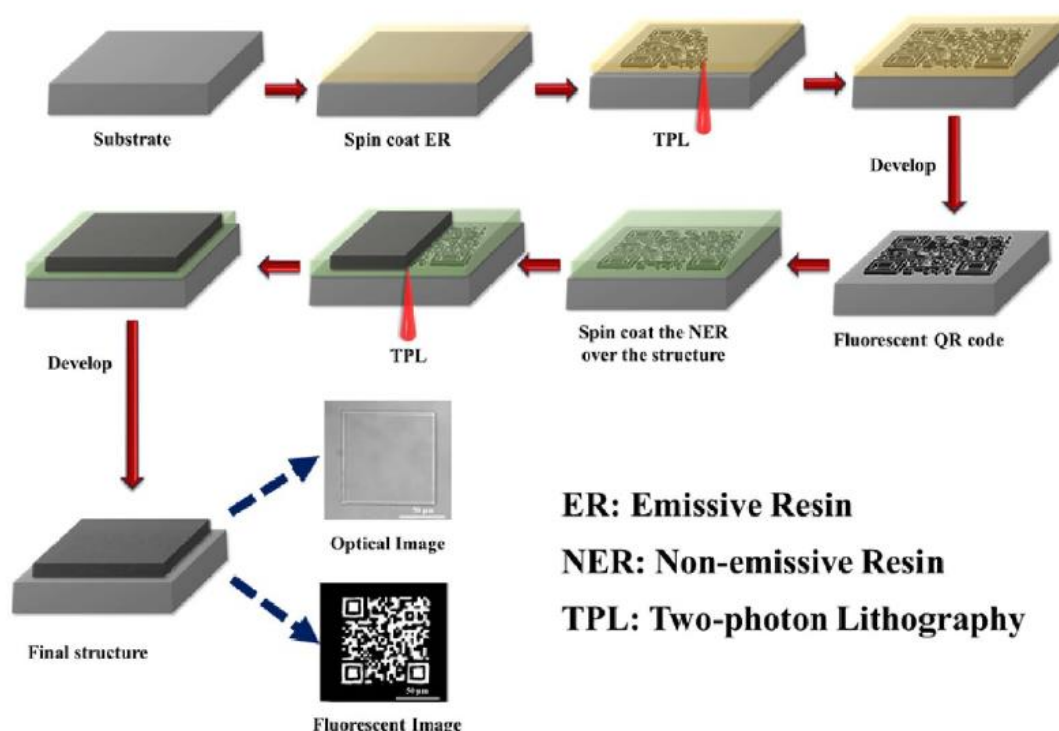


Figure 27: Two-photon lithography/two-photon polymerisation printing of sub-surface photoluminescent nitrogen-doped carbon quantum dots (source: Jaiswal *et al.*, 2021).

Castings made using the nobake sand casting process were modified using material jetting produced 3D printed codes to embed the information on the cast surface via direct part marking (Desavale *et al.*, 2022). In the food industry, the use of 3D printing in food



D2.1. Artificial fingerprinting for tracking raw material flows in complex supply chains.

traceability was explored using the infill of 3D printed food items to create data-embedding patterns within the food using airspace and/or secondary consumable materials, and decoding of the data using backlight illumination (Punpongsanon *et al.*, 2022). Aerosol jet 3D printing has been used to create microscale luminescent patterns of europium-doped yttrium oxide at relatively low temperatures, suitable for traceability and anti-counterfeiting use via photoluminescence spectral analysis (Lin *et al.*, 2023), see Figure 28. Photoluminescent and mechanoluminescent ZnS/CaZnOS-based ceramics were 3D printed using vat photopolymerisation, such that both irradiation and mechanical force result in the objects producing luminescence, with possible applications to anti-counterfeiting mentioned (Wang *et al.*, 2023), see Figure 28.

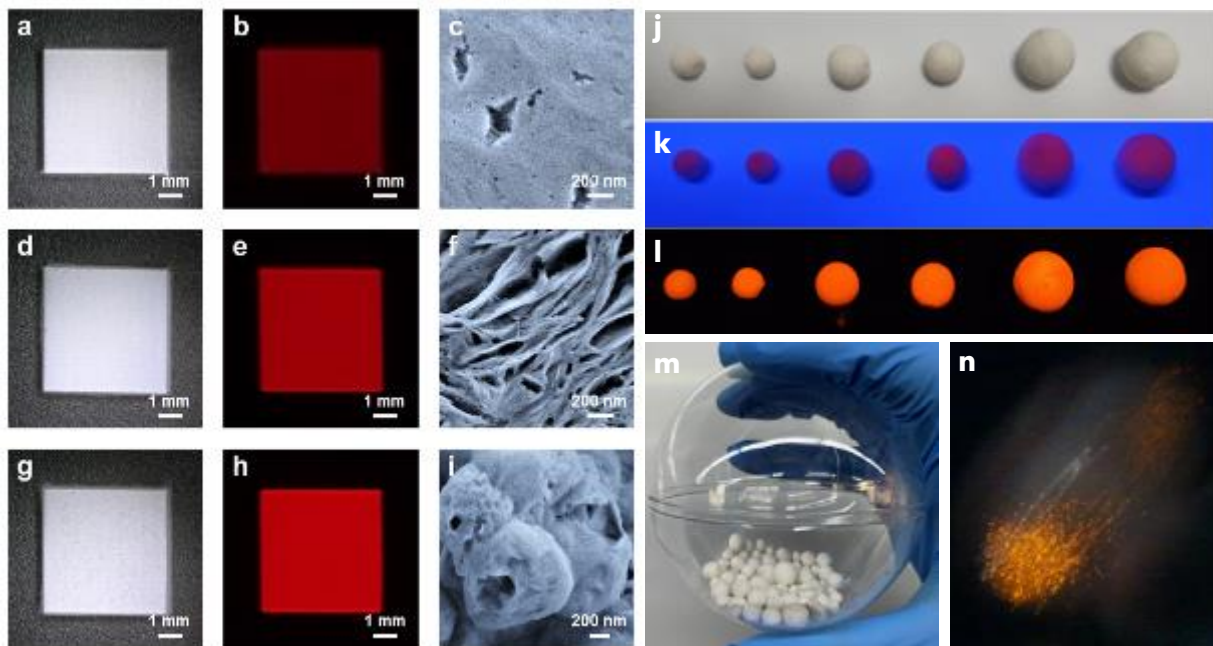


Figure 28: (a-i) Photos, UV luminescence images, and SEM images of aerosol jet 3D printed nanospheres, with g-i deposited at higher temperatures than a-f and producing predominantly spherical and highly luminescent nanosphere structures (source: Lin *et al.*, 2023). (j-n): Photoluminescent and mechanoluminescent ZnS/CaZnOS-based 3D printed ceramic spheres; j - photo, k - 290nm photoluminescence, l - 339nm photoluminescence, m - photo of spheres in plastic ball, n - mechanoluminescence of spheres agitated inside plastic ball in dark (source: Wang *et al.*, 2023).

In the identification and tracking of 3D printed parts, nanoscale quantum dots were added as suspensions in photopolymer materials using material jetting. These were detected at low concentrations when embedded within three dimensional objects using fluorescent microscopy, and their microscale random distribution used as the authentication data (Ivanova *et al.*, 2014). This random distribution represents physical unclonable functions (PUFs) (Arppe & Sørensen, 2017), as outlined in section 4.2.3.9 above. Chemical taggants have been incorporated into directed energy deposition 3D printed objects using a multi-material system, and detected using X-ray fluorescence spectroscopy (Flank *et al.*, 2017). Air pockets introduced internally within 3D printed objects such that they are invisible by eye but visible via computational imaging were used for encoding information (Li *et al.* 2017).

Quick response (QR) codes have been introduced internally in 3D printed components produced by powder bed fusion by incorporating multiple metallic materials in one object,



in this case copper alloy within a stainless-steel object. Surface temperature, 2D X-ray imaging and X-ray fluorescence were used to identify the codes within the printed objects (Wei *et al.* 2018), see Figure 29. In a separate study, QR codes were embedded into parts using contrasting materials or materials and air. The QR code was printed internally, and split across multiple layers of the print, using a range of 3D printing techniques including material extrusion, material jetting and powder bed fusion. X-ray Computer Tomographic (XCT) imaging was used to scan the code non-destructively inside the 3D printed object (Chen *et al.* 2018). The internally printed QR code was subjected to further obfuscation by increasing the number of print layers it was spread across (up to 23), increasing the number of parts it was split into (up to 191), rotating the code to a plane not normal to the build plate, and further obscuring by incorporating a second false QR code at a conventional orientation (Chen, F. *et al.* 2019). Layer thickness was varied for small internal regions of material extrusion 3D printed objects, in order to produce a binary encoding pattern on the surface (Delmotte *et al.* 2019). Optical barcodes within 3D printed objects made with polymer material extrusion and vat photopolymerisation techniques were simulated and printed for complex, non-trivial shapes (Maia *et al.* 2019).

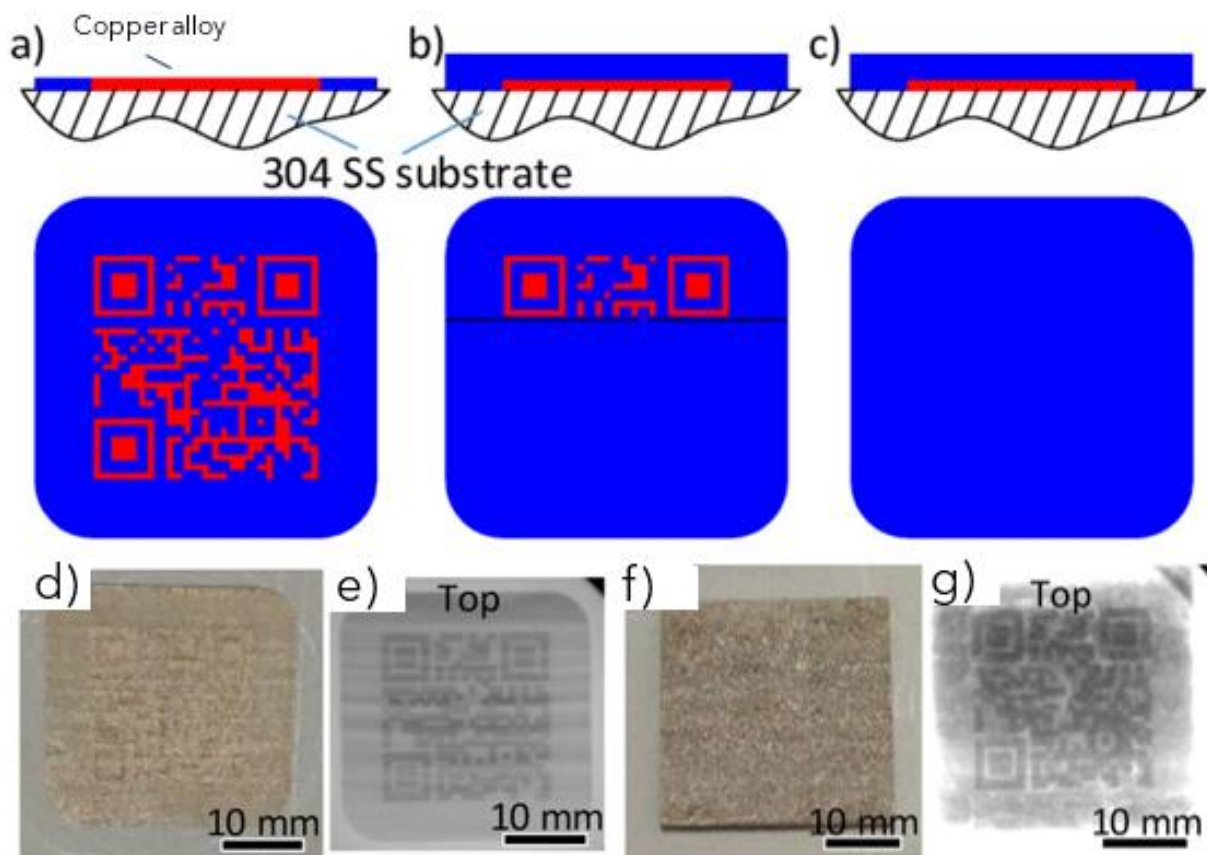


Figure 29: Multi-material powder bed fusion 3D printing of internal QR codes. (a-c): schematic of three levels of concealment (none, partial, full). (d-g): optical and X-ray images of none-concealed and fully concealed samples (source: Wei *et al.* 2018).

QR codes were embedded internally within polymer material extrusion 3D printed objects such that they could be read when light was shone through the object (Gultekin *et al.* 2019). Bar codes were embedded into 3D printed titanium medical tools using the powder bed



D2.1. Artificial fingerprinting for tracking raw material flows in complex supply chains.

fusion method, representing cavities containing non-molten titanium powder. These were read using three methods, eddy current measurements generally used for crack detection in metal products, ultrasonic imaging and X-ray computer tomographic imaging (XCT), which would likely also allow in vivo imaging of the embedded code if the titanium object is an implant (Matvieieva *et al.* 2020). Randomly generated volumetric porous structures were randomly defined internally in 3D printed stainless steel components manufactured using powder bed fusion, leading to density differences that could be imaged using eddy current reading. These again represent physical unclonable functions (PUFs). Similarly, magnetic permeability was modified using multi-material directed energy deposition 3D printing of magnetically soft low carbon steel and paramagnetic steel, again producing differences that could be identified using eddy current reading (Eisenbarth *et al.* 2020), see Figure 30. The use of magnetic property grading in 3D printed components for coding information has been investigated. Using direct energy deposition 3D printing of non-magnetic 316L stainless steel, regions of ferromagnetic 430 or 17-4PH stainless steels were embedded. Magnetic flux normal to the object surface was recorded as an intensity map, and it was suggested that magnetic barcodes or QR codes embedded could be placed within the 3D printed object using these techniques (Salas *et al.* 2022), see Figure 31.

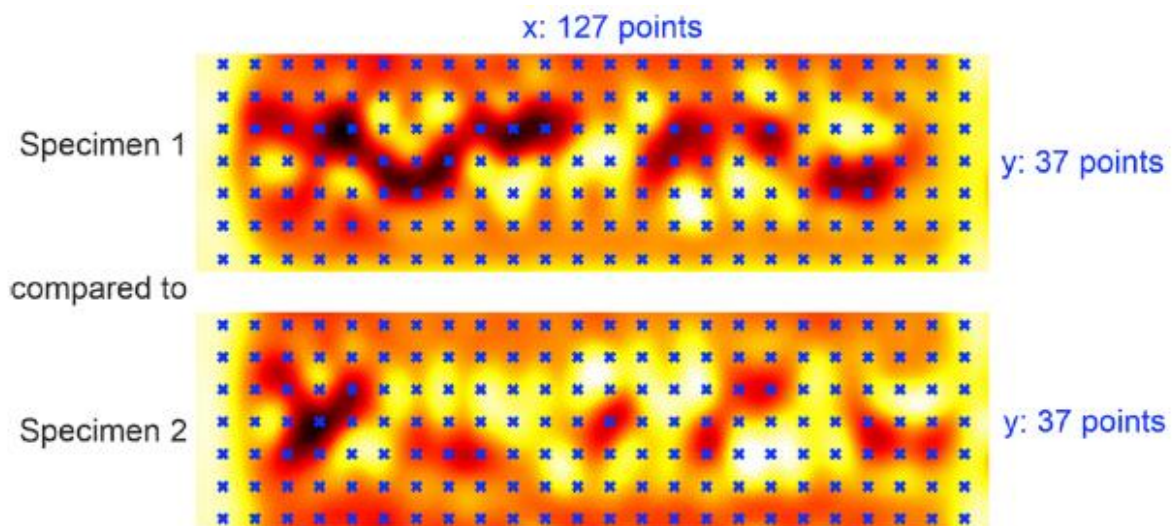


Figure 30: Magnetic permeability differences in directed energy deposition multi-material steel 3D printing revealed by eddy current reading. Grid can be used for comparison and individual coding (source: Eisenbarth *et al.* 2020).

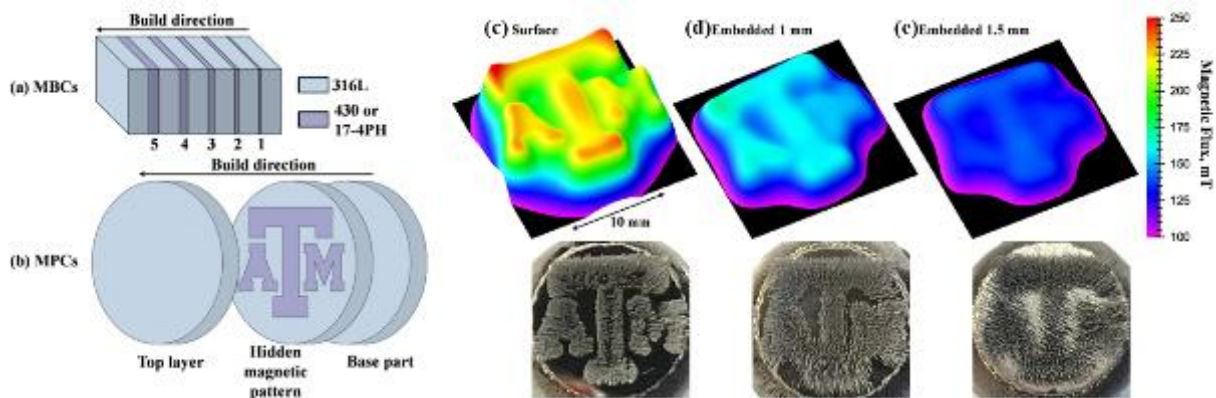


Figure 31: Ferromagnetic multi-material steel directed energy deposition 3D printing of internally coded information. a) Schematic for MBC's – magnetic band composites of non-magnetic 316L and magnetic 430 steel. b) Schematic for MPC's – magnetic pattern composites. c-e) magnetic flux (upper) and iron filing (lower) patterns for MPC's on c) surface, d) 1 mm embedded below surface, and e) 1.5 mm embedded below surface (source: Salas *et al.*, 2022).

The inclusion of particles including rare earth elements in 3D printing materials at parts per million levels, for detection via optical spectroscopy, has been applied to a wide range of 3D printing techniques (Doyle 2022). Linear barcodes and 2D QR codes were embedded into powder bed fusion 3D printed 316 L stainless steel objects by altering the local solidification conditions, allowing control of crystallographic texture, the size of constituent crystal grains, their lattice orientations and phases. Detection is via directional reflectance microscopy. These were the first fully dense bar/QR codes embedded into a single alloy – previous work required either pockets of porosity, with potentially detrimental effects on the mechanical strength of the object, or multiple materials (Sofinowski *et al.*, 2023), see Figure 32. One study aimed to control the degree of polymer crystallinity in material extrusion 3D printing by varying printing parameters such as extrusion temperature, build plate temperature and position in the sample measured, such that it could be measured using differential scanning calorimetry to determine if the object had the degree of crystallinity planned for its manufacture (Cox *et al.*, 2023).

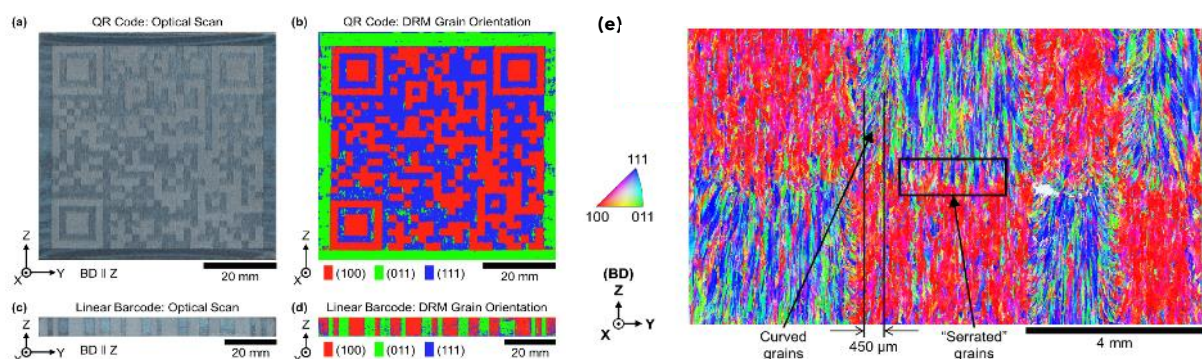


Figure 32: Single material powder bed fusion fully dense 3D printed 316 L stainless steel QR and bar codes via crystallographic texture. (a) optical scanned QR code, (b) directed reflectance microscopy QR code, (c) optical scanned barcode, (d) directed reflectance microscopy barcode, (e) electron backscatter diffraction patterning of data blocks/bits within QR code showing varying crystal grain textures and orientations (source: Sofinowski *et al.* 2023).



6 Conclusions

Artificial taggants use chemical or physical properties to track commodities within global commodities supply chains. Originally, taggants were developed in the 1970s, as an additive in explosives to serve as an identification taggant to track the sale of undetonated explosives. This technology has become further advanced since the 1980s and developed by organisations such as 3M Corporation and Microtrace Solutions LLC.

Taggants are used for brand protection and anti-counterfeiting purposes. The presence or absence of the taggant could alert attention or provide evidence in the event of a crime such as theft, adulteration or substitution. A range of taggants are now commercially available for the property marking of valuable items (e.g., vehicles and electronics), anti-counterfeiting (e.g., currency, clothing and pharmaceutical), tracking (e.g., hazardous chemicals, drugs and explosives) and monitoring (e.g., vehicles and watches).

Taggants technology is highly variable and complex and includes: inks and dyes, micron-sized SU8 (epoxy based negative photoresist) barcodes, cadmium selenide (CdSe), quantum dots (QDs) deposited onto sunflower pollen grains, silicon based photonic crystal, inks containing dispersed CdSe spheres, gold nanoparticles (AuNPs), silver nanoparticles (AgNPs), oxidised indole derivative on silicon nanoparticles (SiNPs), lanthanum-doped up-conversion nanoparticles (UCNP), physical unclonable functions (PUF) keys, carbon nanotubes (CNTs) and deoxyribonucleic acid (DNA).

Unfortunately, there are no existing taggants that might be directly applicable to MaDiTraCe, due to costs, the inclusion of components, which may not be acceptable to the minerals and metals industries, either because of the materials involved or the perception of their inclusion, insufficient data or complex and impracticable detection procedures. As such, existing taggant particles would have to be adapted or an entirely new artificial taggant particle developed. Potentially, silicon from gramineae plants (e.g., rice husks, sugarcane bagasse and wheat straws) could be altered into SiNPs (4 nm), exhibiting strong fluorescence under microwave radiation. This is recommended for experimental research for the MaDiTraCe project owing to its low-cost synthesis, abundance and easy accessibility. In addition, the technology outlined by PUF keys also warrant further investigations for the MaDiTraCe project. Further experimental work is also recommended on existing artificial taggant particles, including for example 'Microtaggant® Identification Particles (MIP)' produced by Microtrace Solutions, in the USA and artificial taggant particles produced by Tailorlux GmbH, in Germany. This research could identify the chemical composition and test the impact of size, geometry, morphology on dispersion to ensure a homogenous coverage and their detectability. Based on material availability and upstream supply chain information, we want to concentrate on Co supply chains during the R&D phase.

MaDiTraCe artificial taggants are envisaged to be: inert, free from metals that are forbidden or restricted in the minerals and metals industries, possess a high encoding capacity, non-toxic, non-radioactive and, easily and cost-effectively detectable.

A wide range of properties and advantages of 3D printing exist over traditional manufacturing including, (a) customisation and mass customisation of products, (b) complex internal and external structures otherwise not possible, (c) wide and growing range of size scales, (d) wide and growing range of materials, (e) reduced weight and waste, both with cost and environmental advantages. In terms of tracking and tracing, there is a





moderate, but growing literature detailing various methods, both for the tracking of 3D printed objects, and (less commonly) of using 3D printing for manufacture of tracking particles or objects to be applied in other industries. Some of these methods borrow materials and techniques from existing tracking methods, while some are unique to 3D printing due to the methodological requirements. Particles could also be produced with shapes designed for optimal dispersion in various levels of the minerals supply chain, a consideration no existing tracking particles have been produced with in mind. Certainly, 3D printing of materials, partially or wholly matching those being traced, and likely in combination with other tracking materials and techniques, holds promise for producing tracking particles for the kinds of multi-material and multi-stage tracking required in the lithium-ion battery and rare earth magnet supply chains being investigated in MaDiTraCe.





7 Bibliography

Akmal, J. S., Salmi, M., Mäkitie, A., Björkstrand, R., & Partanen, J. (2018). Implementation of industrial additive manufacturing: Intelligent implants and drug delivery systems. *Journal of functional biomaterials*, 9(3), 41.

Amnesty International. (2016). This is what we die for: Human rights abuses in the democratic republic of the congo power the global trade in cobalt. In Amnesty International. <https://www.amnesty.org/download/Documents/AFR6231832016ENGLISH.PDF>

Ang, X., Tey, J. Y., Yeo, W. H., & Shak, K. P. Y. (2023). A review on metallic and ceramic material extrusion method: Materials, rheology, and printing parameters. *Journal of Manufacturing Processes*, 90, 28-42.

Arppe, R., & Sørensen, T. J. (2017). Physical unclonable functions generated through chemical methods for anti-counterfeiting. *Nature Reviews Chemistry*, 1(4), Article 4. <https://doi.org/10.1038/s41570-017-0031>

Augé, T., Bailly, L., Bourbon, P., Guerrot, C., Viprey, L., & Telouk, P. (2015). Faisabilité technique d'une traçabilité physico-chimique de l'or de Guyane.

Auzel, F. (2004). Upconversion and Anti-Stokes Processes with f and d Ions in Solids. *Chemical Reviews*, 104(1), 139-174. <https://doi.org/10.1021/cr020357g>

Awad, A., Fina, F., Goyanes, A., Gaisford, S., & Basit, A. W. (2021). Advances in powder bed fusion 3D printing in drug delivery and healthcare. *Advanced Drug Delivery Reviews*, 174, 406-424.

Bai, L., Xie, Z., Wang, W., Yuan, C., Zhao, Y., Mu, Z., Zhong, Q., & Gu, Z. (2014). Bio-Inspired Vapor-Responsive Colloidal Photonic Crystal Patterns by Inkjet Printing. *ACS Nano*, 8(11), 11094-11100. <https://doi.org/10.1021/nn504659p>

Banu, S., Birtwell, S., Galitonov, G., Holmes, D., Zheludev, N., & Morgan, H. (2005). Microfabricated barcodes for particle identification. 252-255. <https://eprints.soton.ac.uk/261200/>

Bagheri, A., & Jin, J. (2019). Photopolymerization in 3D printing. *ACS Applied Polymer Materials*, 1(4), 593-611.

Bain, E. D. (2019). Polymer powder bed fusion additive manufacturing: Recent developments in materials, processes, and applications. *Polymer-Based Additive Manufacturing: Recent Developments*, 7-36.

Beiderbeck, D., Krüger, H., & Minshall, T. (2020). The future of additive manufacturing in sports. *21st Century Sports: How Technologies Will Change Sports in the Digital Age*, 111-132.

Benchmark. (2022). China's lithium ion battery supply chain dominance. Benchmark Source. <https://source.benchmarkminerals.com/article/infographic-chinas-lithium-ion-battery-supply-chain-dominance>

Bhavar, V., Kattire, P., Patil, V., Khot, S., Gujar, K., & Singh, R. (2017). A review on powder bed fusion technology of metal additive manufacturing. *Additive manufacturing handbook*, 251-253.





Bhuiyan, A. A. (n.d.). *Chapter 15 Molecular Luminescence Spectrometry*.

Bloomberg. (2022). The battle to break China's battery-making supremacy, in five charts. Bloomberg Professional Services. <https://www.bloomberg.com/professional/blog/the-battle-to-break-chinas-battery-making-supremacy-in-five-charts/>

Bünzli, J.-C. G. (2010). Lanthanide Luminescence for Biomedical Analyses and Imaging. *Chemical Reviews*, 110(5), 2729–2755. <https://doi.org/10.1021/cr900362e>

Buswell, R. A., De Silva, W. L., Jones, S. Z., & Dirrenberger, J. (2018). 3D printing using concrete extrusion: A roadmap for research. *Cement and Concrete Research*, 112, 37–49.

Buswell, R., Blanco, A., Cavalaro, S., & Kinnell, P. (Eds.). (2022). Third RILEM International Conference on Concrete and Digital Fabrication: Digital Concrete 2022 (Vol. 37). Springer Nature.

Butcher, A. R., & Corfe, I. J. (2021). Geo-inspired science, engineering, construction, art and design. *Geology Today*, 37(5), 184–193.

Calvão, F., & Archer, M. (2021). Digital extraction: Blockchain traceability in mineral supply chains. *Political Geography*, 87, 102381. <https://doi.org/10.1016/j.polgeo.2021.102381>

Catarinucci, L., Tedjini, S., Colella, R., Chietera, F. P., Zannas, K., & Kaddour, D. (2020, February). 3D-Printed barcodes as RFID tags. In 2020 International Workshop on Antenna Technology (iWAT) (pp. 1–4). IEEE.

Chen, Z. (2011). Global rare earth resources and scenarios of future rare earth industry. *Journal of Rare Earths*, 29(1), 1–6. [https://doi.org/10.1016/S1002-0721\(10\)60401-2](https://doi.org/10.1016/S1002-0721(10)60401-2)

Chen, F., Luo, Y., Tsoutsos, N. G., Maniatakos, M., Shahin, K., & Gupta, N. (2018). Embedded tracking codes in additive manufactured parts for product authentication. *Advanced Engineering Materials*, 21(4), 1800495.

Chen, F., Yu, J. H., & Gupta, N. (2019). Obfuscation of embedded codes in additive manufactured components for product authentication. *Advanced engineering materials*, 21(8), 1900146.

Chen, Z., Li, Z., Li, J., Liu, C., Lao, C., Fu, Y., & He, Y. (2019). 3D printing of ceramics: A review. *Journal of the European Ceramic Society*, 39(4), 661–687.

Chen, C., Wang, X., Wang, Y., Yang, D., Yao, F., Zhang, W., & Hu, D. (2020). Additive manufacturing of piezoelectric materials. *Advanced Functional Materials*, 30(52), 2005141.

Cox, J. R., Kipling, I., & Gibbons, G. J. (2023). Ensuring supply chain integrity for material extrusion 3D printed polymer parts. *Additive Manufacturing*, 62, 103403

Chen, G., Shen, J., Ohulchanskyy, T. Y., Patel, N. J., Kutikov, A., Li, Z., Song, J., Pandey, R. K., Ågren, H., Prasad, P. N., & Han, G. (2012). (α -NaYbF₄:Tm³⁺)/CaF₂ Core/Shell Nanoparticles with Efficient Near-Infrared to Near-Infrared Upconversion for High-Contrast Deep Tissue Bioimaging. *ACS Nano*, 6(9), 8280–8287. <https://doi.org/10.1021/nn302972r>

Dade, M. Wallmach, & Laugier, O. (2022). Detailed microparticle analysis providing process relevant chemical and microtextural insights into the black mass. *Minerals* 2022, 12, 119. <https://doi.org/10.3390/min12020119>





D2.1. Artificial fingerprinting for tracking raw material flows in complex supply chains.

Dadhania, S. (2023). 3D Printing and Additive Manufacturing 2023-2033: Technology and Market Outlook. IDTechEx Research Report: <https://www.idtechex.com/en/research-report/3d-printing-and-additive-manufacturing-2023-2033-technology-and-market-outlook/882>

Dalpé, C., Hudon, P., Ballantyne, D. J., Williams, D., & Marcotte, D. (2010). Trace element analysis of rough diamond by LA-ICP-MS: A case of source discrimination? *Journal of Forensic Sciences*, 55(6), 1443-1456. <https://doi.org/10.1111/j.1556-4029.2010.01509.x>

Darton Commodities. (2023). Cobalt Market Review 2023.

De Pastre, M. A., Quinsat, Y., & Lartigue, C. (2022). Effects of additive manufacturing processes on part defects and properties: a classification review. *International Journal on Interactive Design and Manufacturing (IJIDeM)*, 16(4), 1471-1496.

Dehaine, Q., Filippov, L. O., Filippova, I. V., Tijsseling, L. T., & Glass, H. J. (2021). Novel approach for processing complex carbonate-rich copper-cobalt mixed ores via reverse flotation. *Minerals Engineering*, 161, 106710. <https://doi.org/10.1016/j.mineng.2020.106710>

Dehaine, Q., Michaux, S. P., Pokki, J., Kivinen, M., & Butcher, A. R. (2020). Battery minerals from Finland: Improving the supply chain for the EU battery industry using a metallurgical approach. *European Geologist Journal*, 49, 5-11. <https://doi.org/10.5281/zenodo.3938855>

Dehaine, Q., Tijsseling, L. T., Glass, H. J., Törmänen, T., & Butcher, A. R. (2021). Geometallurgy of cobalt ores: A review. *Minerals Engineering*, 160, 106656. <https://doi.org/10.1016/j.mineng.2020.106656>

Delmotte, A., Tanaka, K., Kubo, H., Funatomi, T., & Mukaigawa, Y. (2019). Blind watermarking for 3-D printed objects by locally modifying layer thickness. *IEEE Transactions on Multimedia*, 22(11), 2780-2791.

Desaulty, A.-M., Monfort Climent, D., Lefebvre, G., Cristiano-Tassi, A., Peralta, D., Perret, S., Urban, A., & Guerrot, C. (2022). Tracing the origin of lithium in Li-ion batteries using lithium isotopes. *Nature Communications*, 13(1), 4172. <https://doi.org/10.1038/s41467-022-31850-y>

Desavale, S., Ameri, F., Trueba, L., & Igveh, O. (2022). Direct Part Marking (DPM) Supported by Additively Manufactured Tags to Improve the Traceability of Castings. In IFIP

Dey, A., Roan Eagle, I. N., & Yodo, N. (2021). A review on filament materials for fused filament fabrication. *Journal of manufacturing and materials processing*, 5(3), 69.

Doherty, R. P., Varkevisser, T., Teunisse, M., Hoecht, J., Ketsetzi, S., Ouhajji, S., & Kraft, D. J. (2020). Catalytically propelled 3D printed colloidal microswimmers. *Soft Matter*, 16(46), 10463-10469.

Donnelly, L. J. (2022). Black Mass and the Battery Revolution: An Overview of the Experimental Research Conducted by Alfred H Knight. *Rho Motion Magazine*, Q2, 2022, 8-12.

Donnelly, L. J., Pirrie, D., Power, M., Corfe, I. J., Kuva, J., Lukkari, S., Lahaye, Y, Xun, L. & Butcher, A. (2021a). The sampling and phase characterisation of black mass. 10th World





Conference on Sampling and Blending, Kristiansand, Norway, 31 May to 2 June 2022. Program & Abstracts, 58.

Donnelly, L.J., Pirrie, D., Power, M., Corfe, I., Kuva, J., Lukkari, S., Lahaye, Y. & Butcher, A. (2021b). The Phase Characteristics and Textural Variability of Black Mass. 26th International Congress for Battery Recycling. 22-24 September 2021 Geneva, Switzerland. Abstract only.

Donnelly, L.J., Pirrie, D., Corfe, I., Michaux, S. P. & Butcher, A. (2021c). The Phase Characterization of Black Mass and its Commercial Implications in the Circular Economy. 20th International Automobile Recycling Congress. 23-25 June 2021 Geneva, Switzerland. Abstract only.

Donnelly, L. J., Pirrie, D., Power, M., Corfe, I. Kuva, J., Lukkari, S., Lahaye, & Xuan, L., Butcher, A. 2022. The Phase Characterisation of Black Mass Using Manual, Automated and Interactive Scanning Electron Microscopy with Linked Energy Dispersive Spectrometers (SEM-EDS), X-ray Computed Tomography (Micro-CT) and Laser Ablation Mass Spectrometry (LA-ICP-MS). Abstract for the 10th World Conference on Sampling and Blending, Kristiansand, Norway, 31 May to 2 June 2022, <https://wcsb10.com/>

Donnelly, L., Pirrie, D., Power, M., Corfe, I., Kuva, J., Lukkari, S., Lahaye, Y., Liu, X., Dehaine, Q., Jolis, E. M., & Butcher, A. (2023). The Recycling of End-of-Life Lithium-Ion Batteries and the Phase Characterisation of Black Mass. *Recycling*, 8(4), 59. <https://doi.org/10.3390/recycling8040059>

Donnelly, L. J. and Ruffell, A. 2021. Emerging applications of forensic geology. In: Donnelly, L. J., Pirrie, D., Harrison, M., Ruffell, A. and Dawson, L. (eds). *A Guide to Forensic Geology*. Geological Society, London, 171-187, <https://doi.org/10.1144/GFG.8>

Doyle, S. (2022). Unique tags for printed parts. *Engineering & Technology*, 17(10), 25-25.

Duong, B., Liu, H., Li, C., Deng, W., Ma, L., & Su, M. (2014). Printed Multilayer Microtaggers with Phase Change Nanoparticles for Enhanced Labeling Security. *ACS Applied Materials & Interfaces*, 6(11), 8909-8912. <https://doi.org/10.1021/am501668x>

Edinburgh Instruments, 2023. Granite. (n.d.). Photon Upconversion, Triplet Annihilation, Excited State Absorption. Edinburgh Instruments. Retrieved 29 August 2023, <https://www.edinst.com/blog/photon-upconversion/>

Eisenbarth, D., Stoll, P., Klahn, C., Heinis, T. B., Meboldt, M., & Wegener, K. (2020). Unique coding for authentication and anti-counterfeiting by controlled and random process variation in L-PBF and L-DED. *Additive Manufacturing*, 35, 101298.

Elements. (2023a). Visualizing China's Dominance in Battery Manufacturing (2022-2027). Visual Capitalist. <https://www.visualcapitalist.com/chinas-dominance-in-battery-manufacturing/>

Elements. (2023b). Where Are Clean Energy Technologies Manufactured? Visual Capitalist. <https://elements.visualcapitalist.com/where-are-clean-energy-technologies-manufactured/>

European Commission. (2020). Regulation of the European Parliament and of the Council concerning batteries and waste batteries, repealing. Directive 2006/66/EC and amending Regulation (EU) No 2019/1020. <https://eur-lex.europa.eu/legal-content/EN/TXT/?uri=CELEX%3A52020PC0798>





D2.1. Artificial fingerprinting for tracking raw material flows in complex supply chains.

Flank, S., Nassar, A. R., Simpson, T. W., Valentine, N., & Elburn, E. (2017). Fast authentication of metal additive manufacturing. *3D Printing and Additive Manufacturing*, 4(3), 143-148.

Gäbler, H. E., Schink, W., & Gawronski, T. (2020). Data evaluation for cassiterite and coltan fingerprinting. *Minerals*, 10(10), 1-15. <https://doi.org/10.3390/min10100926>

Gäbler, H.-E., Melcher, F., Graupner, T., Bahr, A., Sitnikova, M. A., Henjes-Kunst, F., Oberthür, T., Brätz, H., & Gerdes, A. (2011). Speeding Up the Analytical Workflow for Coltan Fingerprinting by an Integrated Mineral Liberation Analysis/LA-ICP-MS Approach. *Geostandards and Geoanalytical Research*, 35(4), 431-448. <https://doi.org/10.1111/j.1751-908X.2011.00110.x>

Gao, Y. T., Wu, T. H., & Zhou, Y. (2021). Application and prospective of 3D printing in rock mechanics: A review. *International Journal of Minerals, Metallurgy and Materials*, 28, 1-17.

Garzaniti, N., Golkar, A., & Fortin, C. (2018). Optimization of multi-part 3D printing build strategies for lean product and process development. In *Product Lifecycle Management to Support Industry 4.0: 15th IFIP WG 5.1 International Conference, PLM 2018, Turin, Italy, July 2-4, 2018, Proceedings 15* (pp. 488-497). Springer International Publishing.

Gibson, I., Rosen, D., Stucker, B., Khorasani, M., Gibson, I., Rosen, D., ... & Khorasani, M. (2021). Sheet lamination. *Additive Manufacturing Technologies*, 253-283.

Goh, G. D., Yap, Y. L., Tan, H. K. J., Sing, S. L., Goh, G. L., & Yeong, W. Y. (2020). Process-structure-properties in polymer additive manufacturing via material extrusion: A review. *Critical Reviews in Solid State and Materials Sciences*, 45(2), 113-133.

Gooch, J., Daniel, B., Abbate, V., & Frascione, N. (2016). Taggant materials in forensic science: A review. *TrAC Trends in Analytical Chemistry*, 83, 49-54. <https://doi.org/10.1016/j.trac.2016.08.003>

Gooch, J., Goh, H., Daniel, B., Abbate, V., & Frascione, N. (2016). Monitoring Criminal Activity through Invisible Fluorescent "Peptide Coding" Taggants. *Analytical Chemistry*, 88(8), 4456-4460. <https://doi.org/10.1021/acs.analchem.6b00263>

Gooch, J., Koh, C., Daniel, B., Abbate, V., & Frascione, N. (2015). Establishing evidence of contact transfer in criminal investigation by a novel 'peptide coding' reagent. *Talanta*, 144, 1065-1069. <https://doi.org/10.1016/j.talanta.2015.07.014>

Gopinathan, J., & Noh, I. (2018). Recent trends in bioinks for 3D printing. *Biomaterials research*, 22, 1-15.

Griffiths, C. A., Howarth, J., De Almeida-Rowbotham, G., Rees, A., & Kerton, R. (2016). A design of experiments approach for the optimisation of energy and waste during the production of parts manufactured by 3D printing. *Journal of cleaner production*, 139, 74-85.

Gülcan, O., Günaydın, K., & Tamer, A. (2021). The state of the art of material jetting—a critical review. *Polymers*, 13(16), 2829.

Gültekin, S., Ural, A., & Yaman, U. (2019). Embedding QR codes on the interior surfaces of FFF fabricated parts. *Procedia Manufacturing*, 39, 519-525.





Gupta, C. K., & Krishnamurthy, N. (2004). Extractive metallurgy of rare earths. CRC Press. http://books.google.com/books?hl=en&lr=&id=F0Bte_XhzoAC&oi=fnd&pg=PP1&dq=Extractive+metallurgy+of+rare+earths&ots=g13uanlCKm&sig=Vsw_MxOgZ1fg8GAR3ftKgx dEJ-c

Han, S., Qin, X., An, Z., Zhu, Y., Liang, L., Han, Y., Huang, W., & Liu, X. (2016). Multicolour synthesis in lanthanide-doped nanocrystals through cation exchange in water. *Nature Communications*, 7(1), Article 1. <https://doi.org/10.1038/ncomms13059>

Hickman, D. (2017). What are Fluorescence and Phosphorescence? *Chemistry Views*. https://www.chemistryviews.org/details/education/10468955/What_are_Fluorescence_and_Phosphorescence/

Hines, M. A., & Guyot-Sionnest, P. (1996). Synthesis and Characterization of Strongly Luminescing ZnS-Capped CdSe Nanocrystals. *The Journal of Physical Chemistry*, 100(2), 468-471. <https://doi.org/10.1021/jp9530562>

Hyun, D. C., Levinson, N. S., Jeong, U., & Xia, Y. (2014). Emerging Applications of Phase-Change Materials (PCMs): Teaching an Old Dog New Tricks. *Angewandte Chemie International Edition*, 53(15), 3780-3795. <https://doi.org/10.1002/anie.201305201>

IEA. (2022). Global Supply Chains of EV Batteries. 68. <https://www.iea.org/reports/global-supply-chains-of-ev-batteries>

IEA. (2023). Energy Technology Perspectives. In *Energy Technology Perspectives*. <https://doi.org/10.1787/9789264109834-en>

International Conference on Advances in Production Management Systems (pp. 244-251). Springer Nature Switzerland.

International Organization for Standardization (2021). Additive manufacturing – General principles – Fundamentals and vocabulary. (ISO/ASTM Standard No. 52900:2021). Retrieved from <https://www.iso.org/standard/74514.html>

ISEAL. (2016). Chain of Custody: Models and Definitions. https://www.isealalliance.org/sites/default/files/resource/2017-11/ISEAL_Chain_of_Custody_Models_Guidance_September_2016.pdf

Ivanova, O., Elliott, A., Campbell, T., & Williams, C. B. (2014). Unclonable security features for additive manufacturing. *Additive Manufacturing*, 1, 24-31.

Jaiswal, A., Rani, S., Singh, G. P., Saxena, S., & Shukla, S. (2021). Two-photon lithography of fluorescence-encoded quick-read micro-code for anti-counterfeiting applications. *Journal of Physics: Photonics*, 3(3), 034021.

Jara, A. D., Betemariam, A., Woldetinsae, G., & Kim, J. Y. (2019). Purification, application and current market trend of natural graphite: A review. In *International Journal of Mining Science and Technology* (Vol. 29, Issue 5, pp. 671-689). China University of Mining and Technology. <https://doi.org/10.1016/j.ijmst.2019.04.003>

Jiang, K., Zhang, L., Lu, J., Xu, C., Cai, C., & Lin, H. (2016). Triple-Mode Emission of Carbon Dots: Applications for Advanced Anti-Counterfeiting. *Angewandte Chemie International Edition*, 55(25), 7231-7235. <https://doi.org/10.1002/anie.201602445>





Jones, D. (1974). Joyful three-dimensional doodling. *New Scientist*, 03/10/1974.

Jordan, J. M. (2019). Additive manufacturing ("3D printing") and the future of organizational design: some early notes from the field. *Journal of Organization Design*, 8(1), 5.

Jordens, A., Cheng, Y. P., & Waters, K. E. (2013). A review of the beneficiation of rare earth element-bearing minerals. *Minerals Engineering*, 41, 97–114.
<https://doi.org/10.1016/j.mineng.2012.10.017>

Kaikkonen, H., Kivinen, M., Dehaine, Q., Pokki, J., Eerola, T., Bertelli, M., & Friedrichs, P. (2022). Traceability methods for cobalt, lithium, and graphite production in battery supply chains. https://tupa.gtk.fi/raportti/arkisto/20_2022.pdf

Kang, H., Lee, J. W., & Nam, Y. (2018). Inkjet-Printed Multiwavelength Thermoplasmonic Images for Anticounterfeiting Applications. *ACS Applied Materials & Interfaces*, 10(7), 6764–6771. <https://doi.org/10.1021/acsami.7b19342>

Kantareddy, S. N. R., Bhattacharyya, R., & Sarma, S. (2017, May). Towards low-cost object tracking: Embedded RFID in golf balls using 3D printed masks. In *2017 IEEE International Conference on RFID (RFID)* (pp. 137–143). IEEE.

Keegan, E., Richter, S., Kelly, I., Wong, H., Gadd, P., Kuehn, H., & Alonso-Munoz, A. (2008). The provenance of Australian uranium ore concentrates by elemental and isotopic analysis. *Applied Geochemistry*, 23(4), 765–777. <https://doi.org/10.1016/j.apgeochem.2007.12.004>

Keegan, E., Wallenius, M., Mayer, K., Varga, Z., & Rasmussen, G. (2012). Attribution of uranium ore concentrates using elemental and anionic data. *Applied Geochemistry*, 27(8), 1600–1609. <https://doi.org/10.1016/j.apgeochem.2012.05.009>

Kydd, P. H. (1982). U.S. Patent No. 4,359,353. Washington, DC: U.S. Patent and Trademark Office.

Li, D., Nair, A. S., Nayar, S. K., & Zheng, C. (2017, October). Aircode: Unobtrusive physical tags for digital fabrication. In *Proceedings of the 30th annual ACM symposium on user interface software and technology* (pp. 449–460).

Li, F., Wang, X., Xia, Z., Pan, C., & Liu, Q. (2017). Photoluminescence Tuning in Stretchable PDMS Film Grafted Doped Core/Multishell Quantum Dots for Anticounterfeiting. *Advanced Functional Materials*, 27(17), 1700051. <https://doi.org/10.1002/adfm.201700051>

Li, Q., Chen, F., Kang, J., Su, J., Huang, F., Wang, P., Yang, X., & Hou, Y. (2021). Physical Unclonable Anticounterfeiting Electrodes Enabled by Spontaneously Formed Plasmonic Core-Shell Nanoparticles for Traceable Electronics. *Advanced Functional Materials*, 31(18), 2010537. <https://doi.org/10.1002/adfm.202010537>

Li, W., Mille, L. S., Robledo, J. A., Uribe, T., Huerta, V., & Zhang, Y. S. (2020). Recent advances in formulating and processing biomaterial inks for vat polymerization-based 3D printing. *Advanced healthcare materials*, 9(15), 2000156.

Li, Q., He, Y., Chang, J., Wang, L., Chen, H., Tan, Y.-W., Wang, H., & Shao, Z. (2013). Surface-Modified Silicon Nanoparticles with Ultrabright Photoluminescence and Single-Exponential Decay for Nanoscale Fluorescence Lifetime Imaging of Temperature. *Journal of the American Chemical Society*, 135(40), 14924–14927. <https://doi.org/10.1021/ja407508v>





Lin, A., Zhang, Y., Zhao, D., Wu, Y., Wang, S., Li, J., ... & Gu, F. (2023). Flexible droplet printing of prominently luminescent patterns of europium-doped yttrium oxide nanospheres. *Additive Manufacturing*, 63, 103412.

Lin, Q.-Y., Palacios, E., Zhou, W., Li, Z., Mason, J. A., Liu, Z., Lin, H., Chen, P.-C., Dravid, V. P., Aydin, K., & Mirkin, C. A. (2018). DNA-Mediated Size-Selective Nanoparticle Assembly for Multiplexed Surface Encoding. *Nano Letters*, 18(4), 2645-2649. <https://doi.org/10.1021/acs.nanolett.8b00509>

Li, R., Zhang, Y., Tan, J., Wan, J., Guo, J., & Wang, C. (2016). Dual-Mode Encoded Magnetic Composite Microsphere Based on Fluorescence Reporters and Raman Probes as Covert Tag for Anticounterfeiting Applications. *ACS Applied Materials & Interfaces*, 8(14), 9384-9394. <https://doi.org/10.1021/acsami.6b02359>

Liu, N., Huo, K., McDowell, M. T., Zhao, J., & Cui, Y. (2013). Rice husks as a sustainable source of nanostructured silicon for high-performance Li-ion battery anodes. *Scientific Reports*, 3(1), Article 1. <https://doi.org/10.1038/srep01919>

Lyu, Y., Fang, Y., Miao, Q., Zhen, X., Ding, D., & Pu, K. (2016). Intraparticle Molecular Orbital Engineering of Semiconducting Polymer Nanoparticles as Amplified Theranostics for in Vivo Photoacoustic Imaging and Photothermal Therapy. *ACS Nano*, 10(4), 4472-4481. <https://doi.org/10.1021/acs.nano.6b00168>

Lyu, Y., Zhen, X., Miao, Y., & Pu, K. (2017). Reaction-Based Semiconducting Polymer Nanoprobes for Photoacoustic Imaging of Protein Sulfenic Acids. *ACS Nano*, 11(1), 358-367. <https://doi.org/10.1021/acs.nano.6b05949>

Maia, H. T., Li, D., Yang, Y., & Zheng, C. (2019). LayerCode: Optical barcodes for 3D printed shapes. *ACM Transactions on Graphics (TOG)*, 38(4), 1-14.

Mancini, L., Eslava, N. A., Traverso, M., & Mathieux, F. (2020). Responsible and sustainable sourcing of battery raw materials. In JRC Technical Report. <https://doi.org/10.2760/562951>

Martinez, D. W., Espino, M. T., Cascolan, H. M., Crisostomo, J. L., & Dizon, J. R. C. (2022). A comprehensive review on the application of 3D printing in the aerospace industry. *Key engineering materials*, 913, 27-34.

Matvieieva, N., Neupetsch, C., Oettel, M., Makdani, V., & Drossel, W. G. (2020). A novel approach for increasing the traceability of 3D printed medical products. *Current Directions in Biomedical Engineering*, 6(3), 315-318.

Monticeli, F., Neves, R., Ornaghi, H., & Almeida, J. (2021). A systematic review on high-performance fiber-reinforced 3D printed thermoset composites. *Polymer Composites*, 42, 3702-3715.

Martyna, A., Gäbler, H.-E. E., Bahr, A., & Zadora, G. (2018). Geochemical wolframite fingerprinting – the likelihood ratio approach for laser ablation ICP-MS data. *Analytical and Bioanalytical Chemistry*, 410(13), 3073-3091. <https://doi.org/10.1007/s00216-018-1007-9>

Melcher, F., Dietrich, V., & Gäbler, H. E. (2021). Analytical Proof of Origin for Raw Materials. *Minerals* 2021, Vol. 11, Page 461, 11(5), 461. <https://doi.org/10.3390/MIN11050461>



D2.1. Artificial fingerprinting for tracking raw material flows in complex supply chains.

Melcher, F., Sitnikova, M. A., Graupner, T., Martin, N., Oberthür, T., Henjes-kunst, F., Gäbler, E., Gerdes, A., Brätz, H., Davis, D. W., Dewaele, S., & Groves, D. I. (2008). Fingerprinting of conflict minerals: columbite-tantalite ("coltan") ores. *SGA News*, 23, 1-13.

Meng, F., McNeice, J., Zadeh, S. S., & Ghahreman, A. (2021). Review of Lithium Production and Recovery from Minerals, Brines, and Lithium-Ion Batteries. *Mineral Processing and Extractive Metallurgy Review*, 42(2), 123-141.

<https://doi.org/10.1080/08827508.2019.1668387>

Metalor (2021). Metalor and the University of Lausanne unveil a ground-breaking "Geoforensic Passport" to validate the origin of every gold doré. Press Release.

Mishra A., Khoshsima S., Tomše T., Podmiljšak B., Šturm S., Burkhardt C., Žužek K. (2023). Short-Loop Recycling of Nd-Fe-B Permanent Magnets: A Sustainable Solution for the RE₂Fe₁₄B Matrix Phase Recovery. *Materials*, 16, 6565. <https://doi.org/10.3390/ma16196565>

Mitchell, C., & Deady, E. (2021). Graphite resources, and their potential to support battery supply chains, in Africa - BGS Open Report OR/21/039.

Munk, L. A., Hynek, S. A., Bradley, D. C., Boutt, D., Labay, K., & Jochens, H. (2016). Lithium Brines: A Global Perspective. In *Rare Earth and Critical Elements in Ore Deposits*. Society of Economic Geologists. <https://doi.org/10.5382/Rev.18.14>

Nachal, N., Moses, J. A., Karthik, P., & Anandharamakrishnan, C. (2019). Applications of 3D printing in food processing. *Food Engineering Reviews*, 11(3), 123-141.

Nam, H., Song, K., Ha, D., & Kim, T. (2016). Inkjet Printing Based Mono-layered Photonic Crystal Patterning for Anti-counterfeiting Structural Colors. *Scientific Reports*, 6(1), Article 1. <https://doi.org/10.1038/srep30885>

Natan, M., Norton, S., Freeman, R., Penn, S., & Walton, I. (2007). U.S. Patent Application No. 11/674,597.).

<https://www.oecd-ilibrary.org/docserver/7536db96-en.pdf?expires=1694097236&id=id&accname=guest&checksum=A6E8B320E5694AA91EBBAA08D68724D8>

Ngo, T. D., Kashani, A., Imbalzano, G., Nguyen, K. T., & Hui, D. (2018). Additive manufacturing (3D printing): A review of materials, methods, applications and challenges. *Composites Part B: Engineering*, 143, 172-196.

Nodehi, M., Ozbakkaloglu, T., & Gholampour, A. (2022). Effect of supplementary cementitious materials on properties of 3D printed conventional and alkali-activated concrete: A review. *Automation in Construction*, 138, 104215.

OECD (2022): Free trade zones and illicit gold flows in Latin America and the Caribbean, OECD Business and Finance Policy Papers, OECD Publishing, Paris.

<https://doi.org/10.1787/7536db96-en>.

Oezkan, B., Sameni, F., Karmel, S., Engstrøm, D. S., & Sabet, E. (2021). A systematic study of vat-polymerization binders with potential use in the ceramic suspension 3D printing. *Additive Manufacturing*, 47, 102225.

Park, J., & Moon, J. (2006). Control of Colloidal Particle Deposit Patterns within Picoliter Droplets Ejected by Ink-Jet Printing. *Langmuir*, 22(8), 3506-3513.





<https://doi.org/10.1021/la053450j>

Panda, B., Paul, S., Hui, L., Tay, Y., & Tan, M. (2017). Additive manufacturing of geopolymer for sustainable built environment. *Journal of Cleaner Production*, 167, 281-288.

Pell, R., Tijsseling, L., Goodenough, K., Wall, F., Dehaine, Q., Grant, A., Deak, D., Yan, X., & Whattoff, P. (2021). Towards sustainable extraction of technology materials through integrated approaches. *Nature Reviews Earth & Environment*, 2(10), 665-679. <https://doi.org/10.1038/s43017-021-00211-6>

Pignatelli, F., & Percoco, G. (2022). An application-and market-oriented review on large format additive manufacturing, focusing on polymer pellet-based 3D printing. *Progress in Additive Manufacturing*, 7(6), 1363-1377.

Pochon, A., Desauty, A.-M., Bailly, L., & Lach, P. (2021). Challenging the traceability of natural gold by combining geochemical methods: French Guiana example. *Applied Geochemistry*, 129, 104952. <https://doi.org/10.1016/j.apgeochem.2021.104952>

Pornwilard, M. M., Hansawek, R., Shiowatana, J., & Siripinyanond, A. (2011). Geographical origin classification of gem corundum using elemental fingerprint analysis by laser ablation inductively coupled plasma mass spectrometry. *International Journal of Mass Spectrometry*, 306(1), 57-62. <https://doi.org/10.1016/j.ijms.2011.06.010>

Punpongsanon, P., Miyatake, Y., Iwai, D., & Sato, K. (2022, October). Demonstration of interiqr: Unobtrusive Edible Tags using Food 3D Printing. In *Adjunct Proceedings of the 35th Annual ACM Symposium on User Interface Software and Technology* (pp. 1-3).

Q. Grim, J., Manna, L., & Moreels, I. (2015). A sustainable future for photonic colloidal nanocrystals. *Chemical Society Reviews*, 44(16), 5897-5914. <https://doi.org/10.1039/C5CS00285K>

RCS Global. (2017). Blockchain for Traceability in Minerals and Metals Supply Chains: Opportunities and Challenges. <https://www.rcsglobal.com/wp-content/uploads/2018/09/ICMM-Blockchain-for-Traceability-in-Minerals-and-Metal-Supply-Chains.pdf>

Rao, R. S., Visuri, S. R., McBride, M. T., Albala, J. S., Matthews, D. L., & Coleman, M. A. (2004). Comparison of Multiplexed Techniques for Detection of Bacterial and Viral Proteins. *Journal of Proteome Research*, 3(4), 736-742. <https://doi.org/10.1021/pr034130t>

Raut, H. K., Wang, H., Ruan, Q., Wang, H., Fernandez, J. G., & Yang, J. K. (2021). Hierarchical colorful structures by three-dimensional printing of inverse opals. *Nano Letters*, 21(20), 8602-8608.

Rajeshwar, K., de Tacconi, N. R., & Chenthamarakshan, C. R. (2001). Semiconductor-Based Composite Materials: Preparation, Properties, and Performance. *Chemistry of Materials*, 13(9), 2765-2782. <https://doi.org/10.1021/cm010254z>

Rathaiah, M., Martín, I. R., Babu, P., Linganna, K., Jayasankar, C. K., Lavín, V., & Venkatramu, V. (2015). Photon avalanche upconversion in Ho³⁺-doped gallium nano-garnets. *Optical Materials*, 39, 16-20. <https://doi.org/10.1016/j.optmat.2014.10.050>





D2.1. Artificial fingerprinting for tracking raw material flows in complex supply chains.

Ren, W., Lin, G., Clarke, C., Zhou, J., & Jin, D. (2020). Optical Nanomaterials and Enabling Technologies for High-Security-Level Anticounterfeiting. *Advanced Materials*, 32(18), 1901430. <https://doi.org/10.1002/adma.201901430>

Research Gate (2023) The representation of Stokes-shift and its calculation method. (n.d.). Research Gate. Retrieved 29 August 2023, from https://www.researchgate.net/figure/The-representation-of-Stokes-shift-and-its-calculation-method_fig10_343319896

Rodrigues, T. A., Duarte, V., Miranda, R. M., Santos, T. G., & Oliveira, J. P. (2019). Current status and perspectives on wire and arc additive manufacturing (WAAM). *Materials*, 12(7), 1121.

Salas, D., Ebeperi, D., Elverud, M., Arróyave, R., Malak, R. J., & Karaman, I. (2022). Embedding hidden information in additively manufactured metals via magnetic property grading for traceability. *Additive Manufacturing*, 60, 103261.

Salomon-de-Friedberg, H., & Robinson, T. (2015). Tackling impurities in copper concentrates. *Material Science*.
<https://www.semanticscholar.org/paper/TACKLING-IMPURITIES-IN-COPPER-CONCENTRATES-Salomon-de-Friedberg-Robinson>

Sanderson, K. (2021). The long road to sustainable lithium-ion batteries. *Chemistry World*.
<https://www.chemistryworld.com/features/the-long-road-to-sustainable-lithium-ion-batteries/4013838.article>

Sanei, S., & Popescu, D. (2020). 3D-Printed Carbon Fiber Reinforced Polymer Composites: A Systematic Review. *Journal of Composites Science*, 4 (3), 98.

Savolainen, J., & Collan, M. (2020). How additive manufacturing technology changes business models? – Review of literature. *Additive manufacturing*, 32, 101070.

Schenker, V., Oberschelp, C., Pfister, S. (2022). Regionalized life cycle assessment of present and future lithium production for Li-ion batteries. *Resources, Conservation and Recycling*, 187, 106611. <https://doi.org/10.1016/j.resconrec.2022.106611>

Schmuck, R., Wagner, R., Hörpel, G., Placke, T., & Winter, M. (2018). Performance and cost of materials for lithium-based rechargeable automotive batteries. *Nature Energy*, 3(4), 267–278. <https://doi.org/10.1038/s41560-018-0107-2>

Schütte, P., Melcher, F., Gäbler, H.-E., Sitnikova, M., Hublitz, M., Goldmann, S., Schink, W., Gawronski, T., Ndikumana, A., & Nziza, L. (2018). The Analytical Fingerprint (AFP): Method and Application - Process Manual Version 1.4 (Issue May).
<https://www.bgr.bund.de/mineral-certification>

Schwich, L.; Schubert, T.; Friedrich, B. 2021. Early-stage recovery of lithium from tailored thermal conditioned black mass part 1: Mobilizing lithium via supercritical CO₂-carbonation. *Metals*, 11, pp. 177, <https://doi.org/10.3390/met11020177>

Seman, J., Giraldo, C. H. C., & Johnson, C. E. (2019). Reactive not Proactive: Explosive Identification Taggant History and Introduction of the Nuclear Barcode Taggant Model. *Propellants, Explosives, Pyrotechnics*, 44(4), 397–407.
<https://doi.org/10.1002/prop.201800322>





Shah, J., Snider, B., Clarke, T., Kozutsky, S., Lacki, M., & Hosseini, A. (2019). Large-scale 3D printers for additive manufacturing: design considerations and challenges. *The International Journal of Advanced Manufacturing Technology*, 104(9-12), 3679-3693.

Sing, S. L., & Yeong, W. Y. (2020). Laser powder bed fusion for metal additive manufacturing: perspectives on recent developments. *Virtual and Physical Prototyping*, 15(3), 359-370.

Singh, M., Haverinen, H. M., Dhagat, P., & Jabbour, G. E. (2010). Inkjet Printing—Process and Its Applications. *Advanced Materials*, 22(6), 673-685.

<https://doi.org/10.1002/adma.200901141>

Smith, B. J., Riddle, M. E., Earlam, M. R., Iloeje, C., & Diamod, D. (2022). Rare earth permanent magnets - Supply chain deep dive assessment. In U.S. Department of Energy Response to Executive Order 14017, "America's supply chains."

Sofinowski, K., Wittwer, M., & Seita, M. (2022). Encoding data into metal alloys using laser powder bed fusion. *Additive Manufacturing*, 52, 102683.

Sola, A., Sai, Y., Trinchì, A., Chu, C., Shen, S., & Chen, S. (2021). How can we provide additively manufactured parts with a fingerprint? A review of tagging strategies in additive manufacturing. *Materials*, 15(1), 85.

Svetlizky, D., Das, M., Zheng, B., Vyatskikh, A. L., Bose, S., Bandyopadhyay, A., ... & Eliaz, N. (2021). Directed energy deposition (DED) additive manufacturing: Physical characteristics, defects, challenges and applications. *Materials Today*, 49, 271-295

Terranova, S., Costa, F., Manara, G., & Genovesi, S. (2020). Three-dimensional chipless RFID tags: Fabrication through additive manufacturing. *Sensors*, 20(17), 4740.

Tijsseling, L. T., Dehaine, Q., Rollinson, G. K., & Glass, H. J. (2019). Flotation of mixed oxide sulphide copper-cobalt minerals using xanthate, dithiophosphate, thiocarbamate and blended collectors. *Minerals Engineering*, 138, 246-256.

<https://doi.org/10.1016/j.mineng.2019.04.022>

Tran, T., & Luong, V. T. (2015). Lithium Production Processes. In *Lithium Process Chemistry: Resources, Extraction, Batteries, and Recycling* (pp. 81-124). Elsevier Inc. <https://doi.org/10.1016/B978-0-12-801417-2.00003-7>

Trenfield, S. J., Tan, H. X., Awad, A., Buanz, A., Gaisford, S., Basit, A. W., & Goyanes, A. (2019). Track-and-trace: Novel anti-counterfeit measures for 3D printed personalized drug products using smart material inks. *International journal of pharmaceuticals*, 567, 118443.

Trinchì, A., & Sola, A. (2023). Embedding Function within Additively Manufactured Parts: Materials Challenges and Opportunities. *Advanced Engineering Materials*, 2300395.

Tsai, W.-K., Lai, Y.-S., Tseng, P.-J., Liao, C.-H., & Chan, Y.-H. (2017). Dual Colorimetric and Fluorescent Authentication Based on Semiconducting Polymer Dots for Anticounterfeiting Applications. *ACS Applied Materials & Interfaces*, 9(36), 30918-30924. <https://doi.org/10.1021/acsami.7b08993>

Tumer, E., & Erbil, H. (2021). Extrusion-Based 3D Printing Applications of PLA Composites: A Review. *Coatings*, 11(4), 390.

USGS (2023). Mineral Commodity Summaries 2023. <https://doi.org/https://doi.org/10.3133/mcs2020>





USA Government (1970). Public Law 91-450-OCT. 14, 1970.

Vanderbruggen, A.; Gugala, E.; Blannin, R.; Backmann, K.; Serna-Guerrero, R.; Rudolph, M. 2021. Automated mineralogy as a novel approach for the compositional and textural characterization of spent lithium-ion batteries. *Minerals Engineering*, pp. 169, 106924.

Vock, S., Klöden, B., Kirchner, A., Weißgärber, T., & Kieback, B. (2019). Powders for powder bed fusion: a review. *Progress in Additive Manufacturing*, 4, 383-397.

Wang, P.-X., Hamad, W. Y., & MacLachlan, M. J. (2016). Polymer and Mesoporous Silica Microspheres with Chiral Nematic Order from Cellulose Nanocrystals. *Angewandte Chemie*, 128(40), 12648-12652. <https://doi.org/10.1002/ange.201606283>

Wang, Y., Wang, Y., Bian, F., Shang, L., Shu, Y., & Zhao, Y. (2020). Quantum dots integrated biomass pollens as functional multicolor barcodes. *Chemical Engineering Journal*, 395, 125106. <https://doi.org/10.1016/j.cej.2020.125106>

Weißgärber, T., & Kieback, B. (2019). Powders for powder bed fusion: a review. *Progress in Additive Manufacturing*, 4, 383-397.

Wang, X., Gao, D., Su, F., Zheng, Y., Li, X., Liu, Z., ... & Chen, Z. (2023). Photopolymerization 3D printing of luminescent ceramics. *Additive Manufacturing*, 73, 103695.

Wei, C., Sun, Z., Huang, Y., & Li, L. (2018). Embedding anti-counterfeiting features in metallic components via multiple material additive manufacturing. *Additive Manufacturing*, 24, 1-12.

Wen, X., Zhang, B., Wang, W., Ye, F., Yue, S., Guo, H., ... & Lou, J. (2021). 3D-printed silica with nanoscale resolution. *Nature Materials*, 20(11), 1506-1511.

Windolf, H., Chamberlain, R., Delmotte, A., & Quodbach, J. (2022). Blind-Watermarking–Proof-of-Concept of a Novel Approach to Ensure Batch Traceability for 3D Printed Tablets. *Pharmaceutics*, 14(2), 432.

Wotherspoon, A., Vance, L., Davis, J., Hester, J., Gregg, D., Griffiths, G., Zhang, Y., Palmer, T., Keegan, E., Blagojevic, N., Loi, E., & Hill, D. (2014). Investigating Macro - and Micro - Scale Material Provenancing Signatures in Uranium Ore Concentrates / Yellowcake. IAEA International Conference on Advances in Nuclear Forensics.

Wu, S., Liu, B., Su, X., & Zhang, S. (2017). Structural Color Patterns on Paper Fabricated by Inkjet Printer and Their Application in Anticounterfeiting. *The Journal of Physical Chemistry Letters*, 8(13), 2835-2841. <https://doi.org/10.1021/acs.jpclett.7b01372>

Wu, Y., Zhong, Y., Chu, B., Sun, B., Song, B., Wu, S., Su, Y., & He, Y. (2016). Plant-derived fluorescent silicon nanoparticles featuring excitation wavelength-dependent fluorescence spectra for anti-counterfeiting applications. *Chemical Communications*, 52(43), 7047-7050. <https://doi.org/10.1039/C6CC02872A>

Xiong, L., Chen, Z., Tian, Q., Cao, T., Xu, C., & Li, F. (2009). High Contrast Upconversion Luminescence Targeted Imaging in Vivo Using Peptide-Labeled Nanophosphors. *Analytical Chemistry*, 81(21), 8687-8694. <https://doi.org/10.1021/ac901960d>

Xu, L., Chen, J., Song, J., Li, J., Xue, J., Dong, Y., Cai, B., Shan, Q., Han, B., & Zeng, H. (2017). Double-Protected All-Inorganic Perovskite Nanocrystals by Crystalline Matrix and Silica for





Triple-Modal Anti-Counterfeiting Codes. *ACS Applied Materials & Interfaces*, 9(31), 26556–26564. <https://doi.org/10.1021/acsami.7b06436>

Yakovlev, A. V., Milichko, V. A., Vinogradov, V. V., & Vinogradov, A. V. (2016). Inkjet Color Printing by Interference Nanostructures. *ACS Nano*, 10(3), 3078–3086. <https://doi.org/10.1021/acsnano.5b06074>

Yan, C., Byrne, D., Ondry, J. C., Kahnt, A., Moreno-Hernandez, I. A., Kamat, G. A., Liu, Z.-J., Laube, C., Crook, M. F., Zhang, Y., Ercius, P., & Alivisatos, A. P. (2022). Facet-selective etching trajectories of individual semiconductor nanocrystals. *Science Advances*, 8(32), eabq1700. <https://doi.org/10.1126/sciadv.abq1700>

Yao, W., Tian, Q., Liu, J., Wu, Z., Cui, S., Ding, J., Dai, Z., & Wu, W. (2016). Large-scale synthesis and screen printing of upconversion hexagonal-phase NaYF₄:Yb³⁺,Tm³⁺/Er³⁺/Eu³⁺ plates for security applications. *Journal of Materials Chemistry C*, 4(26), 6327–6335. <https://doi.org/10.1039/C6TC01513A>

Zabyelina, Y., and van Uhm, D. (2020). *Illegal Mining : Organized Crime, Corruption, and Ecocide in a Resource-Scarce World*. Cham, SWITZERLAND: Springer International Publishing AG.

Zhao, R., Wittig, N., De Angelis, G., Yuan, T., Hirsch, M., Birkedal, H., & Amstad, E. (2023). Additive Manufacturing of Porous Biominerals. *Advanced Functional Materials*, 2300950.

Zhou, Y., Zhou, X., Park, D. J., Torabi, K., Brown, K. A., Jones, M. R., Zhang, C., Schatz, G. C., & Mirkin, C. A. (2014). Shape-Selective Deposition and Assembly of Anisotropic Nanoparticles. *Nano Letters*, 14(4), 2157–2161. <https://doi.org/10.1021/nl500471g>

Ziaee, M., & Crane, N. B. (2019). Binder jetting: A review of process, materials, and methods. *Additive Manufacturing*, 28, 781–801.





D2.1. Artificial fingerprinting for tracking raw material flows in complex supply chains.

Web sites:

3M Security Solutions

- <https://multimedia.3m.com/mws/media/630248O/3m-light-reveal-authentication-products.pdf?&fn=3MLightRevealAuthen.pdf>
- https://www.3m.com/3M/en_US/company-us/about-3m/history/timeline/

Applied DNA Science

- <https://adnas.com/>

Authentix

- <https://authentix.com/solution-technologies/markers-tagants/>

European Union: Battery Revolution:

- https://environment.ec.europa.eu/topics/waste-and-recycling/batteries_en

European Union: Critical Raw materials (CRM) Act 2020

- https://single-market-economy.ec.europa.eu/sectors/raw-materials/areas-specific-interest/critical-raw-materials_en

European Union: Directive on Corporate Sustainability Due Diligence

- https://environment.ec.europa.eu/topics/waste-and-recycling/batteries_en
- https://commission.europa.eu/business-economy-euro/doing-business-eu/corporate-sustainability-due-diligence_en

German Supply Chain Act

- <https://corporatejustice.org/news/german-supply-chain-act-comes-into-force/>

Haelixa

- https://www.haelixa.com/category_cases/precious-metals/

IGF

- <https://www.iisd.org/publications/report/illicit-financial-flows-conflict-artisanal-small-scale-gold-mining>

INTERPOL

- <https://www.interpol.int/en/News-and-Events/News/2022/The-devastating-impact-of-illegal-gold-mining-in-Latin-America>
- https://www.interpol.int/content/download/16493/file/2021%2007%2027%20ENG_LISH%20PUBLIC%20VERSION_FINAL_Illegal%20gold%20mining%20in%20Central%20Africa.pdf
- <https://igarape.org.br/en/guidance-note-on-combating-environmental-crime-lessons-from-fighting-illegal-gold-mining-in-the-amazon->





[basin/#:~:text=The%20note%20offers%20a%20catalogue,activities%20within%20and%20across%20countries.](#)

IUGS-IFG

- <https://geoforenses.com/about-special-project/>

Luminex and SmartWater

- <https://www.luminexcorp.com/eu/xtag-technology/SmartWater>
<https://shop.smartwater.com/>
- <https://detertech.com/smartspray/>

MaDiTraCe

- <https://cordis.europa.eu/project/id/101091502/fr>
- www.maditrace.eu
- www.cera4in1.org

Microtrace Solutions

- <https://www.microtracesolutions.com/technologies/implement-independently/microtaggant-identification-particles>

OECD

- <https://mneguidelines.oecd.org/mining.htm>
- <https://www.oecd-ilibrary.org/docserver/7536db96-en.pdf?expires=1694097236&id=id&accname=guest&checksum=A6E8B320E5694AA91EBBAA08D68724D8>

Selectamark Security Systems

- <https://www.selectamark.co.uk/>

Tailorlux GmbH

- <https://www.tailorlux.com>

THEMIS

- <https://www.wearethemis.com/uk/insight/financial-crime-research/gold-more-illicit-flows-following-russias-invasion-of-ukraine/>

TraceTag International

- <https://www.tracetag.com/>

UNODC


- https://www.unodc.org/documents/Wildlife/UNODC_Response_Framework_Minerals.pdf
- <https://www.unodc.org/unodc/en/environment-climate/illegal-mining.html>
- https://sherloc.unodc.org/cld/uploads/pdf/Illegal_Mining_and_Trafficking_in_Metals_and_Minerals_E.pdf



8 Appendices

8.1 Appendix I: MaDiTraCe Questionnaire

ALFRED H KNIGHT


MADITRACE

Commercial-in-Confidence

MaDiTraCe

Material and Digital Traceability for the Certification of critical raw materials

INDUSTRY PARTICIPANT QUESTIONNAIRE

PARTICIPANT DETAILS

| | |
|--------------------|--|
| Company Name | |
| Contact Name(s) | |
| Date | |
| Time | |
| AHK Interviewer(s) | |

Introduction

'MaDiTraCe', is a European Union funded research project, which commenced in January 2023 and has a three years duration. The project aims to enlarge and integrate a portfolio of technological solutions reinforcing the reliability of critical raw material tracking and the transparency of complex supply chains. AHK are contributing to a work package to develop artificial fingerprinting technologies, to be used as 'material passports' for key commodities including but not limited to lithium, graphite, cobalt, and rare earth elements (minerals/metals with a focus on neodymium) in two complex supply chains, namely rechargeable lithium-ion batteries and magnets. AHK also has interests for the potential development of artificial taggant particles for base metal and precious metal mineral commodities.

AHK are leading, with input from the Geological Survey of Finland (GTK), a review and evaluation of existing methods for the potential use of artificial taggant particles. An analysis of the requirements for the mining, minerals and metals industries is being undertaken to ensure any solutions provided are fit-for-purpose and commercially relevant.

The following questionnaire aims to gather stakeholder input to guide the specifications of appropriate materials (e.g., minerals, metals, bioplastic composites containing minerals and/or metals) for the development of prototype artificial taggant particles and subsequent large-scale production of artificial taggant particles.

AHK DISTRIBUTION ONLY
MaDiTraCe 2023



ALFRED H KNIGHT

During 2023,2024 and 2025 AHK and GTK will be performing laboratory-based experimental research followed by field testing of new artificial taggant particles to help determine their physical and chemical characteristics, properties, behaviour and suitability as a potential tracer, when mixed in a sample bag bulk cargo, refined metal commodities, or other products of the lithium-ion and magnet supply chains. The experimental work conducted will also seek to verify if the homogeneous distribution of artificial taggant particles has been achieved, and assess the impacts of transportation, storage time, and environmental conditions. Methods for the cost-effective and practicable detection of the artificial taggant particles also form part of this research.

Questionnaire:

1. Are there any aspects of your operation or supply chain where you feel the use of an artificial taggant would be beneficial (such as to improve traceability of feed material or products)?

2. With respect to the elemental composition of each product material or intermediate material:
 - a. Are there any elements / other materials that should be excluded (i.e. zero-tolerance)?
 - b. Are there any elements / other materials that should be limited, and what are these limits?
 - c. Are there any elements / other materials that are not of concern (e.g. those that are easily removed by production processes)?

| Elements / other materials | Not Permitted | Permitted within limits | No Restriction | Comments |
|----------------------------|--------------------------|--------------------------|--------------------------|----------|
| Antimony (Sb) | <input type="checkbox"/> | <input type="checkbox"/> | <input type="checkbox"/> | |
| Arsenic (As) | <input type="checkbox"/> | <input type="checkbox"/> | <input type="checkbox"/> | |
| Bismuth (Bi) | <input type="checkbox"/> | <input type="checkbox"/> | <input type="checkbox"/> | |
| Cadmium (Cd) | <input type="checkbox"/> | <input type="checkbox"/> | <input type="checkbox"/> | |
| Chlorine (Cl) | <input type="checkbox"/> | <input type="checkbox"/> | <input type="checkbox"/> | |
| Carbon (C) | <input type="checkbox"/> | <input type="checkbox"/> | <input type="checkbox"/> | |
| Iron (Fe) | <input type="checkbox"/> | <input type="checkbox"/> | <input type="checkbox"/> | |
| Lead (Pb) | <input type="checkbox"/> | <input type="checkbox"/> | <input type="checkbox"/> | |
| Mercury (Hg) | <input type="checkbox"/> | <input type="checkbox"/> | <input type="checkbox"/> | |
| Nickel (Ni) | <input type="checkbox"/> | <input type="checkbox"/> | <input type="checkbox"/> | |

AHK DISTRIBUTION ONLY
MaDITraCe 2023





ALFRED H KNIGHT

| Elements / other materials | Not Permitted | Permitted within limits | No Restriction | Comments |
|--|--------------------------|--------------------------|--------------------------|----------|
| Phosphorus (P) | <input type="checkbox"/> | <input type="checkbox"/> | <input type="checkbox"/> | |
| Silicon (Si) | <input type="checkbox"/> | <input type="checkbox"/> | <input type="checkbox"/> | |
| Selenium (Se) | <input type="checkbox"/> | <input type="checkbox"/> | <input type="checkbox"/> | |
| Sulphur (S) | <input type="checkbox"/> | <input type="checkbox"/> | <input type="checkbox"/> | |
| Tellurium (Te) | <input type="checkbox"/> | <input type="checkbox"/> | <input type="checkbox"/> | |
| Tin (Sn) | <input type="checkbox"/> | <input type="checkbox"/> | <input type="checkbox"/> | |
| Rare earth elements (Ce, Dy, Er, Eu, Gd, Ho, La, Lu, Nd, Pr, Pm, Sm, Sc, Tb, Tm, Yb and Y) | <input type="checkbox"/> | <input type="checkbox"/> | <input type="checkbox"/> | |
| Oil-based plastics | <input type="checkbox"/> | <input type="checkbox"/> | <input type="checkbox"/> | |
| Non-oil-based plastics | <input type="checkbox"/> | <input type="checkbox"/> | <input type="checkbox"/> | |
| Ceramics | <input type="checkbox"/> | <input type="checkbox"/> | <input type="checkbox"/> | |
| Blomaterials | <input type="checkbox"/> | <input type="checkbox"/> | <input type="checkbox"/> | |
| Others (please specify) | <input type="checkbox"/> | <input type="checkbox"/> | <input type="checkbox"/> | |
| | <input type="checkbox"/> | <input type="checkbox"/> | <input type="checkbox"/> | |
| | <input type="checkbox"/> | <input type="checkbox"/> | <input type="checkbox"/> | |
| | <input type="checkbox"/> | <input type="checkbox"/> | <input type="checkbox"/> | |
| | <input type="checkbox"/> | <input type="checkbox"/> | <input type="checkbox"/> | |
| | <input type="checkbox"/> | <input type="checkbox"/> | <input type="checkbox"/> | |

3. Specific to your operation, are there any other requirements or restrictions with respect to the properties of an artificial taggant (e.g. particle size, appearance, resistance to temperature/pH, magnetism, etc.)?



ALFRED H KNIGHT

4. Would your organisation be willing to participate in a trial of the artificial taggants by?

a. Providing sample material for laboratory-based tests?

Yes ☐

No ☐

b. Testing prototype artificial taggant particles on a consignment/shipment of cargo?

Yes ☐

No ☐

The information you have provided will be used for research and development of artificial taggant particles and may be shared with the MaDiTraCe project partners for this purpose. Your contribution to this project is appreciated and we would like to credit your organisation in any future project publications. However, responses can be anonymised for publication if necessary. Please tick one of the two options:

My organisation consents to being named as a contributor in future publications ☐

Provided responses and information shall be anonymised for publication ☐

Thank you for your participation.

AHK DISTRIBUTION ONLY
MaDiTraCe 2023





8.2 Appendix II: Photolithography or Photochemical Machining

The geometry of the particle and pattern needed to be produced is drawn using a CAD software and printed onto a photographic film (silver halides or di-azo films). A light sensitive material (photoresist) is layered onto the substrate. The pattern is applied onto the surface, this helps ensure the unmasked regions are exposed to light.

There are two kinds of photoresist processes that take place: positive photoresist and negative photoresist. In the case of the former, the photo-sensitive material becomes degraded by light and the developer, which was used to coat over it, dissolves away the regions that were exposed to light (Figure AIII.1). This leaves behind a coating where the mask was placed. In case of the latter, strengthening through polymerisation or crosslinking takes place by usage of light. The developer dissolves away only the regions that were not exposed to the light. This leaves behind a coating of the areas where the mask not placed.

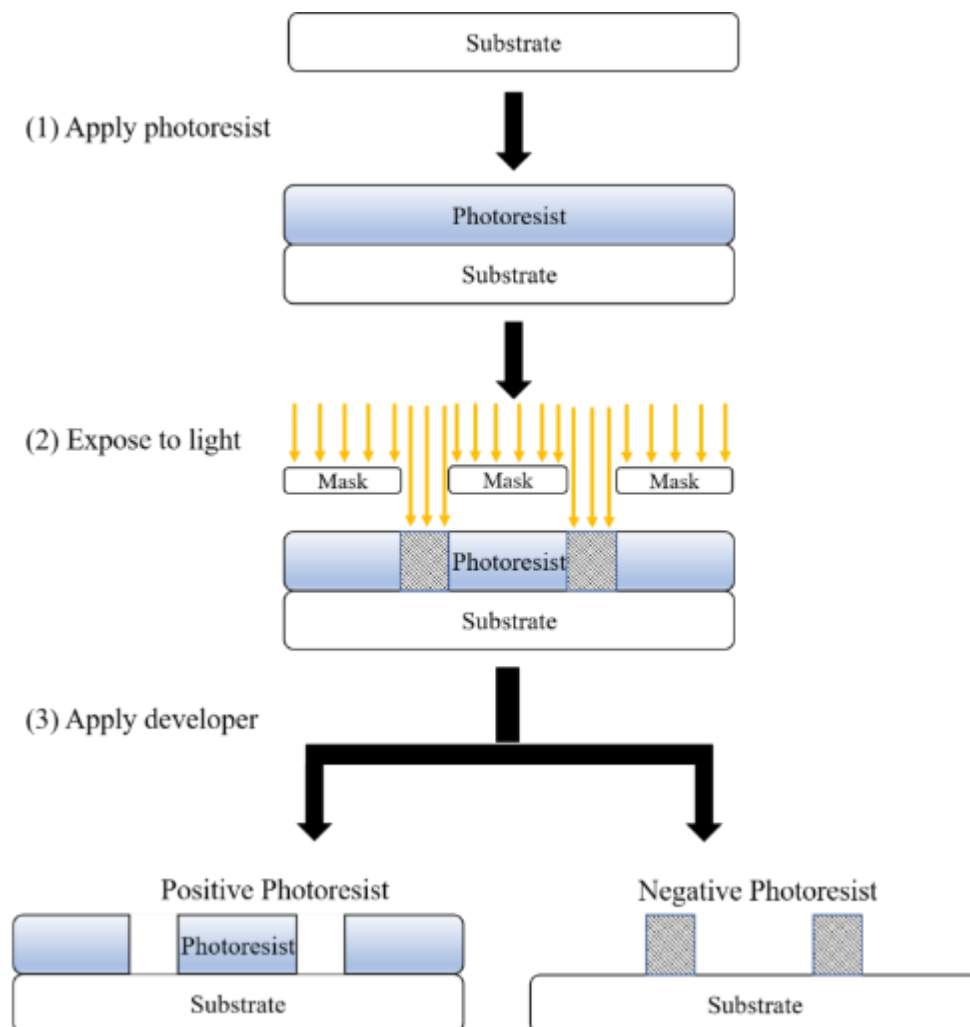


Figure AIII.1: Photolithography procedure (Rao *et al.*, 2004).

8.3 Appendix III: Stokes shift and Anti-Stokes shift

When there is a spectral shift in photonic energy from high to low between an incident and emitted light source respectively, it is termed as Stokes Shift. The shift extent depends on the fluorophore. More polar solvents produce larger shifts. Anti-Stokes Shift is the opposite of Stokes Shift (Figure A.V1).

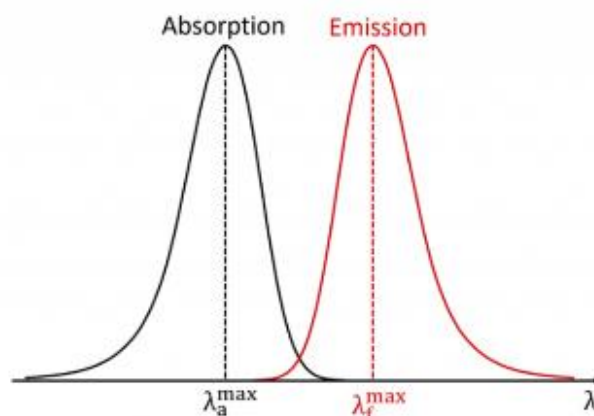


Figure AIV.1 Wavelength increase in Stokes Shift Hines, M. A., & Guyot-Sionnest (Research Gate, 2023)

There are three types of fluorescence possible: Downshifting (DS), Upconversion (UC), and Downconversion (DC). DS luminescence absorbs a photon with high energy and emits a lower energy photon. UC converts two or more photons with low energy into one high energy photon. UC luminescence therefore exhibits Anti-Stokes Shift. UC has been greatly used in bio-imaging, sensing devices, light harvesting using solar cells and cancer treatment. DC absorbs one photonic energy and emits two or more photons. Upconversion consists of three (1,2,3) energy states. Initially, electron resides at the 1st state. On absorption of 1st photon, electron is excited to an intermediate 2nd stage. On absorption of 2nd photon, excitation to the 3rd stage takes place. The electron relaxes back (a certain initial phononic, non-radiative energy is released) to the 1st state, the released photon has higher energy than both the initial incident photons (Figure AV.2).

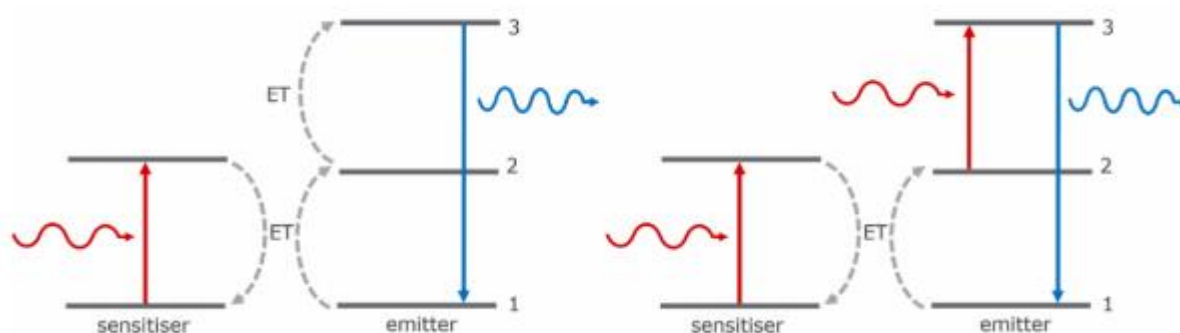


Figure AIV.2: (left) sequential energy transfer in UC, and (right) excited state absorption UC (Edinburgh Instruments, 2023).

Conditions required for UC to take place include the following:

1. The 2nd electronic orbital stage has to be sufficiently long-lived, and
2. photon flux must be high enough such that a 2nd photon is absorbed prior to relaxation of 1st photon from state 2.



8.4 Appendix IV: Photoluminescence

The energy absorbed from incident light helps excite electrons to higher energy orbitals (Figure AIV.1). On relaxing back to the lower orbital, the electron emits energy in the form of photons producing luminescence. Photoluminescence is of two types (Table AV.1).

Table AV.1: Fluorescence and phosphorescence difference.

| Fluorescence | Phosphorescence |
|---|---|
| Occurs for the duration light energy is incident on the material. | Continues to generate luminescence for a period even after removal of light source. |

The spin angular momentum of a molecule at its ground state is 0 since all orbitals are filled, therefore all electron spins are anti-parallel. When the electron is excited from highest occupied molecular orbital (HOMO) to lowest occupied molecular orbital (LUMO), there exists 2 unpaired electrons. The new excited electron can have the following states (Figures AIV.2 and AIV.3):

1. Singlet (s_1): Owing to electron selection rules, electrons cannot change their spin orientation ($s=0$). Hence, the number of degenerate states = $2s + 1 = 2 [(1/2) + (-1/2)] = 1$.
2. Triplet (T_1): If the electron has parallel spin, $s=1$. Number of degenerate states = 3.

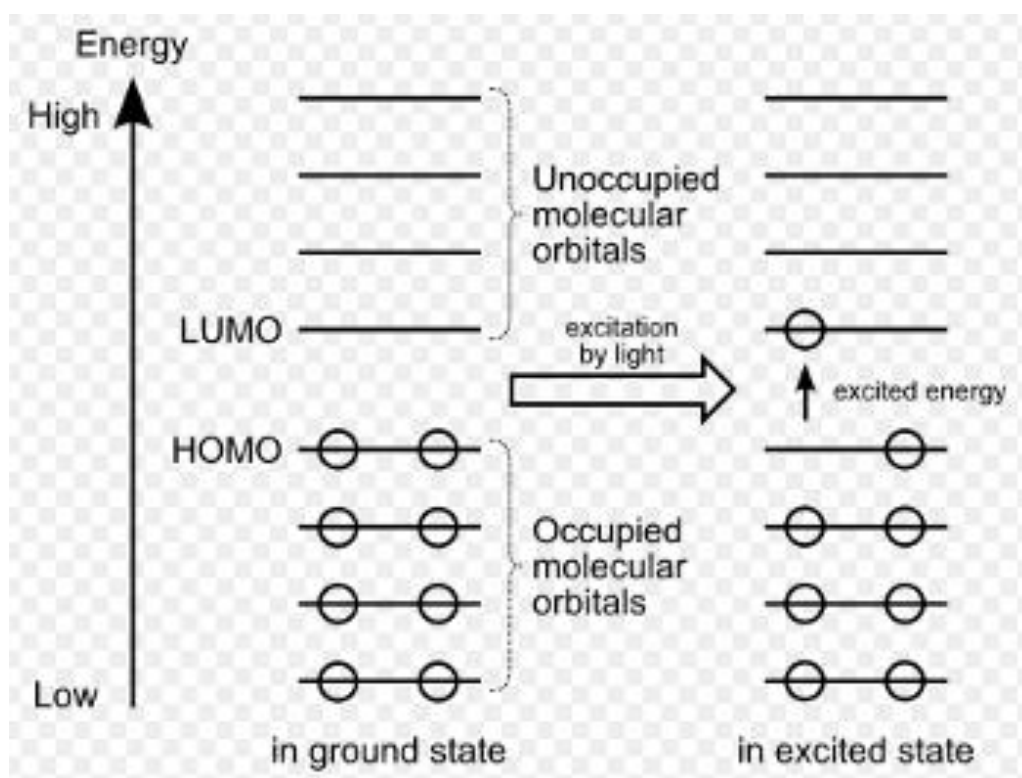


Figure AV.1: Electron excitation (Hickman, 2017).

In fluorescence, while going through vibrational relaxation, non-radiative energy is released initially followed by photonic energy on reaching the lowest energy in s_1 stage. It is only found in atoms or molecules with distinct energy gap between s_0 and s_1 .

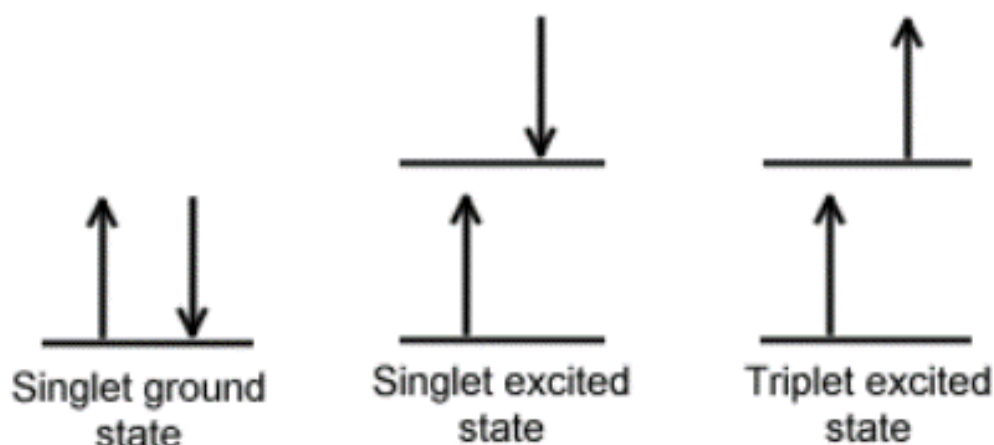


Figure AV.2: Electronic states (Hickman 2017).

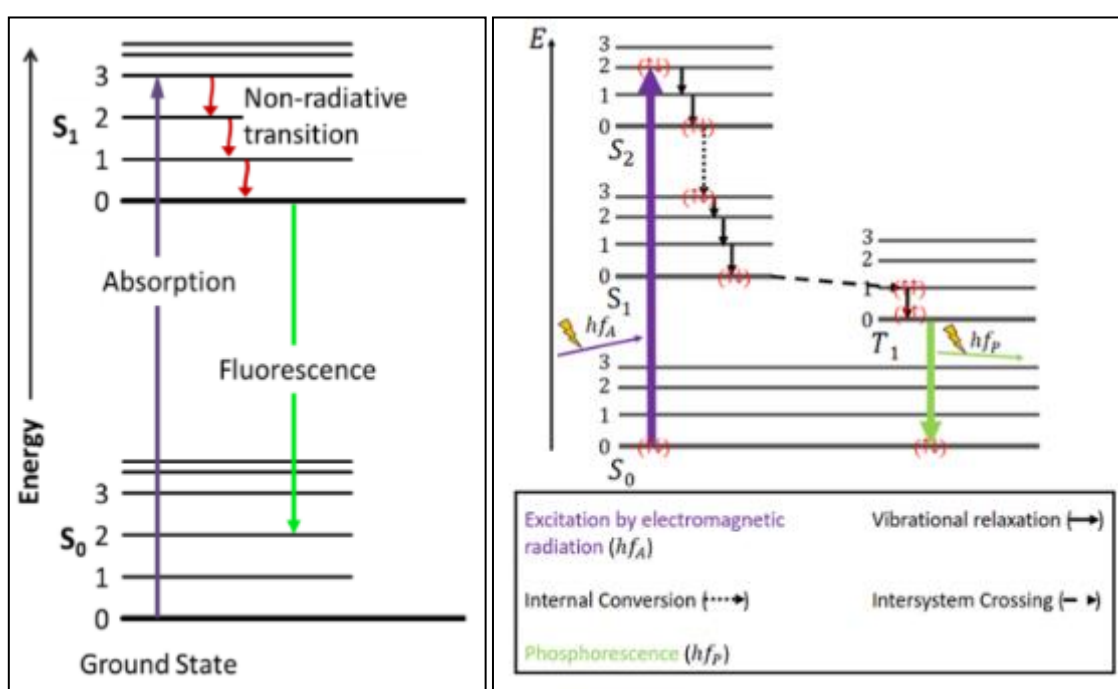


Figure AVV.3: Fluorescence (left) and phosphorescence (right) energy diagram (Hickman 2017).

In phosphorescence, both unpaired electrons end up having the same spin. There exist 4 states in total: s_0 , s_1 , s_2 and T_1 which lies between s_0 and s_2 . The release of energy through vibrational relaxation and internal conversion while maintaining the same spin remains the same here, but only until the s_1 state is reached. Intersystem crossing (ISC) occurs since the T_1 state is energetically more favourable than the s_1 state. It is associated with a spin reversal from singlet to triplet. ISC is forbidden due to "spin-orbit coupling".